Retention and Enhancement of Biomolecule Activity on Quantum Dots

A Thesis Submitted for the Degree
of
Doctor of Philosophy
at
The University of Edinburgh
by
Manish Gupta, *MPharm*

Department of Chemistry
University of Edinburgh
2010

Abstract

Quantum dots (QDs) are semiconductor nanoparticles which have emerged as powerful fluorescent probes for biological imaging applications due to their unique size-dependent optical and electrical properties. QDs have several advantages over small organic dyes and fluorescent proteins such as size-tunable photoluminescence, wide excitation-narrow emission properties, improved brightness and high resistance to photobleaching and degradation. So far QDs have been used to track individual biomolecules, but for this application a widespread concern is that biomolecules can lose activity when they are attached to QDs because these are multivalent and large. Thus, recent attention has turned toward labelling strategies which enable site-specific recognition and controlling the number of molecules that can be attached to a single QD down to a single molecule with retention of activity. Apart from showing ability to recognise appropriate biological partners, relatively little is known about the biological activity of biomolecules attached to QDs.

In this thesis various strategies for preserving and enhancing the activity of biomolecules on QDs were developed to address and investigate these aspects and to extend the biological applications of QDs.

Nitrilotriacetic acid (NTA)-modified QDs were used for site specific labelling of a hexahistidine (His_6)-tagged Glutathione-S-Transferase (GST). GSTs catalyse nucleophilic substitution reactions between glutathione and a wide range of endogenous and xenobiotic electrophiles, which makes them important detoxifying enzymes and anticancer targets. The hydrophobic CdSe-ZnS (core-shell) QDs were made water soluble by ligand exchange with dihydrolipoic acid and coupled to NTA-Ni via an amide bond. Ni-NTA capped QD were capable of binding recombinant *S. japonicum* His_6-GST selectively. As a result of the His_6 tag's ability to provide a docking site for the QD away from the active site, the GST molecules bound to these QDs retained their catalytic activity. In contrast, the non specific binding which takes place in the absence of the His_6 tag leads to loss of catalytic activity.

Hydrophobic interactions were used to functionalize CdSe-ZnS QDs with Kdo_2-lipid A –the lipopolysaccahride (LPS) present in the outer membrane of *E.coli*. These constructs were used as pathogen models to investigate how pathogens and pathogen associated molecular patterns (e.g. LPS) interact and are processed by the immune system. The ability of

QDs to enhance the biological activity of a biomolecule was demonstrated *in vitro* and *in vivo* for the first time. QD-LPS micelles were able to induce stronger production of cytokines in macrophages and dendritic cells *in vitro* and a model antigen (DNP-OVA) *in vivo* than control LPS.

Also presented in this thesis is the first attempt to exploit the multivalency and site specific labelling properties of NTA-Ni-decorated QDs to mimic the surface of a parasite. The focus here was on the *Plasmodium falciparum* malaria merozoite, which has MSP 1 as major component of its surface. Conjugation of a recombinant form of His_6-MSP-1 hybrid to three different types of NTA-Ni-decorated QDs was accomplished. Morever, by changing the linker units separating the QDs and Ni-NTA complexes it was possible to control the number of MSP 1 molecules attached to each QD.

Acknowledgement

I am grateful to all the people who helped me through good and bad times during my dissertation work. First and foremost, I would like to express my sincere gratitude to my supervisor Dr Juan Mareque Rivas for giving me this interesting project and leading me into the field of nanobiotechnology. I have to thank him for his thoughtful and patient guidance, motivation and encouragement. You are the best supervisor a student could ask for. Dr. Dominic Campopiano, my co-supervisor, for his ideas and help throughout this thesis.

I want to express my sincere gratitude to Prof. David Dryden and Dr Simon Daff for allowing me to have access to the spectrophotometer and centrifuge in their respective laboratories.

I have to thank the people who collaborated with me - Anne Caniard for providing GST; Tom Barr for performing biological studies in LPS project and Lynne Harris for providing MSP.

I acknowledge Dr. V Ganesh for helping me in XPS studies. I would like to thank Dr. Wuzong Zhou and Ross Blackley at EaStCHEM-St. Andrews for the HRTEM studies.

Many thanks to my present and former colleagues Martin, Carmen, Pilar, Ganesh, Laurent, Nina, Angeles, Jose, and Daniela for making the lab a nice working environment. I am especially thankful to Venu, Kallol, Arindam and Rakesh for keeping me afloat whenever life and research wasn't going so great. I wish to thank my family for providing a loving environment for me, my parents, my brother Ashish for their unconditional love and infinite support. Finally, I am grateful to my wife Shraddha who helped me remain focused and determined in pursuit of my goals. I also want to thank her for her love and patience.

And last but not least I am very grateful for financial support provided by the EastCHEM fellowship.

Declaration

I hereby declare that, except where specific reference is made to other sources, the work contained in this thesis is the original work of my own research since the registration of the PhD degree in October 2006, and any collaboration has been clearly indicated. This thesis has been composed by myself and has not been submitted, in whole or in part, for any other degree, diploma or other qualification.

(Manish Gupta)

November 2010

Abbreviations

a.u.	Arbitrary Unit
BCA	Bicinchoninic acid
°C	Degree Celsius
Cy3	Cyanine 3 dye molecule
Cy5	Cyanine 5 dye molecule
Cys	Cysteine
Da	Dalton
DHLA	Dihydrolipoic acid
DOC	Deoxycholate
DMF	N, N-Dimethylformamide
DNA	Deoxyribonucleic acid
Dpa	Dipicolylamine
E. Coli	Escherichia Coli
ELISA	Enzyme-linked immunosorbent assay
ε	Extinction Coefficient
EDC	1-Ethyl-3-[3-dimethylaminopropyl]carbodiimide
EDTA	Ethylene Diamine Tetraacetic Acid
EYFP	Enhanced Yellow Fluorescent protein
FACS	Fluorescence Activated Cell Sorting
FRET	Fluorescence resonance energy transfer
FWHM	Full width at half maximum
FISH	Fluorescence in situ hybridization
GFP	Green fluorescent protein
GSH	Glutathione
GST	Glutathione-S-Transferases
HDA	Hexadecylamine
HEPES	4-(2-Hydroxyethyl)-Piperazine-1-Ethanesulfonic Acid
h	Hour
His_6	Hexahistidine
His_6-GST	Hexahistidine tagged Glutathione-S-Transferases
HIV	Human immunodeficiency virus
HNP	protonated *para*- nitrophenol
ICP-OES	Inductively Coupled Plasma – Optical Emission Spectrometry

IL-6	Interleukin-6
IgG	Immunoglobulin G
IgM	Immunoglobulin M
IMAC	Immobilized Metal Affinity Chromatography
LPS	Lipopolysaccharide
mAb	Monoclonal Antibody
MRI	Medical Resonance Imaging
MSP	Merozoite Surface protein
mM	Millimolar
Me_2Zn	Dimethylzinc
min	Minute
mL	Milliliter
MMP	Magnetic Microparticle
MW	Molecular weight
μg	Microgram
μL	Microliter
μm	Micromolar
NCs	Nanocrystals
NHS	N-hydroxysuccinimide
nm	Nanometer
nmol	Nanomole
NPs	Nanoparticles
NTA	Nitrilotriacetic acid
PAGE	Polyacrylamide Gel Electrophoresis
PBS	Phosphate-buffered saline
PEG	polyethylene glycol
PEG-PE	Poly (ethylene glycol) Phosphatidylethanolamine
pmol	Picomole
PMB	Polymyxin B
QDs	Quantum dots
QY	Quantum Yield
RNA	Ribonucleic acid
RNase	Ribunuclease
RT	Room Temperature
SDS	Sodium Dodecyl Sulfate

SMCC	Sulfosuccinimidyl-4-(*N*-maleimmidomethyl)cyclohexane-1-carboxylate
SPR	Surface Plasmon esonance
TBP	Tri-butyl phosphine
TEM	Transmission Electron Microscopy
TEMED	N, N, N', N'-Tetramethylethylenediamine
(TMS)2S	bis(Trimethylsilyl) Sulfide
TOP	Tri-octyl phosphine
TOPO	Tri-octyl phosphine oxide
TNF_{α}	Tumour Necrosis Factor-α
UV	Ultraviolet
U-GST	Untagged Glutathione-S-Transferases
Vis	Visible Wavelengths
XPS	X-ray photoelectron spectroscopy

Contents

Chapter 2

Chapter 3

1.1 Nanotechnology

Nanotechnology (from the Latin *nanus* and Greek *nanos* for dwarf) is the science which deals with materials having dimensions between 0.1-100 nm (1 nm = 10^{-9} m) (Figure 1.1). These materials are called nanomaterials. Nanotechnology is a fast growing field which uses the knowledge of various fields like materials science, interface and colloid science, supramolecular chemistry, chemical engineering and biological engineering.[1] In 1965 Nobel laureate Richard Feynman said "There is plenty of room at the bottom". His vision has been proven correct by the unprecedented growth of nanotechnology during last decade or so.[2]

An important feature of nanomaterials is that they exhibit properties which are different from those of small molecules and bulk materials, as will be illustrated below with representative examples.[3]

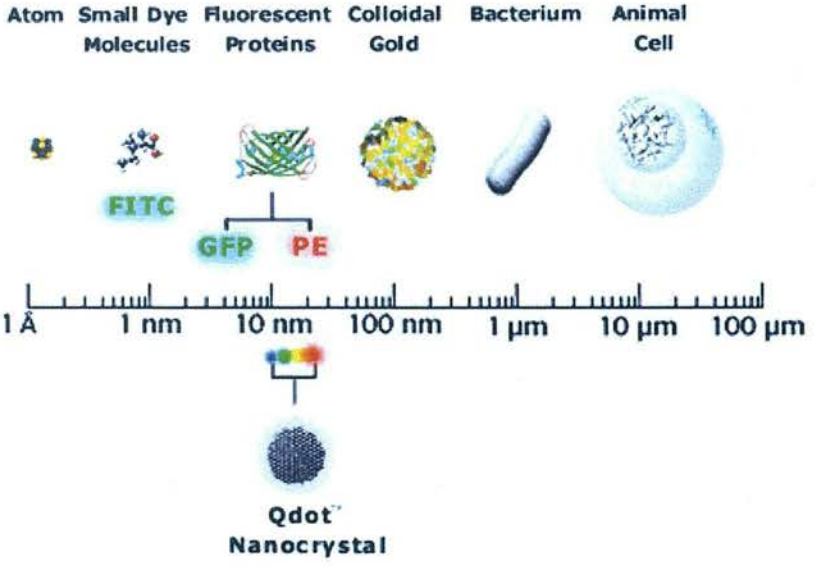

Figure 1.1 Nanometre-Sized Comparison *(taken from Rosenthal et al.[3])*.

1.2 Colloidal Nanoparticles

1.2.1 Colloids

The term *colloid* is originated from the greek word 'kolla' for glu. Colloids are biphasic mixtures which contain a dispersed phase (or discontinuous phase) dispensed uniformly in a finely divided state in a dispersion medium (or continuous phase). In colloidal systems the dispersed phase lies in the 1-100 nm range, and therefore they are an important class of nanomaterials. Colloidal systems, like other nanomaterials, have high surface-to-volume

ratios and this is important for many applications. When a beam of light is allowed to pass through a colloidal dispersion, the path of light gets illuminated. This phenomenon was observed by John Tyndall in 19th century and so called the "Tyndall effect". Colloids and colloidal nanoparticles have been important for many centuries. Alchemists used two important forms of colloidal gold, namely potable gold and Purple of Cassius, for making ruby glass. In 1856 Michael Faraday prepared and studied the first colloidal gold by reducing an aqueous solution of gold chloride with phosphorus to form a ruby coloured liquid. Some common examples of colloids are milk, fogs, smoke, hair sprays, pigmented ink and blood (Table 1.1)[4]

Dispersed Phase	Dispersed Medium	Name	Examples
Liquid	Gas	Liquid aerosol	Fog , sprays
Solid	Gas	Solid aerosol	Smoke, dust
Gas	Liquid	Foam	Foams
Liquid	Liquid	Emulsion	Milk , mayonnaise
Solid	Liquid	'Sol' or colloidal solution Paste at high concentration	Au sol, Ag sol Toothpaste
Gas	Solid	Solid foam	Expanded polystyrene
Liquid	Solid	Solid emulsion	Opal , pearl
Solid	Solid	Solid suspension	Pigmented plastics

Table 1.1 Classification of colloidal systems

1.2.2 Classification and applications of colloidal nanoparticles

Colloidal nanoparticles can be classified on the basis of the type of material they are made of into organic and inorganic nanoparticles. Various other criteria are used to characterize these systems including particle size, polydispersity, colloidal stability and surface charge density.[5] Nanoparticles are also widely used in biology and medicine due to their unique size dependent properties. A nanoparticle having various functional groups can be used for targeting specific receptors and cells. Paul Erlich proposed this concept at the beginning of the 20th century and it was called 'magic bullet'.[6] Inorganic nanoparticles made of gold, silver, iron and platinum are used for a variety of purposes including biomolecular recognition,[7] delivery,[8] sensing,[9] tissue engineering, [10] MRI contrast imaging.[11] Noble metal (e.g. gold and silver) nanoparticles demonstrate surface plasmon resonance (SPR). In SPR the surface of these metals is exposed to electromagnetic radiation. The free electrons in the metal (d electrons in silver and gold) are polarized to one surface by the incident light and oscillate in resonance with the radiation frequency forming a standing oscillation (Figure

1.2). For instance, this oscillation results into a characteristic absorption peak at 520 nm for gold nanoparticles. Molecules which are bonded to the metal can cause a change in the electron density on the nanoparticle surface leading to shifts in the SPR absorption maximum.[12]

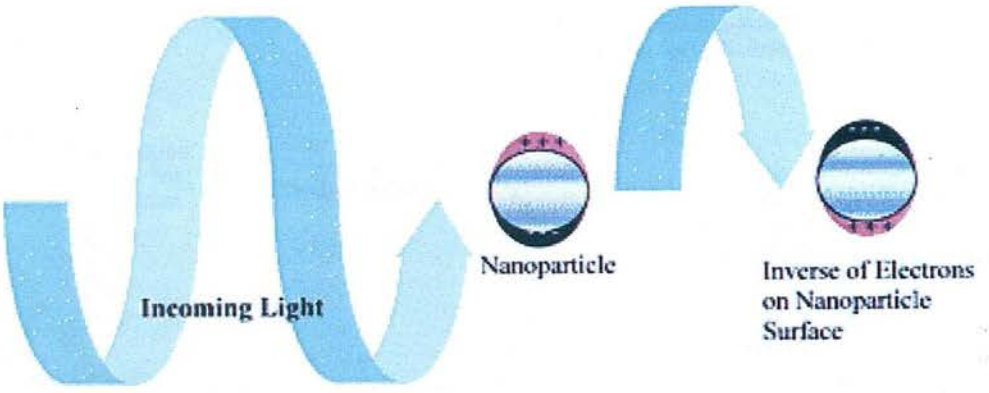

Figure 1.2 Origin of surface plasmon resonance due to coherent interaction of the electrons in the conduction band with light *(taken from Eustis et al.[12])*.

Thus, gold and silver nanoparticles are widely used for detecting biomolecules in DNA analysis,[13] immunoassays[14] and bioimaging applications[15] (Table 1.2). Non-noble metal nanoparticles like iron nanoparticles are widely used in protein purification, separation and concentration. Their magnetic properties make their isolation very easy after binding to proteins.[16]

In some cases more than one type of metal nanoparticle is used in the same experiment because they bring complementary features. For example, in a recent study magnetic microparticles (MMPs) were coated with a primary antibody targeting a specific antigen like prostate specific antigen (PSA). Gold nanoparticles were immobilized with a secondary antibody for PSA, and through a sense strand to multiple short DNA duplexes that are unique to PSA. After MMPs with the primary antibody react with antigen and subsequently with the gold nanoparticles having secondary antibody, they can be easily separated from unbound species taking advantage of the magnetic properties of the MMPs. The antisense strand can be released from the MMP-nanoparticle assembly by heating and the amount of oligonucleotide can be determined by using a DNA microarray (Figure 1.3). Because the mixed nanoparticle assembly carries many copies of DNA per protein binding event, the signal is significantly amplified and PSA could be detected at 30 aM (10^{-18} M) concentration by using this method.[17]

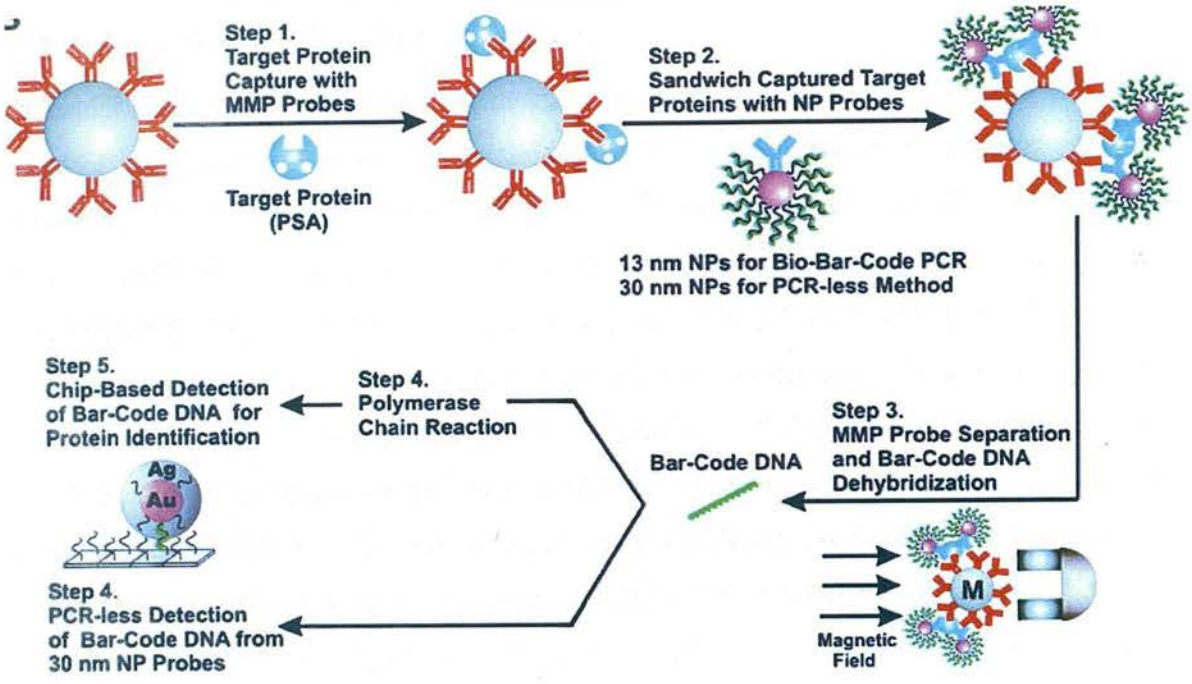

Figure 1.3 The bio–barcode assay method *(taken from Nam et al.[17])*.

Name of particle	Size Domain	Example of applications
Inorganic nanoparticles		
1.Gold nanoparticles	10-30 nm	Colorimetric detection of DNA sequences
2. Silver nanoparticles	2-10 nm	Protein purification
3. Iron nanoparticles	2-10 nm	Medical imaging
4. Platinum nanoparticles	2-10 nm	Labels for chip-based DNA detection
5.QDs	2-10 nm	Detection and quantification of biological molecules
Organic nanoparticles		
1. Carbon nanotubes and fullerenes	A few nanometers	DNA targeting
2. Dendrimers	10–50 nm	DNA chips
3. Polyelectrolyte (complexes natural and synthetic polymers)	50-200 nm	Drug targeting, Vaccination
4. Self-assemblies of polyethylene oxide block copolymers	50-200	Stealth drug delivery systems
5. Latexes	20–1000 nm	Solid-phase assays, vaccination, two dimensional arrays

Table 1.2 Various colloidal nanoparticles with applications.

1.2.3 Synthesis of colloidal nanoparticles

Colloidal systems are commonly synthesized by precipitation,[5,18] polymerization[5,19] and self assembly processes.[5,20] Inorganic particles like those made of gold or silver are typically prepared by a precipitation process (Figure 1.4) involving three steps. In the first step metal ions are reduced to metal atoms. In the second step these metal atoms aggregate forming a small nuclei having diameter of less than 1 nm. In last step further growth of the nanoparticle takes place by the deposition of atoms or microclusters on the newly formed nuclei. Usually a water-soluble polymer (e.g. poly(N-vinyl-2-pyrrolidine, PVP) is added to stabilise the final metal nanoparticles (Figure 1.4).[5] Semiconductor nanoparticles, which are the focus of this thesis work, can also be prepared adopting the precipitation method (see below). In contrast, organic nanoparticles are most commonly made by the polymerization method. For example by polymerization of an organic monomer dispersed in aqueous phase in the presence of an emulsifying agent after the addition of a radical initiator (Figure 1.5).[19]

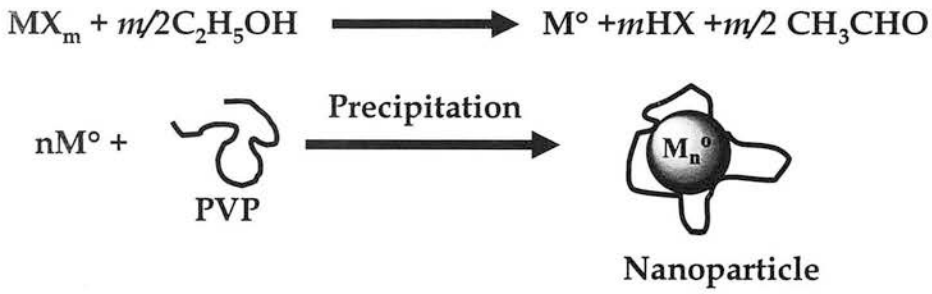

Figure 1.4 Formation of a metal nanoparticle by reduction with an alcohol of metals salts in the presence of of poly(*N*-vinyl-2-pyrrolidone)(PVP) as stabilizer.

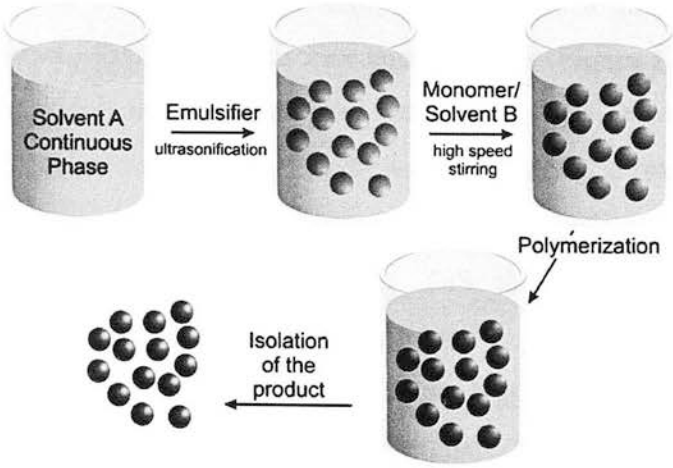

Figure 1.5 Polymerization of olefins in a perfluoralkane/alkane mixture *(taken from Larpent et al.[19])*.

Preparation of colloidal nanoparticles via self-assembly is mostly done by processes which involve micelles. Micelles are formed when the surfactant concentration exceeds the critical

micelle concentration (CMC) in water. In normal micelles, the hydrophobic hydrocarbon chains of surfactants are directed towards the interior of the micelle and the hydrophilic groups are pointing outwards to interact with the aqueous medium surrounding the micelle (Figure 1.6). This method can be applied to prepare stable and biocompatible semiconductor nanoparticles (see below). In reverse micelles, hydrophilic groups are oriented towards the core of micelle and hydrophobic groups are terminated outwards (Figure 1.6). [20]

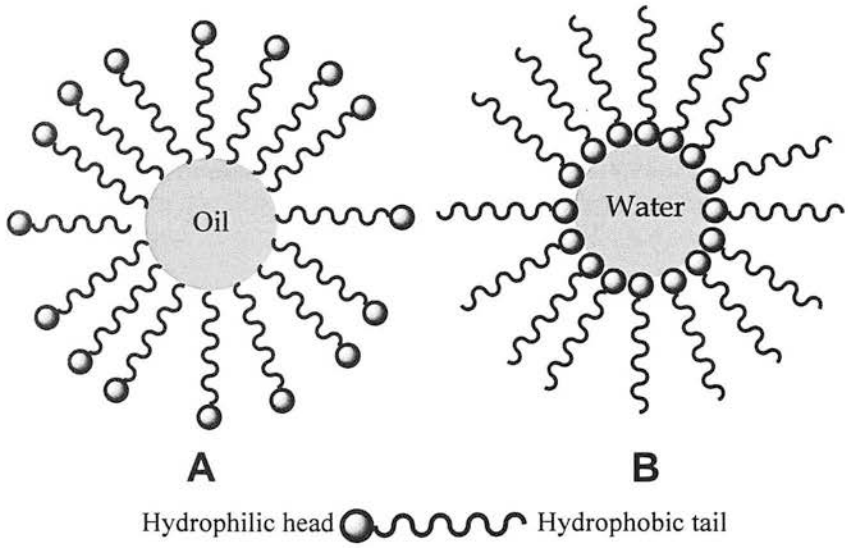

Figure 1.6 Architecture of (A) normal and (B) reverse micelles.

1.3 Quantum Dots (QDs)

QDs are nanocrystals of semiconductor materials with a size range of 1-10 nm, and therefore they contain from several hundreds to a few thousand atoms. QDs are sometimes referred to as 'artificial atoms' because like an atom or a discrete molecule (and unlike bulk semiconductors) they have discrete energy levels (Figure 1.8).[21]

The most widely used QDs are made of group II-VI elements i.e., cadmium sulphide (CdS), [22] cadmium selenide (CdSe), [22] cadmium telluride (CdTe), [22] zinc selenide (ZnSe), [23] and mercury telluride (HgTe).[24] Sometimes these semiconductor cores are also coated with another semiconductor material (e.g. ZnS shells for CdSe cores) for protecting against oxidation and degradation, improving emission properties etc. of the QD.[25] These are referred to as core/shell QDs. In this thesis, the work is focussed on CdSe/ZnS (core/shell) QDs. The surface of QDs is also coated with organic ligands which further tune the physical and chemical properties of the QD (Figure 1.7).[26]

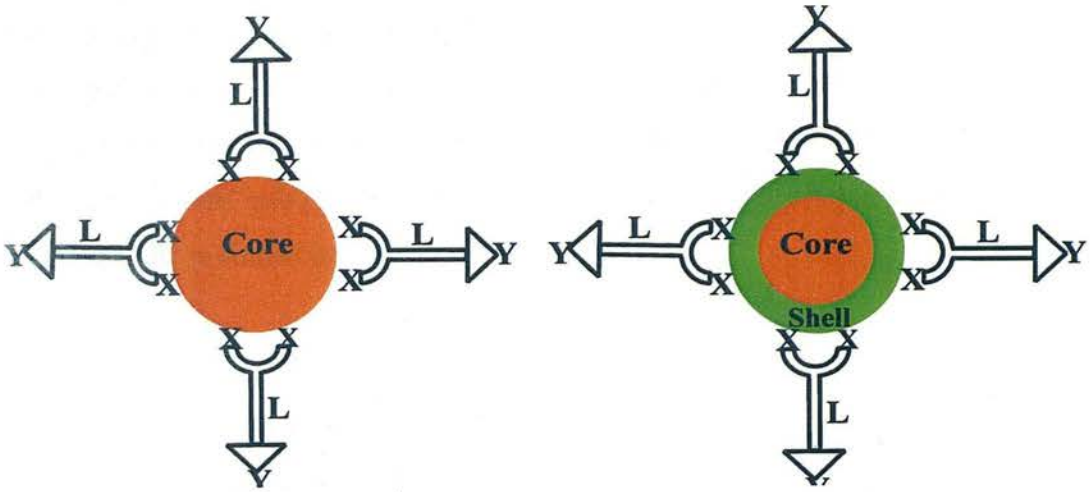

Figure 1.7 Quantum dots composition core and core/shell (X represents the groups attached to QD surface, L represents the linker and Y represents groups for functionalization).

1.3.1 Optical properties of QDs

There are significant differences between the electronic and optical properties of QDs and bulk semiconductors which make these materials of considerable current interest. In a bulk semiconductor the energy levels in the valence and conduction bands are continuous whereas in QDs energy levels are discrete (Figure 1.8). When an electron jumps from the valence band to the conduction band it forms a hole in the valance band and the hole-electron pair is called an *exciton*. The distance between hole and electron is called the exciton Bohr radius[27] and varies from material to material.[28] When the radius of the semiconductor crystal becomes smaller than the exciton Bohr radius then the density of states becomes more like that found in discrete atoms.[29] This causes the band gap energy to increase and depend upon the size of the nanocrystal.

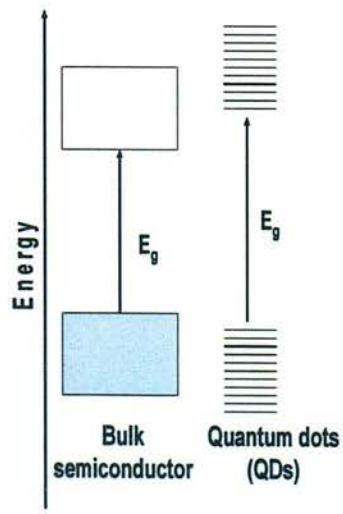

Figure 1.8 Energy level diagram for semiconductors and QDs.

Thus, for exciting an electron in a QD, the energy required is always higher than the band gap energy for the bulk material (E_g) (Figure 1.8). As a result the absorption spectrum of QDs reflects atomic-like transitions of which the so-called 'first absoption peak' or first 'excitonic peak' is the lowest energy required to excite an electron.[30,31] A typical absorption spectrum for a CdSe QD is shown in Figure 1.5.

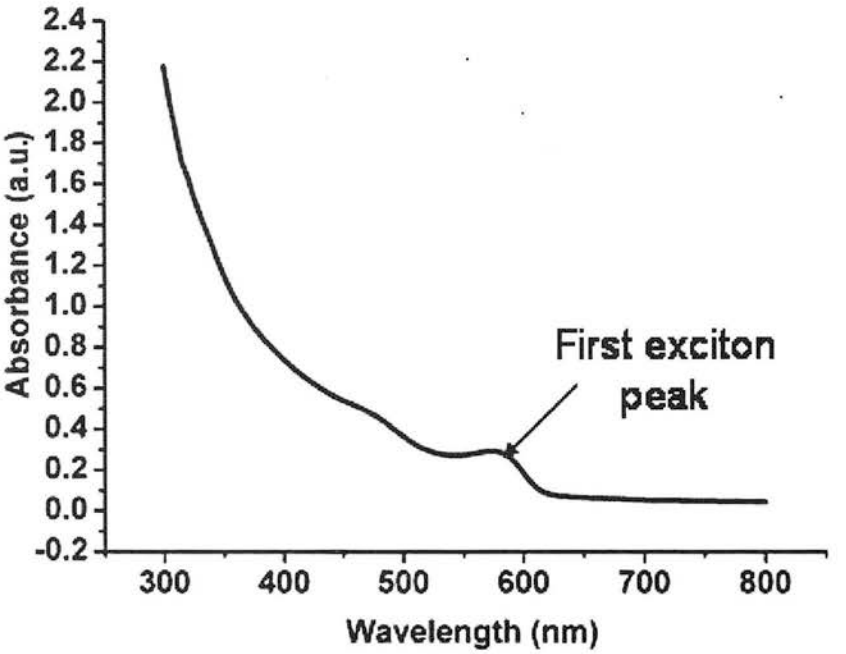

Figure 1.9 Absorption spectrum of a CdSe QD.

The position of this peak for QDs of the same semiconductor material will be different for different sizes. This is because the electrons behave like 'particles in a 3D box'.
For a particle in a 1D box the particle energy is proportional to the dimension of the box ($1/d^2$) as follows

$E_{well,1d} = 1/8\ h^2/md^2$ (where h = Plank's constant , m = free electron mass and d = width of well)

For a QD the box is a sphere and the lowest energy level is then

$E_{well,3d(sphere)} = 1/2\ h^2/md^2$

The minimum energy E_g required for creating an electron-hole pair in a QD is made up of several contributions.

The first contribution is the band gap energy for the bulk material $E_{g(bulk)}$. Another important contribution comes from the confinement energy which is

$E_{well} = E_{well}(E^-) + E_{well}(h^+) = h^2/2m^*d^2$ (1) (E^- represents the electron, h^+ represents the hole; m^* is the reduced mass of exciton). In this expression m^* is given by

$1/m^* = 1/m_e + 1/m_h$ (where m_e = effective mass of electron and m_h = effective mass of hole)

For a large particle (bulk: $d \rightarrow \infty$) so this energy tends to become zero.
For calculating the energy required to create an electron-hole pair a Coulombic interaction terms (E_{coul}) has to be considered. This Coulomb interaction is based on the attraction between the electron and the hole multiplied by a screening coefficient which depends on the dielectric constant of the semiconductor ε and dielectric constant of vacuum ε_o. Because d is small for a QD then this term can also be significant.

$E_{coul} = -1.8\ e^2/2\pi\varepsilon\varepsilon_o d$ (2)

Thus, estimating the size-dependent energy gap of a spherical shape QD can be done by using following equation.

$E_g(dot) = E_g\ (bulk) + E_{Well} + E_{Coul}$ (3)

So by inserting equation (1) and (2) into expression (3) we get

$E_g(dot) = E_g\ (bulk) + h^2/2m^*d^2 - 1.8\ e^2/2\pi\varepsilon\varepsilon_o d$

So the band gap for QDs depends upon two size dependent terms: the confinement energy which changes as a function of $1/d^2$ and the Coulomb attraction which changes as a function of 1/d. Thus, quantum confinement becomes very important in small QDs.[32]

When the hole and electron recombine, it results into emission of light by fluorescence,[33] which therefore is also size-dependent. As the size of the QD decreases the band gap increases and the fluorescence emission shifts towards the red (Figure 1.10).

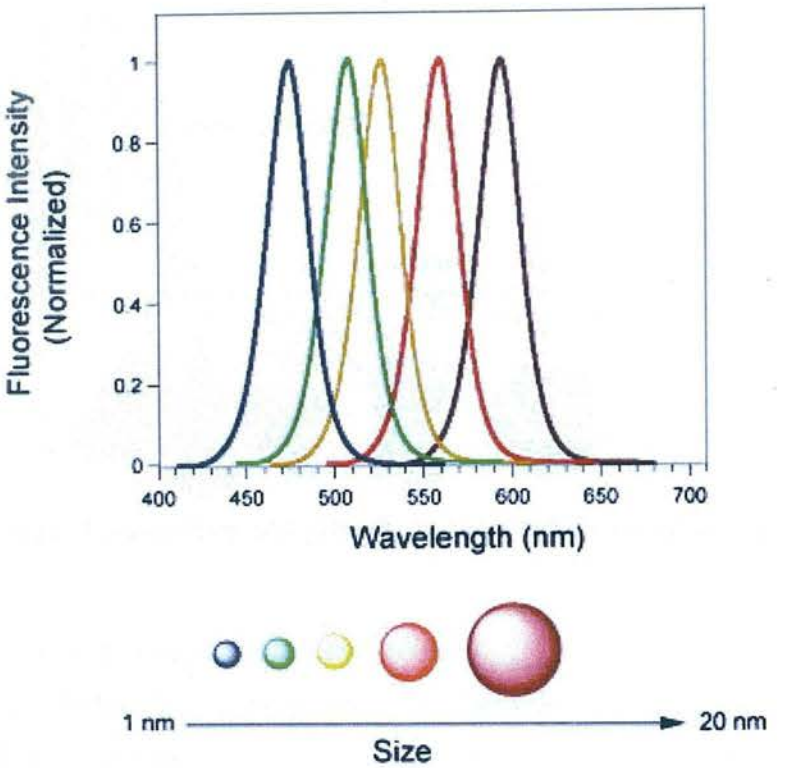

Figure 1.10 Emission spectra of different size CdSe nanoparticles (*taken from Zhou et al.*[34]).

1.3.2 Synthesis of QDs

Because QDs are nanocrystalline materials, their formation involves a nucleation and crystal growth process. In 1950 LaMer and Dinegar proposed that the formation of colloids of sulphur occurs by a nucleation process which depends on the concentration of precursor, and that is followed by incorporation of the remaining precursors in solution to these initially formed nuclei.[35] In this model, when the solution is supersaturated and reaches a critical threshold then nucleation starts, causing a drop in the concentration. The nucleation process stops once this drop in concentration reaches a critical threshold value, at which point the nuclei formed grow.[35] QD synthesis employs the same principle but at higher temperatures.

Synthesis of QDs is commonly done by the hot-injection method. As the name suggests in this method nucleation and growth of particles is achieved by rapid injection of reagent into hot solvent, which quickly increases the precursor concentration in the reaction mixture above the nucleation threshold. This starts the nucleation process which can be quenched by fast cooling after achieving the desired QD size (Figure 1.11).[36]

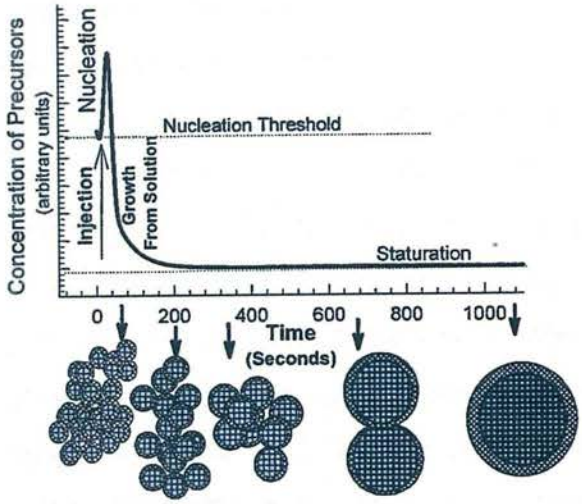

Figure 1.11 Stages of nucleation and growth for the preparation of QDs *(taken from Murray et al.[35b])*.

1.3.2.1 CdSe core (nanoparticle) synthesis

One of the first colloidal QDs were produced by Ramsden and Graztzel[37] by adding H_2S to an aqueous solution of $Cd(NO_3)_2$ or by rapid mixing of Na_2S and $Cd(NO_3)_2$. They reported luminescence data and transmission electron microscopy (TEM) images of the particles formed. In 1985 Nozik *et al.*[38] found that size quantization has a very significant effect on the optical properties of CdS and PbS colloidal properties.Two years later Henglein developed further the synthesis and properties of CdS nanoparticles by first precipitating Cd^{2+} ions with stoichiometric amounts of H_2S (injected in) followed by the addition of NaOH and excess Cd^{2+} ions. In this synthesis the creation of a shell of the large band gap material $Cd(OH)_2$ on the surface of CdS nanoparticle act as fluorescence activator. This provides an electronic barrier at the surface of the nanoparticles, which prevents the charge carrier from escaping the core.[39] In 1988 Streigerwald and Brus demonstrated that IR, NMR and X-ray photoelectron spectroscopies, in conjunction with scanning and high resolution electron microscopy can be used to characterise QDs,[40] which was an extraordinary advance in terms of particle characterization.

Murray *et al.*[41] reported the first synthesis of CdSe nanoparticles using organometallic compounds,[42-44] and found that these are excellent precursors in QD synthesis. The method is based on the pyrolysis of organometallic reagents like dimethyl cadmium and bis(trimethylsilyl) selenium by injection into hot coordinating solvents like tri-*n*-octylphosphine oxide (TOPO) and tri-*n*-octylphosphine (TOP). In this method, the coordinating solvent provides temporary discrete nucleation and permits controlled growth of nanocrystals. The reaction involves combining the appropriate metallic or organometallic

precursors (zinc, cadmium or mercury species) with the corresponding chalcogen precursors (sulphur, selenium or tellurium species) in a coordinating solvent at high temperature. Preferably TOPO is used due to its surfactant properties. Sometimes TOPO is used in combination with other surfactants or co-solvents such as TOP, TBP, hexadecylamine or stearic acid. In these reaction conditions, particle nucleation takes place in a very short time span, and is followed by epitaxial growth and nanocrystal annealing at slightly lower temperature.[45] Epitaxial growth reaches a point where the size distribution is narrow. The larger particles grow from the smaller more soluble particles (Figure 1.11).[46] This point is also called the bright point because from this point photoluminescence efficiency decreases.[47] At this point the reaction is quenched by lowering the temperature. This is the most reliable and reproducible procedure for the synthesis of high-quality QDs.[48] Nanoparticle size and growth can be manipulated to a certain extent by controlling the initial precursor concentration, temperature and length of growth period. This method yields samples with narrow distributions (<5% rms in diameter) having uniform size, shape and surface passivation. This method has been applied to QDs with CdS, CdSe and CdTe cores, leading to nanocrystals with sharp absorption and emission features at room temperature, and ~10-times brighter fluorescence than Rhodamine 640.[41, 48]

Peng *et al.*[49] have developed a new approach for the synthesis of CdS and CdSe nanoparticles which involves the reaction of CdO as cadmium precursor and hexylphosphonic acid or tetradecylphosphonic acid as ligands. This was the first study in which non-pyrophoric precursors are used, making QD synthesis safer and less expensive. This new synthetic procedure works significantly better than the previous synthesis based on the use of dimethyl cadmium as a cadmium source. Moroever, this approach for synthesizing high-quality semiconductor nanocrystals works under mild conditions and is simple, making it well suited for bulk nanoparticle synthesis.

All these methods are based on the hot-injection technique. However, an alternative QD synthetic procedure involves mixing precursors at room temperature and subsequent heating to a certain temperature to initiate nucleation; this method is called the heating-up method. In 2005 Cao's[50] group synthesised CdSe QDs without using phosphine ligands using the heating-up method. Phosphine ligands are air, moisture-sensitive and costly compounds. They used cadmium myristate as a cadmium precursor because myristate decomposes above 226 °C. Elemental selenium was used with octadecene (a non-coordinating solven) for the CdSe core synthesis because octadecene dissolves selenium above 190 °C. Thus, the

formation of CdSe is possible at a temperature of ~ 240 °C. Nowadays octadecene is widely used in QD synthesis because of its physical properties (liquid at room temperature), lower price and environmentally friendly nature.

1.3.2.2 Shell Growth

It was found that defects on QD particle surfaces and poor surface passivation can reduce the fluorescence quantum yields. For improving the quantum yield of these materials the semiconductor core can be capped with a wider band gap inorganic layer. The main advantage of capping the core is that the exciton photogenerated in the core is protected from the environment, preventing non-radiative recombination pathways. These QDs are often referred to as core/shell QDs.[25]

Bawendi *et al.*[25] and Hines *et al.*[51] synthesized the first prototype of core/shell QD. ZnS-capped CdSe QDs were prepared by using organometallic reagents in a two-step single-flask method (Figure 1.12). In this method, purified CdSe nanoparticles are suspended in coordination solvent. The capping material, usually diethyl zinc and hexamethyl disilathiane dissolved in TOP are then slowly added at elevated temperature (Figure 1.8). The temperature chosen for this addition is very important. It should be high enough to favour epitaxial crystalline growth but low enough to prevent nucleation of ZnS crystal and Ostwald ripening of CdSe core. Thus, the shell growth temperature is around 160-220°C. ZnS capping increases the particle size of QDs, resulting in a red shift of the photoluminescence wavelength. At the same time Danek *et al.*[52] provided another example of a core/shell QD by passivating CdSe nanocrystals electronically and chemically with a ZnSe. Some typical examples of core/shell QDs include CdS shell on CdSe core,[25] ZnS shell on CdSe core,[25] ZnS shell on CdS core,[53] and CdS shell on CdSe core.[54]

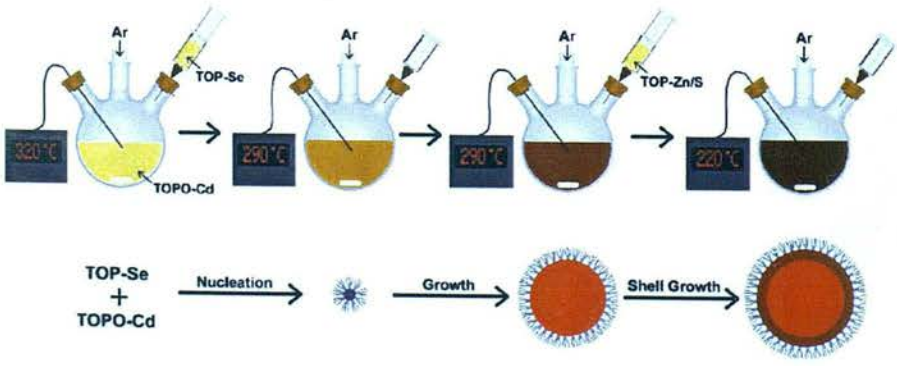

Figure 1.12 Scheme for making CdSe/ZnS QDs *(taken form Bailey et al.[55])*.

Recently Zhu *et al.*[56] developed a phosphine-free synthesis of CdSe/ZnS (core /shell) QDs. They reported a simple method for making QDs by using cadmium stearate, oleylamine, paraffin liquid, zinc acetate dihydrate and sulphur powder. The shell of ZnS was grown over the CdSe core by using the seeding growth technique. In this technique first the shell was made by mixing Zn and S precursors in the CdSe core reaction mixture. This growth cycle was repeated many times for yielding desirable size core/shell QDs.

1.3.3 Water Solubilization of QDs

QDs are generally synthesised using organic solvents thus they are hydrophobic in nature. This makes them unsuitable for biological applications. It is therefore important to make them hydrophilic. There are three main approaches to prepare water-soluble QDs: 1) hydrophobic ligands on QDs surface are replaced by bifunctional hydrophilic ligands, 2) hydrophobic QDs can be encapsulated in amphiphilic polymers by using hydrophobic-hydrophobic interactions to provide water-soluble QDs and 3) hydrophobic QDs can be encapsulated in a silica shell which imparts protection from the environment and water solubility.

1.3.3.1 Ligand Exchange

QDs synthesised in organic solvents have TOP, TOPO,[41,57] tetradecylphosphonic acids[57] or oleic acid[50] on the surface. These hydrophobic ligands can be replaced by water-soluble bifunctional ligands (Figure 1.13). In these ligands one end binds to the QD surface, and the other, has functional groups free for reaction with biomolecules and to confer water solubility.[57] Typical biofunctional ligands are mercaptocarbonic acids,[58] 2-aminoethanethiol,[59] dithiothreitol,[60] dihydrolipoic acid,[61] oligomeric phosphines,[62] peptides[63] and dendrons.[64]

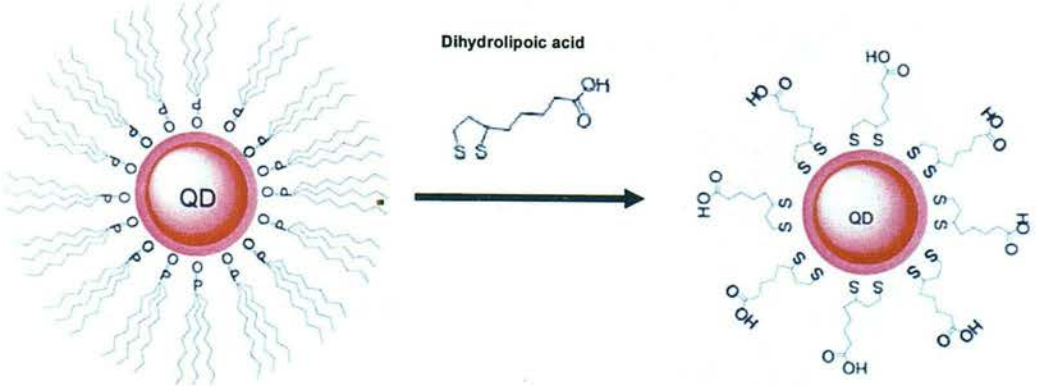

Figure 1.13 Water solubilization strategies for hydrophobic QDs by ligand exchange using dihydrolipoic acid *(taken from Zhou et al.[34])*.

1.3.3.2 Encapsulation by amphiphilic polymers

Phospholipids like 1,2-dipalmitoyl-sn-glycero-3-phosphoethanolamine-n-[methoxy (polyethylene glycol)] and 1,2-dipalmitoyl-sn-glycero-3-phosphocholine have both hydrophobic and hydrophilic moieties. The hydrophobic ends form a core inside which QDs can be encapsulated by forming oil-in-water micelles through hydrophobic interactions (Figure 1.14). These micelles provide aqueous solubility via the hydrophilic exterior ends of the phospholipids.[65,66,67] In another interesting approach polyacrylic acids were partially cross-linked with octylamine using 1-ethyl-3-[3-dimethylaminopropyl]carbodiimide (EDC). This makes them amphiphilic and capable of forming micelle-like structures with carboxylic acid groups pointing outwards which encapsulate QDs in the core.[68] Incorporation of polyethylene glycol (PEG) in the surface of QDs is useful because of its low toxicity and because it allows the QD to have longer circulation times in biological environments than other water-soluble QDs.[48]

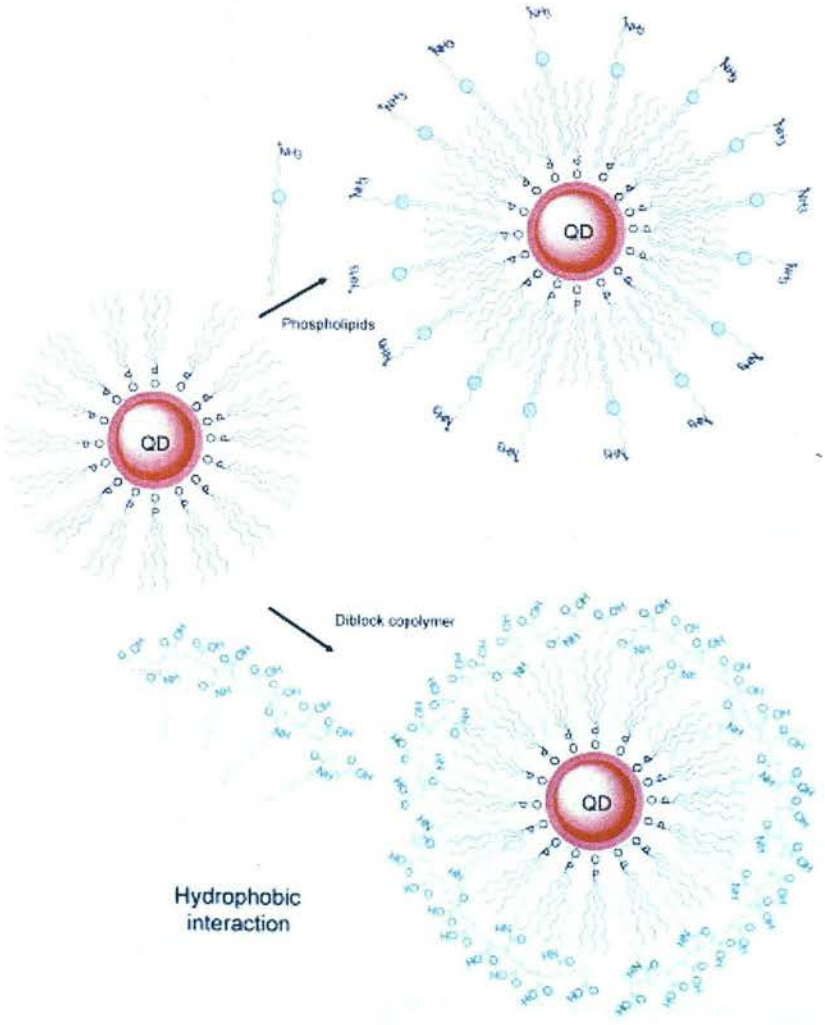

Figure 1.14 Encapsulation strategies for hydrophobic QDs nanoparticles *(taken from Zhou et al.[34]).*

1.3.3.3 Silica Encapsulation

QDs can also be encapsulated in silica for water solubilization.[69,70] In a typical procedure QDs are embedded in a siloxane shell and then functionalized with thiol and/or amine groups (Figure 1.15).[69] Introduction of these organosilicone molecules on the QD surface, however, typically causes a decrease in photoluminescence. But Selvan *et al.*[70] recently described a simple, yet effective strategy in which CdSe QDs were embedded in silica by using the reverse micro emulsion technique having a quantum yield of 20% in water (compared to 17% for typical hydrophobic CdSe/ZnS QDs). In general, SiO_2-coated QDs show less in-vitro cytotoxicity than other water soluble QDs (e.g. coated with mercaptoacetic acid).

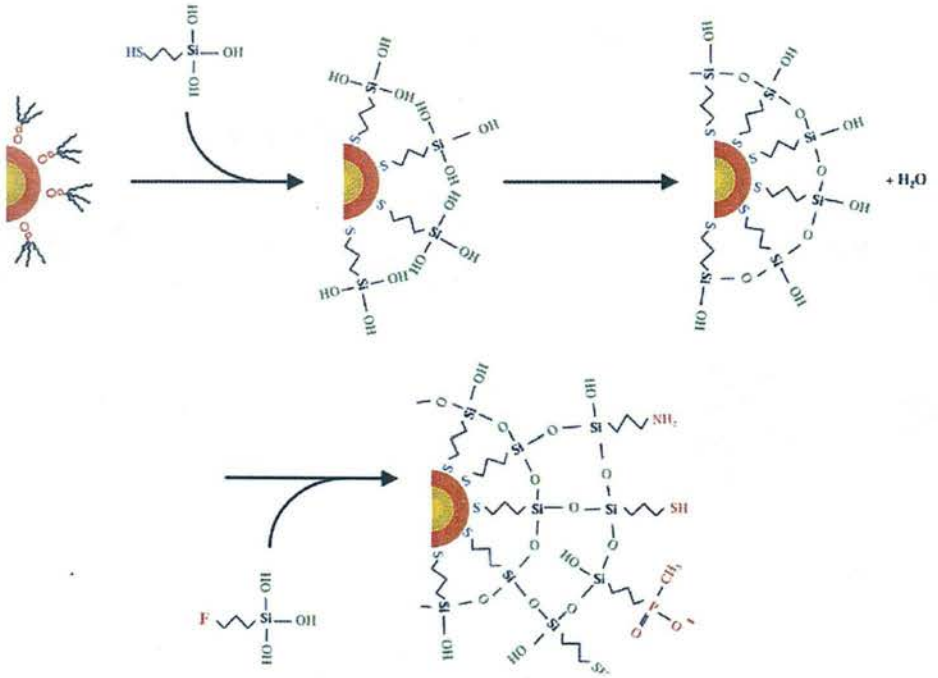

Figure 1.15 Scheme showing silanization method and subsequent functionalization with F = amine, thiol, phosphate etc. *(taken from Gerion et al.[69]).*

1.3.4 Bioconjugation to QDs

For biological applications QDs are conjugated to various biomolecules. It is very important that the activity of conjugated biomolecules is retained so that they can be used further in various biological applications. There are two strategies for attaching biomolecules on QDs: using covalent and noncovalent linkages.

1.3.4.1 Covalent attachment

There are two common covalent linkage strategies for cross linking biomolecules on QDs. These strategies are carbodiimide-mediated amide formation (using EDC)[58] and active ester maleimide-mediated amine and sulfhydryl coupling[71] (using sulfosuccinimidyl 4-[*N*-

maleimidomethyl] cyclohexane-1-carboxylate (sulfo-SMCC)) (Figure 1.16 and 1.17). There is an advantage in using the carboxylate-amine condensation method in that most proteins contain primary amines and carboxylic groups which can be used for carbodiimide-mediated amide formation. The disadvantage is that it does not provide control over the site of attachment. Free sulfhydryl groups are rarely found in proteins and they are usually unstable in presence of oxygen. This makes this approach less widely applicable but it provides better site-specificity than amide bond formation.

Chan *et al.*[58] used carbodiimide coupling chemistry to link transferrin and immunoglobulin G (IgG) to mercaptoacetic acid coated QDs (CdSe/ZnS), and these proteins were able to still bind to their appropriate biological partners.

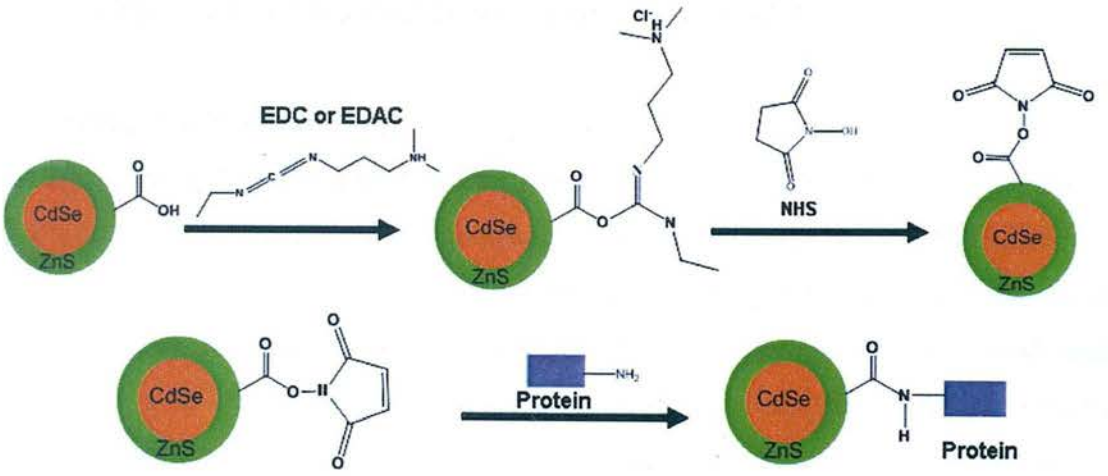

Figure 1.16 Covalent coupling between carboxylic acid (-COOH) coated QDs and primary amines (-NH_2) on proteins.

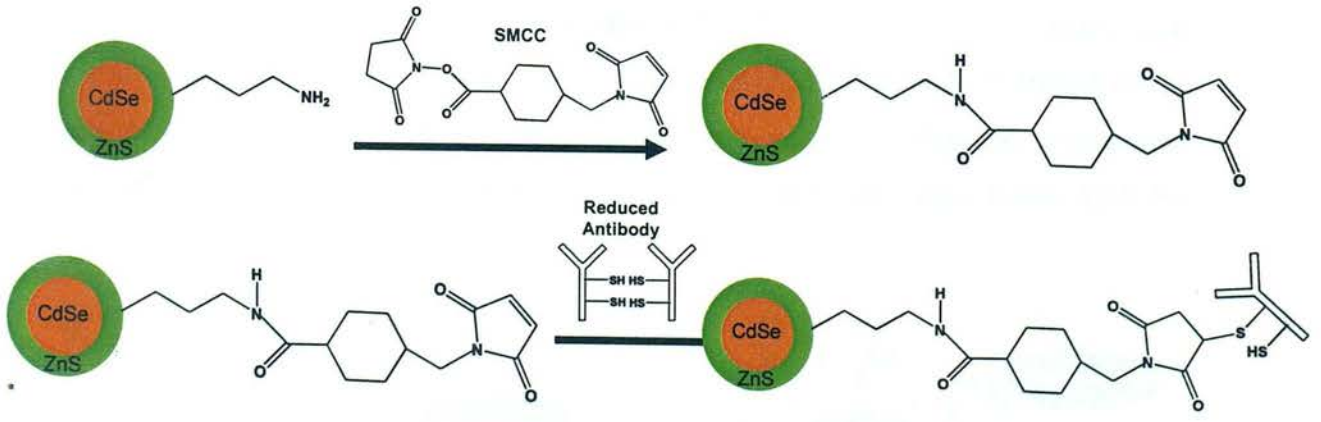

Figure 1.17 QD conjugation to antibody fragments via disulphide reduction and sulfhydryl-amine coupling.

Pathak *et al.*[60] prepared water-soluble QDs by coating them with dithiothreitol. These hydroxyl-terminated QDs were then coupled with different oligonucleotide sequences via a

carbamate linkage. This linkage led to conjugates that were stable for months and have high aqueous solubility. Further these QDs-oligonucleotide conjugates were used in detection of chromosome abnormalities or mutations by using fluorescence in situ hybridization (FISH) procedures.

Pellegrino and coworkers[72] used QDs coated with a preactivated amphiphilic polymer containing multiple anhydride units which are highly reactive towards primary amines, allowing attachment of proteins via the formation of peptide bond linkages. This method can be very useful for making biodegradable drug delivery systems.[40]

Mitchell *et al.*[73] used 3-mercaptopropionic acids to passivate the QD surface so that it can easily displaced by alkyl thiol-capped oligonucleotides. This was the first attempt where nanoaparticle were modified successfully with single stranded DNA.

1.3.4.2 Noncovalent attachment

Electrostatic interactions, biotin-streptavidin linkages and direct absorption of biomolecules on QD are three types of non-covalent linkage used for attaching biomolecules on QDs.

Electrostatic interactions are based on electrostatic attraction between QD and biomolecules (Figure 1.18). For example, Mattoussi and co-workers[74] conjugated lipoic acid-capped CdSe/ZnS QDs with a negatively charged surface to a recombinant protein having a maltose binding protein attached to a positively charged leucine zipper domain at the C-terminus. In another study, Dixit *et al.*[75] encapsulated QDs inside a viral capsid. This process is driven primarily by electrostatic interactions between negatively charge QDs and the positively charged internal compartment of the brome mosaic virus (BMV) capsid. In this study QDs were coated with four different types of ligands: lipids, DNA, DHLA and HS-PEG-COOH. Niemeyer *et al.*[76] used electrostatic interaction between positively charged cytochrome $P450_{BS\beta}$ and negatively charged mecaptoacetic acid coated CdS and CdSe QD for bioconjugation.

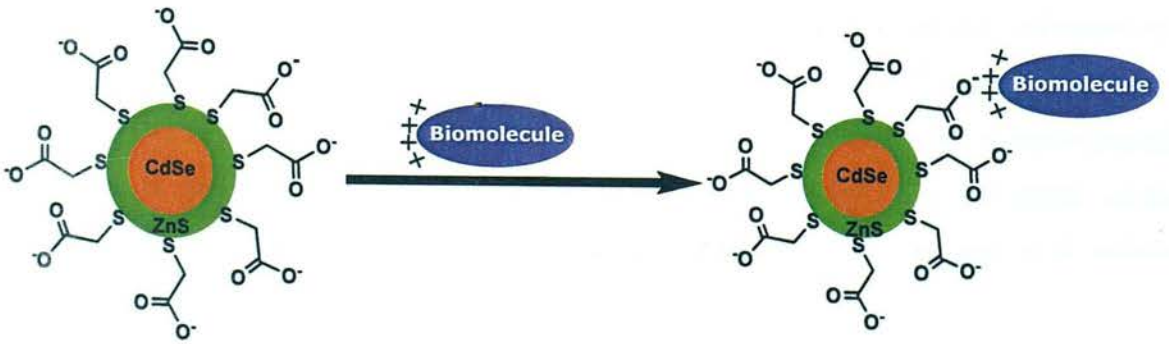

Figure 1.18 Scheme showing QD conjugation to biomolecule using electrostatic interaction.[74]

Mattoussi and co-workers[77] reported a new non-covalent coupling strategy for linking biomolecules on QDs. CdSe/ZnS core/shell QDs were attached to polyhistidine tagged proteins (Figure 1.19) exploiting the high binding affinity of histidine for the metal (Zn^{2+}) rich surface of the QD (CdSe/ZnS). In this way, several his-tagged peptides and proteins, including a maltose binding protein (MBP) were successfully attached to QDs.[78]

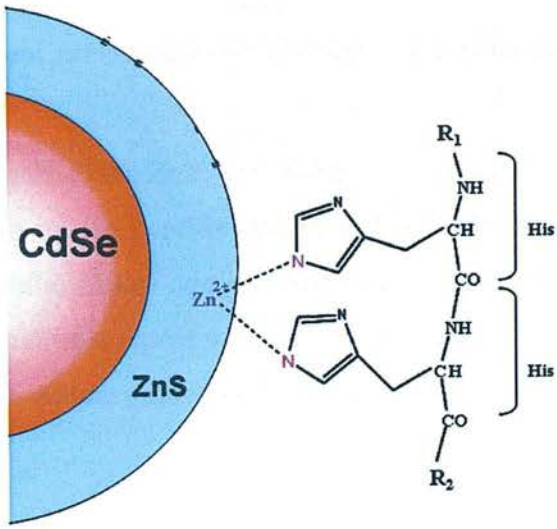

Figure 1.19 Scheme showing QD conjugation to biomolecule using coordination bonds *(taken from Sapsford et al.[77]).*

Streptavidin is a protein that has very high affinity for biotin ($K_d = 10^{-15}$ M) and therefore can be used for attaching QD-streptavidin conjugates to biotinylated biomolecules or vice-versa (Figure 1.20). In general, QDs are targeted to the protein of interest using biotin-streptavidin recognition using a three-layer strategy involving a primary antibody which binds to the target protein, a QD coated with streptavidin and biotinylated secondary antibody which binds the primary antibody and the QD.[79] Another approach used by Bruchez *et al.*[80] involved attaching covalently streptavidin to QDs and used these streptavidin-coated QDs to label F-actin filaments on fibroblasts by using biotinylated phalloidin, a molecule which specifically binds to filamentous F-actin but not to globular G-actins. This method was very effective and did not lead to non-specific binding to other parts of cells. Howarth *et al.*[81] used a streptavidin conjugated QD to specific proteins by tagging them with a 15-amino acid acceptor peptide (AP) which is specifically biotinylated by the *E. coli* enzyme BirA. The advantage of this approach is that it produces smaller conjugates and therefore interferes less with cellular events.

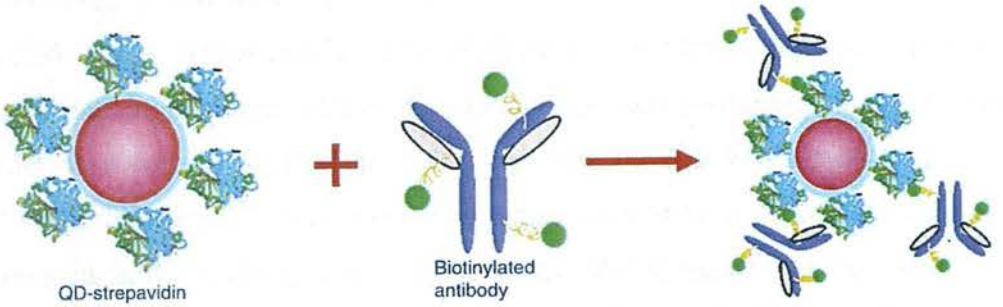

Figure 1.20 Noncovalent conjugation of streptavidin-coated QDs to biotinylated antibodies *(taken from Xing et al.[82])*.

In a different approach CdSe/ZnS semiconductor nanocrystals were immobilized with synthetic phytochelatin related peptide (Figure 1.21).[83] These synthetic phytochelatin-related peptides have hydrophilic linker domain made up of glutamic acid residues and adhesive domain composed of multiple repeat units of cysteines pairs. The adhesive domain is used for anchoring peptide on nanocrystals while aqueous solubility is provided by hydrophilic domain.

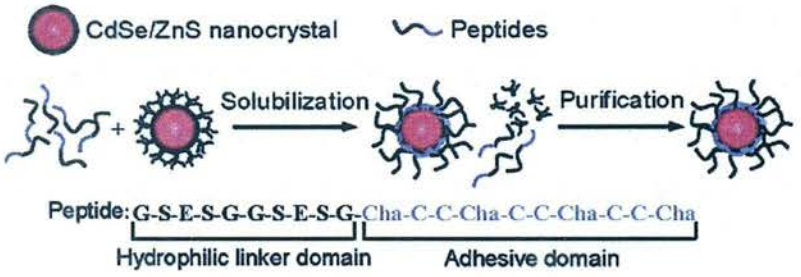

Figure 1.21 Schematic representation of the surface coating chemistry of CdSe/ZnS nanocrystals with phytochelatin-related α-peptides *(taken from Pinaud et al.[83])*.

1.4 Fluorescent tool box for biological labelling

Visualization, tracking and quantification of molecules and events in living cells with high accuracy and precision provide a platform to understand these complex systems. There are three types of tools which are widely used in fluorescence cell labelling: small organic dyes, fluorescent proteins, and since recently, QDs.[84] Small organic dyes have long history as a labelling agent in biology. Organic dyes commonly used in biology are fluoresceins, rhodamines, cyanine dyes and alexa dyes. There are some limitations with organic dyes like short Stokes shift, low photostability and high susceptibility for photobleaching. But their low cost, availability and easy to use property makes them very popular in cell labelling.[85] Fluorescent proteins are also popular for bioimaging applications. The first fluorescent

proteins used in cell labelling were phycobiliproteins and photosynthetic antenna pigments extracted from cyanobacteria. Phycobiliproteins contains multiple bilin chromophores encapsulated in a protein matrix for minimising self-quenching, making them two times brighter than organic dyes. But their large size (~ 200 kD) limits their usage in many labelling applications.[84] They are more often used with antibody conjugates for surface labelling in flow cytometry and enzyme linked immunoassays. A new era in cell labelling was started after the discovery and development of green fluorescent proteins (GFP).[85-87] GFP was first isolated from jelly fish Aequoera victora[86] and later it was cloned.[87] In 2008 the Noble prize for chemistry was awarded to Osamu Shimomura, Martin Chalfie and Roger Y. Tsien for the discovery and development of the GFP which shows the importance of these proteins in cell labelling. As the name suggests GFP emits green fluorescence under excitation by U.V. light. The chromophore which is responsible for absorbance and fluorescence of GFP is *p*-hydroxybenzylidene-imidazolidinone. Expression of green fluorescent protein fused to other proteins of interest is widely used in cell biology for studying their functions. But there are also some limitations in using GFP type proteins in labelling. They form aggregates inside the cells which causes toxicity. There are also some issues regarding their photostability as they photobleach upon extended excitation.[88] In recent years a new class of fluorophores which has shown great promise in cell labelling are QDs. QDs are ideal candidates for biological imaging because they have large extinction coefficients, large Stokes shifts, and high photostability.[85] QD having different emission profiles can be excited using a single exciting source; this is a very useful property as it gives an opportunity to use QDs of different colours in the same labelling experiment. But there are also some difficulties in using QD as biological labels. As their size increases after bioconjugation, it becomes more difficult for them to cross the cell membrane and they can also be cytotoxic.[89]

All these fluorophores have benefits as well as limitations which makes their use selective (some are better than others for specific applications) (Table 1.3).

Fluorophores for examination of	Small organic dyes (antibody-targeted)	QDs (antibody-targeted)	Fluorescent proteins
Endogenous proteins	++	+	-
Clinical specimens	++	+	-
Animals	Ex vivo	Ex vivo	Transgene live
Primary tissues	++	+	Transgene/virus
Live cells in culture	Surface	Surface	++
Multiple proteins at once	++	++	++
Dynamic interactions	+/-	+/-	++
Turnover/synthesis	-	-	+
Protein microarrays	++	+	-
In gel fluorescence	-	-	+
Western blot	-	+	-
Major advantages	Diversity of properties	Bright and photostable	Live cells and specificity
Major limitations	Targeting in live cells	Targeting and penetration	Ectopic expression
Improvements expected	Generic conjugated primary antibodies	Smaller, diversity of properties	Better properties, generic sensors

Table 1.3 Different types of flurophores for biological labelling[84]. Applicability ranges from most optimal (++) to generally not applicable (-), and (+/-) indicates applicable in some cases

1.5 Applications of QDs in Biological Imaging

1.5.1 Imaging of fixed cells and tissues

Imaging of fixed cells provides important data about the activities which are taking place within a cell or a heterogeneous cell population. QDs have been used in many fixed cell staining studies. For example, Bruchez *et al.*[80] labelled nuclear antigens and F-actin filaments using QDs of different colours in fixed mouse fibroblasts which were simultaneously excited with 363 nm light.

QDs are also used in fluorescence in situ hybridization (FISH) for mapping or detecting genomic sequences. FISH is a technique in which single stranded DNA, hybridized with targeted sequence(s) of complimentary nucleic acid which is further detected by a probe like QDs or organic dyes. QDs were functionalized with DNA by using carbamate linkages and used for binding selectively Y chromosome in human sperm cells (Figure 1.22).[60]

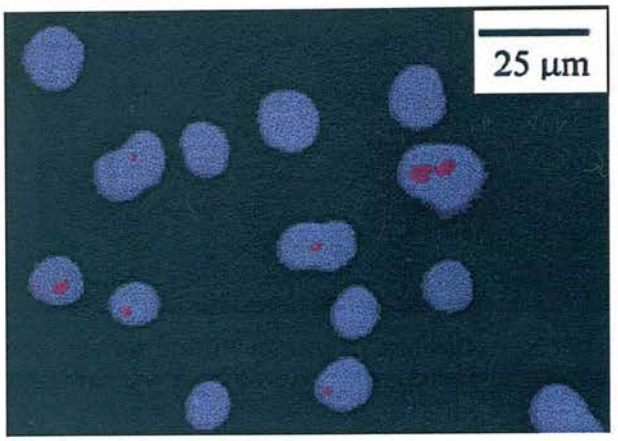

Figure 1.22 Fluorescence micrograph of in situ hybridization of red quantum (λ_{max}= 609 nm, fwhm = 38 nm) dot probe(s) for the Y chromosome in human sperm cells *(taken from Pathak et al.[60])*.

Wu *et al.*[79] linked QDs to IgGs and streptavidin and these bioconjugates were used to label the cancer marker Her2 on the surface of fixed and live cancer cells. They were also used in staining actin and microtubule fibers in the cytoplasm and in detecting nuclear antigens. The photostability between QDs (QD-608) and organic dyes (Alexa 488) was compared. It was found that under the conditions used in this experiment Alexa 488 had lost 50% of it initial intensity even after 10 seconds, and after three minutes it had lost all its fluorescence (Figure 1.23). In contrast the QD fluorescence intensity was never compromised.

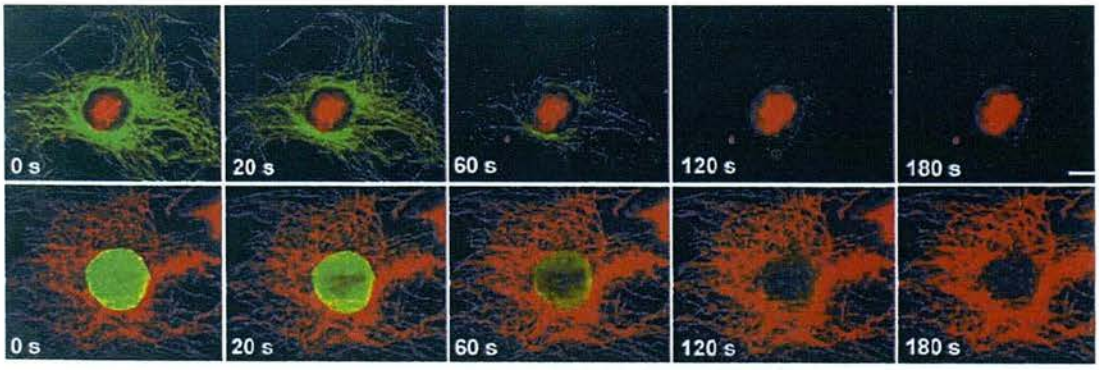

Figure 1.23 Nuclear antigens were labeled with QD 630–streptavidin (red), and microtubules were labeled with Alexa 488 conjugated to anti-mouse IgG (green) *[taken from Wu et al.[79]]*.

QDs have been used also as cancer cell biomarkers. For example, Sukhanova *et al.*[90] prepared (CdSe/ZnS) QDs in which cysteine molecules are bound to the QD via sulfhydyl groups, a layer of poly(allylamine) polymer is bound to negatively charged carboxylate groups of cysteine by electrostatic interactions to label MCF7r breast adenocarcinoma cells. In these

QDs the amine groups of the polymer are used to covalently attach anti-mouse polyvalent goat antibodies which recognise *p*-glycoproteins (p-gp) overexpressed in membrane of these cancer cells.

1.5.2 Live cell imaging

The availability of probes for live cell imaging is very limited and QDs can make a significant contribution in this area. However, for better understanding of the cell's intracellular assembly it is important to cross the plasma membrane barrier. There are four methods to surpass the plasma membrane barrier: microinjection, non specific uptake, protein or peptide specific uptake and uptake induced by receptor-ligand recognition.[91]

Chan and Nie[58] covalently conjugated transferrin on mercaptoacetic acid-coated CdSe/ZnS QDs. They found that the QD-transferrin conjugates were taken up by cancer cells by receptor-mediated endocytosis. This work revealed that QDs retain their optical properties *in vivo* and have potential to be used as intracellular labels. Dubertret *et al.*[92] achieved live cell imaging of *Xenopus* embryo cells by microinjecting the PEG-coated CdSe/ZnS QDs having green emission into single embryo cells (Figure 1.24). Microscopic fluorescence imaging was utilized for real time monitoring of cell lineage and differentiation. It was also found that the embryos exhibited normal growth even with the injection of over 1 billion QD particles per cell.

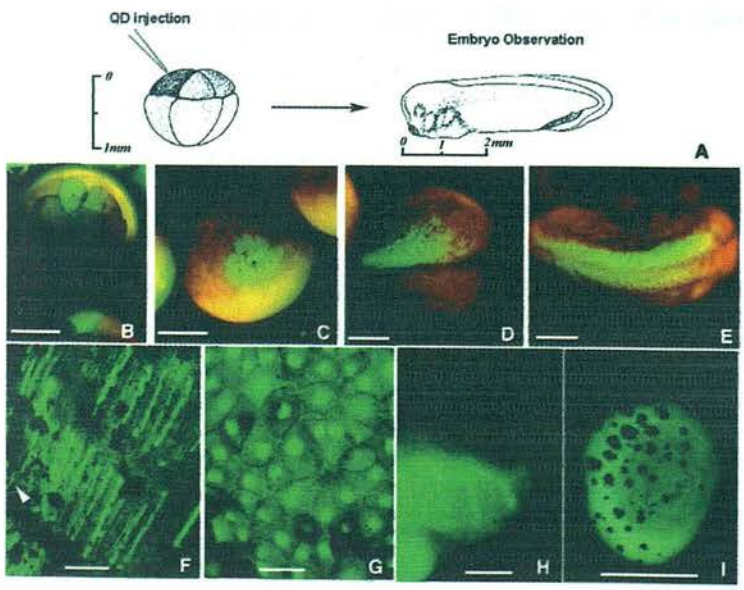

Figure 1.24 Quantum dot labelling of *Xenopus* embryos at different stages showing the specific intracellular localizations of the QDs (*taken form Dubertret et al.*[92]).

Dahan *et al.*[93] used antibody-bound red QDs for detecting plasma membrane glycine receptors (GlyRs) on neuronal cells (Figure 1.25). After formation of QD-GlyR conjugate within synapatic and extrasynaptics domains, real time diffusion for single QD-GlyR was observed for more than twenty minutes.

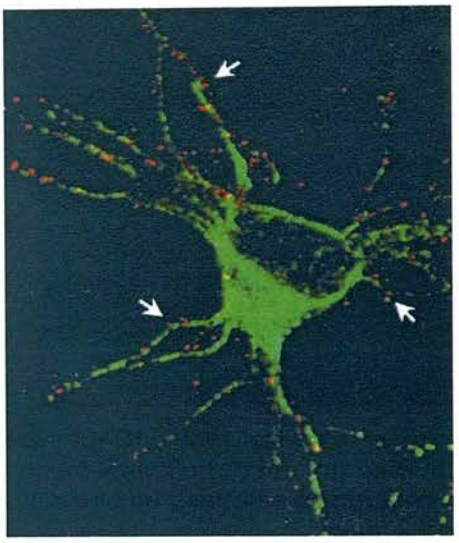

Figure 1.25 QDs as a marker for GlyR localization in neurons QD-GlyRs (red) detected over the somatodendritic compartment identified by microtubule-associated protein-2 (green). Arrows ark clusters of QD-GlyRs located on dendrites *(taken form Dahan et al.* [93]*).*

Lidke and co-workers[94] used the peptide specific uptake approach for studying the intracellular structure of human epithelial carcinoma cells. Preparation of QDs – EGF (epidermal growth factor) conjugate was done for labelling erbB (epidermal growth factor receptor). They observed receptor binding in real time with quantification of binding and internalization.

1.5.3 *In vivo* animal imaging

For *in vivo* imaging a probe must contain a targeting motif with high affinity for a specific tissue, and a fluorescent domain that emits light on binding to the target. The targeting domain must be modular so that any tissue could be imaged. There are also other requirements the probe must meet. It must minimize non-specific interactions, it must have long term stability and it should have a proper metabolism mechanism. QDs have large surface area which provides the possibility of attaching many functional units for enhancing the binding.[91]

Akerman *et al* [95] reported the first studies on *in vivo* animal imaging with QDs. CdSe/ZnS QDs with either green or red emission were given intravenously to mice. QDs were attached to lung targeting peptide and targeted to the lung vasculature. QDs were also linked with

tumour homing peptides for targeting to tumour blood vessels. They coated QDs with peptide alone or with both peptide and polyethylene glycol (PEG) and they found PEG coating on QD prevents non-specific uptake. Peptide coated QDs were found excellent in targeting the vascular site without any aggregation.

In 2003 Kim *et al.*[45] fluorescently imaged murine and porcine sentinel lymph nodes after intradermal injection of near infra-red (CdTe)CdSe QDs. Injected QDs were phagocytosized by dendritic cells and then migrated to sentinel lymph node that could then be fluorescently detected even 1 cm under the skin surface.

QDs have also been used in tumour targeting and imaging. Gao *et al.*[96] succeeded in targeting and imaging human prostate cancer in nude mice. A nude mouse lacks thymus and functional immune system so it can be used in studying growth of myeloma cells. They prepared QD probes conjugated to a prostate tumour specific antibody which were successful in targeting selectively human prostate tumours (Figure 1.26).

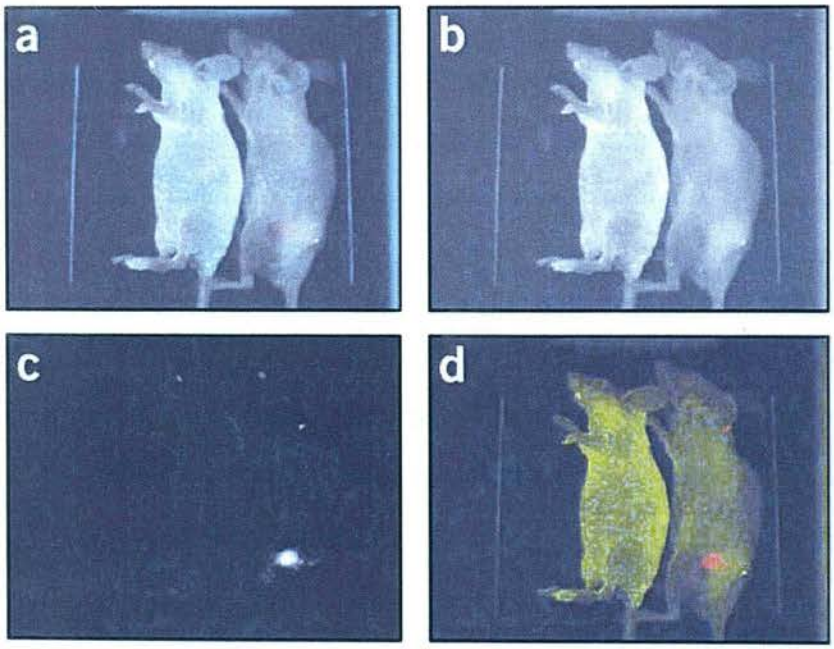

Figure 1.26. Imaging of QD-prostate-specific membrane antigen (PSMA) Ab conjugates in live animals harbored with C4-2 tumor xenografts. Orange-red fluorescoence signals indicate a prostate tumor growing in a live mouse (right)*[taken from Gao et al.[96]]*.

In response to stress and brain injuries astrocytes (macroglial cell types found in the brain) are activated, so they are considered an important key marker in detecting stress conditions in a cell. Maysinger *et al.*[97] observed real time imaging of astrocytes. For this study the GFAP-Luc (lucifrase) transgenic mouse was used in which the bioluminescent luciferase gene which will be expressed in the event of oxidative stress. So in the event of any stress or in response

to foreign nanoparticles these mice will become luminescent. They used a range of QDs and found the PEGylated QDs cause very little tissue damage as compare to other QDs.

1.5.4 Intracellular uptake of QDs

Like for other nanoparticles, intracellular delivery of QD depends upon their size and surface charge. There are specific and non-specific ways of QD intracellular delivery. Micropipette injection, electroporation and biomolecule-mediated specific delivery are distinctive delivery methods,[98] whereas endocytosis is a non-specific entry mode. Endocytosis is a transporting process by which macromolecules and small particles travel from the plasma membrane. It is a very important pathway for cells as they communicate with each other by using endocytosis. They also use endocytosis for supplying nutrients and generating immune responses. Endocytosis can be classified into phagocytosis (uptake of large particles) and pinocytosis (uptake of fluid and solutes). Phagocytosis is found in specialized membranes like those found in macrophages, monocytes and neutrophils. But pinocytosis is found in all mammalian cells.

QDs are commonly delivered to the cells by clathrin-mediated endocytosis which is the most common form of receptor-mediated endocytosis (Figure 1.27). In clathrin- mediated endocytosis the ligand binds to a specific cell surface receptor which is followed by the clustering of ligand receptor complexes in coated pits (these are formed by assembly of cytosolic coat proteins among which clathrin is the main component). Then these coated pits forms intracellular clathrin coated vesicles by pinching off the plasma membrane. After clathrin depolymerises and proton influx acidifies the early formation of endosomes takes place. In next step ligand is released from the endosomes.[99]

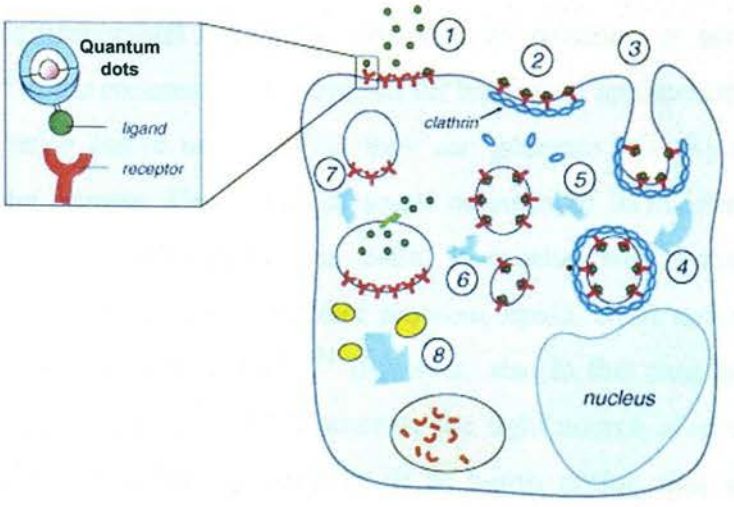

Figure 1.27 Clathrin-mediated endocytosis *(taken from Khalil et al.[99]).*

There are several examples of QD delivery by receptor-induced endocytosis. For example, Chan and Nie[58] conjugated transferrin to QDs by EDC coupling (see section 1.3.4.1), and found that transferrin mediated the endocytsosis of the QDs. Lidke and co-workers[94] used QDs – EGF (epidermal growth factor) conjugates for labelling erbB (see section 1.5.2) and these QDs were also internalized by receptor-mediated endocytosis.

1.5.5 QD Cytotoxicity

The potential cytotoxicity caused by QDs is a key issue for *in vitro* and *in vivo* biological imaging applications. However, investigating and deciding whether QDs (in general) are toxic is challenging. Currently there are no standard methods for synthesising QDs and the organic coatings used to over-coat them are also highly variable. Another complication arises from the fact that cell systems used in each study are often very different. So it is hard to get a reasonable answer about their toxicity. It is generally accepted that there are two mechanisms by which QDs can be toxic: (1) by release of heavy metals from the core of nanocrystals like cadmium, selenium, tellurium etc. (2) by formation of reactive oxygen species (ROS).

The most documented and widely studied QDs for biological applications are made of CdSe and CdTe. Cadmium is a class 1 carcinogen[100] which affects DNA stability severely by stopping DNA repair mechanisms. Cadmium also induces oxidative stress by depleting naturally occurring antioxidants like glutathione (Figure 1.28). In cadmium-containing QDs release of cadmium ions is believed to be the primary mode of cytotoxicity. Release of cadmium ions can be due to oxidation or due to the intracellular acidic environment. In general this type of cytotoxity can be minimized by overcoating the Cd-containing cores with ZnS. Equally, if the nanocrystal is properly protected by polymers or proteins the QDs are mostly non-toxic[101] at the concentrations required for biological applications.

Because QDs are redox active nanoparticles they can generate ROS by energy or electron transfer to molecular oxygen. Generation of small amounts of ROS is sufficient to inhibit proliferation and induce differentiation in cells. It is also well known that at higher concentrations, ROS cause damage to cellular proteins, lipids, DNA and carbohydrates, and that it can cause apoptosis or necrosis.[98,102] However, also in this case the type of material forming the QD affects its toxicity.[103] Moreover, the light source used and the irradiation power and time also affect the cytotoxicity. It is worth noting that although for some

biological applications the phototoxicity of QDs is problematic, it can also be beneficial and be exploited medically (e.g. to kill cancer cells in photodynamic cancer therapy).[104]

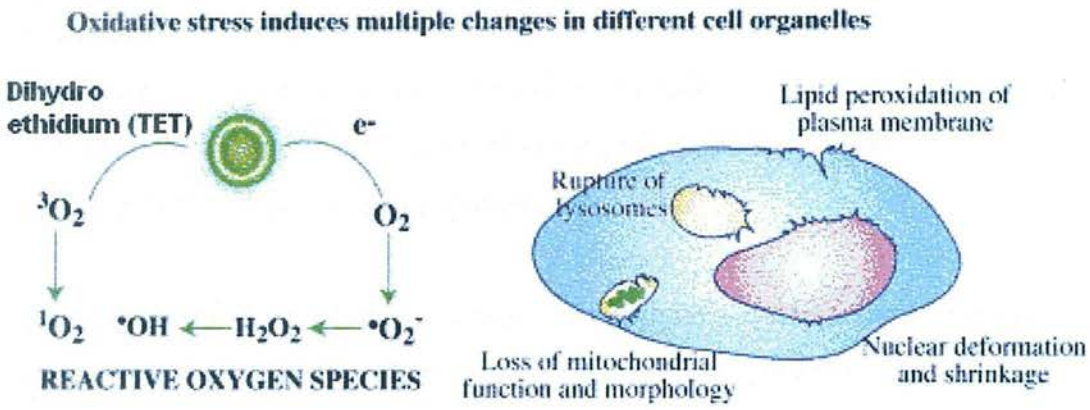

Figure 1.28 ROS produced by QDs can induce organelle damage *(taken from Maysinger et al.[98]).*

1.6 Thesis objectives and overview

The main objectives of this PhD thesis were:

- To develop new strategies to label biomolecules with QDs.
- To investigate the biological activity of molecules which are attached to QDs.
- To exploit QDs for novel biological applications.

Two aspects which this thesis research wanted to investigate and find answers for were:

- Site-specific labelling, is it important to maintain biological activity?
- QD large size and multivalency; are these properties beneficial or a problem?

In this thesis several new strategies for labelling various biomolecules on QDs are devised and the biological activity of the constructs is studied. Ni-NTA modified QDs are used for site specific labelling of the recombinant enzyme glutathione-S-transferase (GST) in Chapter 2. In Chapter 3, the multivalency and hydrophobic nature of QDs are used to site-specifically attach an important immunostimulatory molecule, Kdo_2-Lipid A, which is the main component of the outer membrane of *E. coli* and thus mimics this microbial pathogen. In Chapter 4, site-specific labelling strategies based on Ni(NTA)-His-tagged and multivalency are exploited to anchor a different number of malaria surface protein 1 (MSP 1) molecules and thus develop valuable material to investigate and mimic the early events involved in the recognition and attachment of the merozoite of the malaria parasite *Plasmodium falciparum* to red blood cells.

1.7 References

(1) Riehemann, K.; Schneider, S. W.; Luger, T. A.; Godin, B.; Ferrari, M.; Fuchs, H. *Angew. Chem. Int. Ed.* **2009,** 48, 872-897.

(2) www.feynmanonline.com (01 Dec, 2009)

(3) Rosenthal, S. J.; Wright, D.W. *Nanobiotechnology Protocol;* Humana Press Inc, 2005; pp 9.

(4) Everett, D. H. *Basic principles of colloid science;* Royal Society of Chemistry, 1988, pp10-15.

(5) Elaissari, A. *Colloidal Nanoparticles in Biotechnology;* John Wiley and Sons, Inc. 2008, pp1-6.

(6) Sonvico, F.; Dubernet, C.; Colombo.; Couvreur, P. *Curr. Pharm. Des.* **2005**, *11* 2091-2105.

(7) Raschke,G.; Kowarik, S.; Franzl, T.; Sönnichsen, C.; Klar, T.A.; Feldmann ,J. *Nano Lett.* **2003**, *3*, 935–93.

(8) Plank,C.; Anton, M.; Rudolph,C.; Rosenecker, J.; Krötz, F. *Expert. Opin. Biol. Ther.* **2003**, *3*, 745-758.

(9) Elghanian, R.; Storhoff, J, J.; Mucic, R.C.; Letsinger, L, R.; Mirkin, C.A.; *Science* **1997**, *277*, 1078 – 1081.

(10) Ito, A.; Takizawa, Y.; Honda, H.; Hata, K. I.; Kagami, H.; Ueda, M.; Kobayashi, T. *Tissue. Eng.* **2004**, *10*, 833-840.

(11) Debouttiere, P. J.; Roux, S.; Vocanson, F.; Billotey, C.; Beuf, O.; Favre-Reguillon, A.; Lin, Y.; Pellet-Rostaing, S.; Lamartine, R.; Perriat, P.; Tillement, O. *Adv. Funct. Mater.* **2006**, *16*, 2330-2339.

(12) Eustis, S.; El-Sayed, M. A. *Chem. Soc. Rev.* **2006**, *35*, 209-217.

(13) Authier, L.; Grossiord, C.; Brossier, P.; Limoges, B. *Anal. Chem.* **2001**, *73*, 4450-4456.

(14) Gupta, S.; Huda, S.; Kilpatrick, P. K.; Velev, O. D. *Anal. Chem.* **2007**, *79*, 3810-3820.

(15) Shi, X. Y.; Wang, S. H.; Lee, I.; Shen, M. W.; Baker, J. R. *Biopolymers* **2009**, *91*, 936-942.

(16) Xu, C.; Xu, K.; Gu, H.; Zhong, X.; Guo, Z.; Zheng, R.; Zhang, X.; Xu, B. *J. Am. Chem. Soc.* **2004**,126, 3392-3393.

(17) Nam, J. M.; Thaxton, C. S.; Mirkin, C. A. *Science* **2003**, *301*, 1884-1886.

(18) Sugimoto, T. *Fine particles, synthesis, characterization and mechanism of growth surfactant*, CRC, 2000, pp 2–34.

(19) Larpent, C.; Bernard, E.; Richard, J.; Vaslin, S. *Macromolecules* **1997**, *30*, 354-362.

(20) Burda, C.; Chen, X. B.; Narayanan, R.; El-Sayed, M. A. *Chem. Rev.* **2005**, *105*, 1025-1102.

(21) Alivisatos, P. *Nat. Biotechnol.* **2004**, *22*, 47-52.

(22) Murray, C. B.; Norris, D. J.; Bawendi, M. G. *J. Am. Chem. Soc.* **1993**, *115*, 8706-8715.

(23) Hines, M. A.; Guyot-Sionnest, P. *J. Phys. Chem. B***1998**, *102*, 3655-3657.

(24) Green, M.; Wakefield, G.; Dobson, P. J. *J. Mater. Chem.* **2003**, *13*, 1076-1078.

(25) Dabbousi, B. O; Veiejo, J. R.; Mikulec, F.V.; Heine, J.R.; Mattousi, H.; Ober, R.; Jensen K.F.; Bawendi, M.G. *J. Phys. Chem B.* **1997**, *101*, 9463-9475.

(26) Uyeda, H.T.; Medintz, I. L.; Jaiswal, J.K.; Simon, S.M.; Mattoussi, H. *J. Am. Chem. Soc.* **2005** ,127,3870-3878.

(27) Murphy, C. J.; and Coffer, J.L. *Appl. Spectrosc.*, **2002,** 56, 6A-27A.

(28) Rogach A.L. *Semiconductor nanocrystals quantum dots*; SpringerWienNewYork 2008; pp 46.

(29) Efros, A. L.; Rosen, M. *Annu. Rev. Mater. Sci.* **2000**, *30*, 475-521.

(30) Norris, D. J.; Bawendi, M. G. *Phys. Rev. B.: Condens. Matter.* **1996**, *53*, 16338-16346.

(31) Yu, W. W.; Qu, L. H.; Guo, W. Z.; Peng, X. G. *Chem. Mater.* **2003**, *15*, 2854-2860.

(32) Schimid, G. *Nanoparticles: from Theory to Application*; Wiley-VCH, 2005; pp 21-24

(33) Klimov, V. I. *J. Phys. Chem. B* **2006**, *110*, 16827-16845.

(34) Zhou, M.; Ghosh, I. *Biopolymers* **2007**, *88*, 325-339.

(35) (a) Lamer, V. K.; Dinegar, R. H. *J. Am. Chem. Soc.* **1950**, *72*, 4847-4854. (b) Murray, C. B.; Kagan, C. R.; Bawendi, M. G. *Annu. Rev. Mater. Sci.* **2000**, *30*, 545-610.

(36) Park, J.; Joo, J.; Kwon, S. G.; Jang, Y.; Hyeon, T. *Angew. Chem. Int. Ed.* **2007**, *46*, 4630-4660.

(37) Ramsden, J.J.; Gratzel, M. J *Chem. Soc. Farad. Trans. 1.* **1984**, *80*, 919-933.

(38) Nozik A, J.; Wiliams, F.; Nenadovic, M.T.; Rajh, Micic, O.I. *J. Phys. Chem* **1985**, *89*, 397-399.

(39) Spanhel, L.; Haase,M.; Weller,H.; Henglein, A. *J. Am. Chem. Soc.* **1987**,*109*, 5649-5655.

(40) Steigerwald, M.L.; Alivisatos, A.P.; Gibson, J.M.; Harris, T.D.; Kortan, R.; Muller A.J.; Thayer A.M.; Duncan, T.M.; Douglass, D.C.; Brus, L. E. *J. Am. Chem. Soc.* **1988**, *110*, 3046-3050.

(41) Murray, C. B.; Norris, D. J.; Bawendi, M. G. *J. Am. Chem. Soc.* **1993**, *115*, 8706-8715.

(42) Steigerwald, M. L.; Alivisatos, A. P.; Gibson, J. M.; Harris, T. D.;Kortan, R.; Muller, A. J.; Thayer, A. M.; Duncan, T. M.; Douglas, D. C.; Brus, L. E. *J. Am. Chem. Soc.* **1987**, *110*, 3046-3050.

(43) Brennan, J. G.; Siegrist,T.; Carroll, P. J.; Stuczynski, S. M.; Brus, L. E.; Steigerwald, M. L. *J. Am. Chem. Soc.* **1989**, *111*, 4141-4143.

(44) Stuczynski. S. M.: Brennan. J. G.; Steigerwald, M. L. *Inorg. Chem.* **1989**, 28, 4431-4432.

(45) Trindad, T.; *Chem. Mater.* **2000**, *13*, 3848-3858.

(46) Peng, X.; Wickham, J.; Alivisatos, A.P. *J. Am. Chem. Soc.* **1998**, *120*, 5043-5344.

(47) Qu, L.; Peng X. *J. Am. Chem. Soc.* **2002**, *124*, 2049-2055.

(48) Smith, A.M.; Ruan G.; Rhyner, M.N. *Ann. Biomed. Eng.* **2006**, *34*, 3-14

(49) Peng Z. A.; Peng, X. G. *J. Am. Chem. Soc.* **2001**, *123*, 183-184.

(50) Yang, Y. A.; Wu, H. M.; Williams, K. R.; Cao, Y. C. *Angew. Chem. Int. Ed.* **2005**, *44*, 6712-6715.

(51) Hines, M. A.; Guyot-Sionnest, P. *J. Phys. Chem.* **1996**, *100*, 468-471.

(52) Danek, M.; Jensen, K.I.; Murray, C.B.; Bawendi, M.G. *Chem. Mater.* **1996**, *8*, 173-180.

(53) Youn, H.C.; Baral, S.; Fendeler, J.H. *J. Phys. Chem.* **1988**, *92*, 6320-6327.

(54) Tian, Y.; Newton, T.; Kotov, N.A.; Guldi, D.M.; Fendler, J. *J Phys. Chem.* **1988**, *92*, 6320-6327

(55) Bailey, R.E.; Smith, A.M.; Nie, S. *Physica. E.* **2004,** *25*, 1-12.

(56) Zhu, C. Q.; Wang, P.; Wang, X.; Li, Y. *Nanoscale. Res. Lett.* **2008**, *3*, 213-220.

(57) Yu, W.W.; Chang E.; Drezek, R.; Covin V.L. *Biochem. Biophy. Res. Commun.* **2006**, 781-786.

(58) Chan, W. C.; Nie, S. *Science* **1998**, 281, 2016-2018.

(59) Wuister, S. F.; Swart,I.; Driel, F.V.; Donega, M.C. *Nano. lett.* **2003**, *3*, 503-507.

(60) Pathak, S.; Choi, S. K.; Arnheim, N.; Thompson, M. E. *J. Am. Chem. Soc.* **2001**, *123*, 4103-4104

(61) Mattoussi, H.; Mauro, J. M.; Goldman, E. R.; Anderson, G. P.; Sundar, V. C.; Mikulec, F. V.; Bawendi, M. G. *J. Am. Chem. Soc.* **2000**, *122*, 12142-12150.

(62) Kim, S.; Bawendi M.G. *J. Am. Chem. Soc.* **2003**, *125*, 14652-14653.

(63) Pinaud, F.; King, D.; Moore, H. P.; Weiss, S. *J. Am. Chem. Soc.* **2004**, *126*, 6115-6123.

(64) Guo, W. Z.; Li, J. J.; Wang, Y. A.; Peng, X. G. *Chem. Mater.* **2003**, *15*, 3125-3133.

(65) Michalet, X.; Pinaud, F.F.; Bentolila, L.A.; Tsay J.M.; Doose, S.; Li, J.J,.; Sundaresan, G.; Wu, A.M.; Gambhir, S.S.; Weiss S. *Science* **2005**, *307*, 538-544.

(66) Dubertret, B.; Skourides, P.; Norris, D. J.; Noireaux, V.; Brivanlou, A. H.; Libchaber, A. *Science* **2002**, *298*, 1759-1762.

(67) Fan, H.; Leve, E,W.; Scullin, C.; Gabaldon, J.; Tallant, D.; Bunge, S.; Boyle, T.; Wilson, M.C.; Brinker, C.J. *Nano. Lett.* **2005**, *5*, 645-648.

(68) Mattheakis, L. C.; Dias, J. M.; Choi, Y. J.; Gong, J.; Bruchez, M. P.; Liu, J. Q.; Wang, E. *Anal. Biochem.* **2004**, *327*, 200.

(69) Gerion, D.; Pinaud, F.; William, S.C.; Parak, W.J.; Zanchet, D.; Weiss,S.; Alivisatos A.P.; *J. Phys. Chem . B.* **2001**, *105*, 8861-8871.

(70) Selvan, S.T.; Tan T.T.; Ying Y.J. *Adv. Mater.* **2005**, *17*, 1620-1625.

(71) Xing, Y.; Chaudry, Q.; Shen, C.; Kong, K. Y.; Zhau, H. E.; Wchung, L.; Petros, J. A.; O'Regan, R. M.; Yezhelyev, M. V.; Simons, J. W.; Wang, M. D.; Nie, S. *Nat. Protoc.* **2007**, *2*, 1152-1165.

(72) Pellegrino, T.; Manna, L.; Kudera, S.; *Nano. Lett.* **2004**, *4*, 703-707.

(73) Mitchell, P.G.; Mirkin, C.A.; Letsinger, R.L.; *J. Am. Chem. Soc.* **1999**, *121*, 8122-8123.

(74) Mattoussi, H.; Mauro, J. M.; Goldman, E. R.; Anderson, G. P.; Sundar, V. C.; Mikulec, F. V.; Bawendi, M. G. *J. Am. Chem. Soc.* **2000**, *122*, 12142-12150.

(75) Dixit, S.K.; Goicochea, N.L.; Daniel, M.C.; Murali, A.; Bronstein, L.; De, M.; Stein, B.; Rotello V.M.; Kao C.C.; Dragnea B. *Nano. lett.* **2006**, *6*, 1993-1999.

(76) Ipe, B. I.; Shukla, A.; Lu, H. C.; Zou, B.; Rehage, H.; Niemeyer, C. M. *Chemphyschem* **2006**, *7*, 1112-1118.

(77) Sapsford, K.E.; Pons, T.; Medintz, L.; Higashiya, S.; Brunel, F. M.; Dawson, P. E.; Mattoussi, H. *J. Phys. Chem. C* **2007**, *111*, 11528-11538.

(78) Medintz, I. L.; Clapp, A. R.; Mattoussi, H.; Goldman, E. R.; Fisher, B.; Mauro, J. M. *Nat. Mater.* **2003**, *2*, 630-638.

(79) Wu, X. Y.; Liu, H. J.; Liu, J. Q.; Haley, K. N.; Treadway, J. A.; Larson, J. P.; Ge, N. F.; Peale, F.; Bruchez, M. P. *Nat. Biotechnol.* **2003**, *21*, 41-46.

(80) Bruchez, M.; Moronne, M.; Gin, P.; Weiss, S.; Alivisatos, A. P. *Science* **1998**, *281*, 2013-2016.

(81) Howarth, M.; Takao, K.; Hayashi, Y.; Ting, A. Y. *Proc. Natl. Acad. Sci.* **2005**, *102*, 7583-7588.

(82) Xing, Y.; Chaudry, Q.; Shen, C.; Kong, K. Y.; Zhau, H. E.; Wchung, L.; Petros, J. A.; O'Regan, R. M.; Yezhelyev, M. V.; Simons, J. W.; Wang, M. D.; Nie, S. *Nature Protocols* **2007**, *2*, 1152-1165.

(83) Pinaud, F.; King, D.; Moore, H. P.; Weiss, S. *J. Am. Chem. Soc.* **2004**, *126*, 6115-6123.

(84) Giepmans, B. N. G.; Adams, S. R.; Ellisman, M. H.; Tsien, R. Y. *Science* **2006**, *312*, 217-224.

(85) Wang, F.; Tan, W. B.; Zhang, Y.; Fan, X. P.; Wang, M. Q. *Nanotechnology* **2006**, *17*, R1-R13.

(86) Shimomura, O.; Johnson, F. H.; Saiga, Y. *J. Cell. Comp. Physiol.* **1962**, *59*, 223-239.

(87) Prasher, D. C.; Eckenrode, V. K.; Ward, W. W.; Prendergast, F. G.; Cormier, M. J. *Gene* **1992**, *111*, 229-233.

(88) Tsien, R. Y. *Annu. Rev. Biochem.* **1998**, *67*, 509-544.

(89) Resch-Genger, U.; Grabolle, M.; Cavaliere-Jaricot, S.; Nitschke, R.; Nann, T. *Nat. Methods.* **2008**, *5*, 763-775.

(90) Sukhanova, A.; Devy, M.; Venteo, L.; Kaplan, H.; Artemyev, M.; Oleinikov, V.; Klinov, D.; Pluot, M.; Cohen, J. H. M.; Nabiev, I. *Anal. Biochem.* **2004**, *324*, 60-67.

(91) Smith, A.M.; Gao, X.; Nie, S. *J. Photochem. Photobiol.* **2004**, *80*, 377-385.

(92) Dubertret, B.; Skourides, P.; Norris, D. J.; Noireaux, V.; Brivanlou, A. H.; Libchaber, A. *Science.* **2002**, *298*, 1759-1762.

(93) Dahan, M.; Lévi, S.; Luccardini, C.; Rostaing, P.; Riveau, B.; Triller, A. *Science.* **2003**, *302*, 442-445.

(94) Lidke, D. S.; Nagy, P.; Heintzmann, R.; Arndt-Jovin, D. J.; Post, J. N.; Grecco, H. E.; Jares-Erijman, E. A.; Jovin, T. M. *Nat. Biotechnol.* **2004**, *22*, 198-203.

(95) Akerman, M. E.; Chan, W. C. W.; Laakkonen, P.; Bhatia, S. N.; Ruoslahti, E. *PNAS* **2002**, *99*, 12617-12621.

(96) Gao, X.; Cui Y.; Levenson, R.M.; Chung, L.W.K.; Nie, S. *Nat. Biotechnol.* **2004**, *22*, 969-976.

(97) Maysinger, D.; Behrendt, M.; Lalancette-Herbert, M.; Kriz, J. *Nano Lett.* **2007**, *7*, 2513-2520.

(98) Maysinger, D.; Lovric, J.; Eisenberg, A.; Savic, R. *Eur. J. Pharm. Biopharm.* **2007**, *65*, 270-281.

(99) Khalil, I. A.; Kogure, K.; Akita, H.; Harashima, H. *Pharmacol. Rev.* **2006**, *58*, 32-45.

(100) Rzigalinski, B. A.; Strobl, J. S. Toxicol. Appl. Pharmacol. **2009**, *238*, 280-288.

(101) Jaiswal, J. K.; Mattoussi, H.; Mauro, J. M.; Simon, S. M. *Nat. Biotechnol.* **2003**, *21*, 47-51.

(102) Hild, W. A.; Breunig, M.; Goepferich, A. *Eur. J. Pharm. Biopharm.* **2008**, *68*, 153-168.

(103) Ipe, B. I.; Lehnig, M.; Niemeyer, C. M. *Small* **2005**, *1*, 706-709.

(104) Bakalova, R.; Ohba, H.; Zhelev, Z.; Ishikawa, M.; Baba, Y. *Nat. Biotechnol.* **2004**, *22*, 1360-1361.

2.1 Introduction

2.1.1 Metal-mediated labelling of histidine-tagged proteins

Proteins are widely used in genomics and proteomics. Production of various recombinant proteins with affinity tags has increased exponentially over the years. Affinity tags are exogenous amino acid sequences having high affinity for specific biological or chemical ligands. Various affinity tags are used in protein production and purification (Table 2.1).

Tag	Size (Amino acids)	Comments
His-tag	5–15	Purification under native or denaturing conditions
FLAG	8	Calcium-dependent, mAb-based purification
Streptag II	8	Modified streptavidin, elution with biotin analog
HA-tag	9	Influenza virus hemagglutinin tag, Ab-based purification
Softag1, Softag 3	13, 8	Recognized by polyol-responsive mAb
c-myc	10	mAb-based purification
T7-tag	11–16	mAb-based purification
S-tag	15	S-protein resin affinity purification
Chitin-binding domain	52	Binds only insoluble chitin
Thioredoxin	109	Affinity purification with modified resin
Xylanase 10A	163	Cellulose based capture, elution with glucose
Glutathione *S*-transferase	201	Glutathione or GST-Ab affinity
Maltose binding protein	396	Amylose affinity purification

Table 2.1 Affinity and solubility tags for recombinant proteins.[1]

The most widely used affinity tags are those having a variable number of histidine residues, so-called His-tags. It has been estimated that in molecular biology more than 60% of proteins are expressed with His-tags.[1] Purification of His-tagged proteins is based on immobilized metal affinity chromatography (IMAC). IMAC is a purification technique in which a metal ion is complexed with an immobilized chelating agent for protein purification. Binding of the His-tag to the immobilised metal ions on the solid support of the chromatography column is used for protein separation (Figure 2.1).

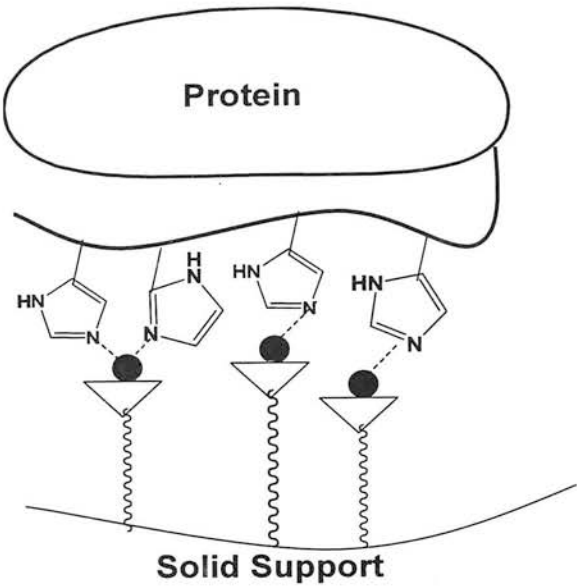

Figure 2.1 Schematic illustration of His tagged protein binding to a metal-chelated affinity support.

Transition metals commonly used as ions in IMAC are Cu(II), Ni(II), Zn(II), Co(II) and Fe(III). All these metals ions are electron pair acceptors and are Lewis acids. In the immobilised chelating agents, electron donor groups like sulphur, oxygen and nitrogen are present and coordinate with metal ions to form stable metal complexes. The remaining metal coordinating sites on the metal are occupied by water molecules and can be exchanged with electron donor groups from the protein like an histidine group. Adsorption of his-tag proteins to IMAC columns is normally accomplished at neutral or slightly basic pH to ensure that the imidazole nitrogen of the histidine residue stays deprotonated.[2] Hochuli *et al.*[3] was the first to use the metal chelator nitrilotriacetic acid (NTA) as an adsorbent in IMAC. NTA occupies four positions in the coordination sphere of the metal ion (Figure 2.2), e.g. Ni^{2+}. The remaining two sites are available for selective protein interactions (i.e. with the His-tag). It has been found that Ni^{2+} binds very strongly to NTA; more strongly than to any other ligand previously used in IMAC.[3]

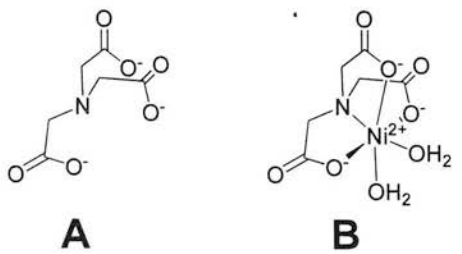

Figure 2.2 Structure of the NTA ligand and of a complex it forms with Ni^{2+} ions.

In several studies Ni-NTA derivatized nanoparticles and organic dyes have been used for site-specific immobilization of his-tagged proteins.

The first study of Ni-NTA mediated his-tagged protein conjugation to organic dyes was reported by Kapanidis *et al.*[4] who attached the widely used cyanine fluorochrome to Ni^{2+}-NTA moieties (Figure 2.3). These constructs were capable of fluorescence labelling an His_6-tagged derivative of the transcriptional activator Catabolite Activator Protein (CAP) upon binding of Ni^{+2} ions to the NTA fragment. They found that compounds 1a and 1b have relatively low affinity for the hexahistidine (His_6) tag ($K_d \geq 10$ μM), whereas 2a and 2b have quite high affinity ($K_d = 1.0$ μM for 2a; $K_d = 0.4$ μM for 2b). All these compounds, however, had poor emission (fluorescence quantum yield < 0.1).

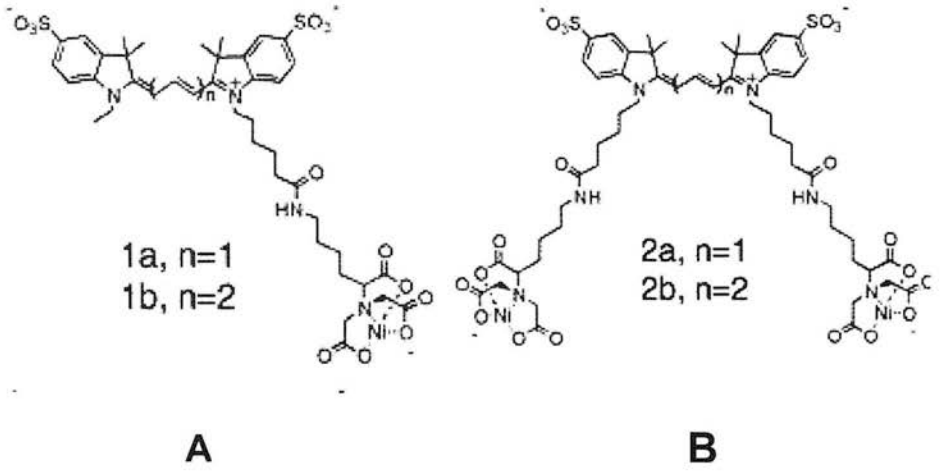

Figure 2.3 Some fluorophores A = $(Ni^{+2}:NTA)_1$ derivatives of Cyanine 3 (1a) and Cyanine 5 (1b); B =$(Ni^{+2}:NTA)_2$ derivatives of Cyanine 3 (2a) and Cyanine 5 (2b) used for protein labelling *(taken from Kapanidis et al.[4]).*

Lata *et al.*[5] designed even higher affinity recognition units for his-tagged proteins by exploiting the concept of multivalent chelator heads (MCHs). In these constructs several NTA moieties (termed bis-, tris-, and tetrakis-NTA) were attached to a fluorescein dye (Figure 2.4). Interactions between these MCHs and polyhistidine (hexahistidine and decahistidine) tagged proteins were studied. It was observed that binding stability improves after increasing the number of NTA moieties linked to fluorescein dye. The stronger binding was observed between the tris-NTA derivative and the His_{10}-tagged protein; $K_d \sim 0.1$ nM.

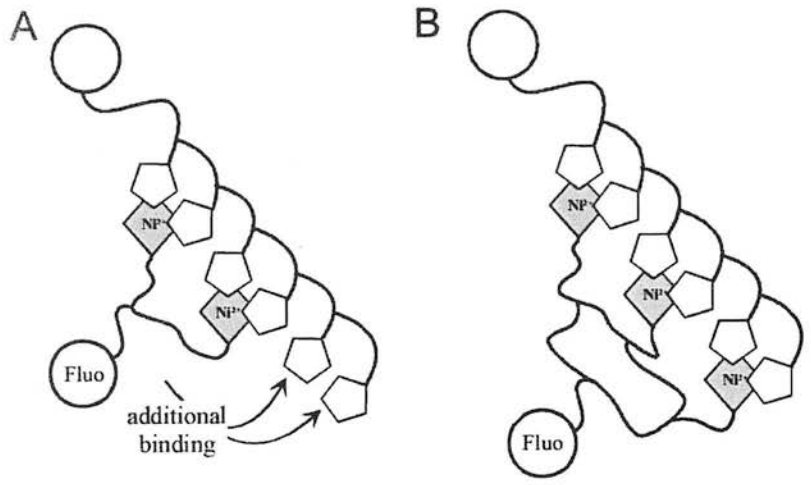

Figure 2.4 Schematic of different scenarios of multivalency in Ni-NTA binding to polyhistidine-tagged proteins *(taken from Lata et al.[5]).*

The problem with these Ni-NTA dye conjugates is still that the paramagnetic Ni^{2+} ions strongly quench the fluorescence of the dye (quantum yields < 0.1), limiting the practical applications of these systems for biological imaging purposes. However, Lippard *et al.*[6] overcame this problem and labelled His_6-tagged extracellular proteins expressed on the outer surface of HeLa and HEK 293-T cells using a different fluorescein-based dye which attached to a single Ni-NTA unit had a fluorescence quantum yield of ~ 0.7. Unfortunately the binding affinity was not as good (K_d = 1-20 μM).

Ni-NTA modified nanoparticles have also been used in site specific labelling of proteins.[7] Xu *et al.*[7] used Ni-NTA modified magnetic (FePt) nanoparticles (less than 10 nm in diameter) for binding, purifying and carrying His_6-tagged green fluorescent proteins (GFP) (Figure 2.5). They found these magnetic nanoparticles have high surface/volume ratio and better solubility than micrometer-sized resins or beads used in IMAC, and provide a simple procedure to obtain pure GFP directly from the mixture of lysed cells in a matter of minutes. The lowest concentration of proteins that was possible to separate using these Ni-NTA modified magnetic nanoparticles was 0.5 pM.

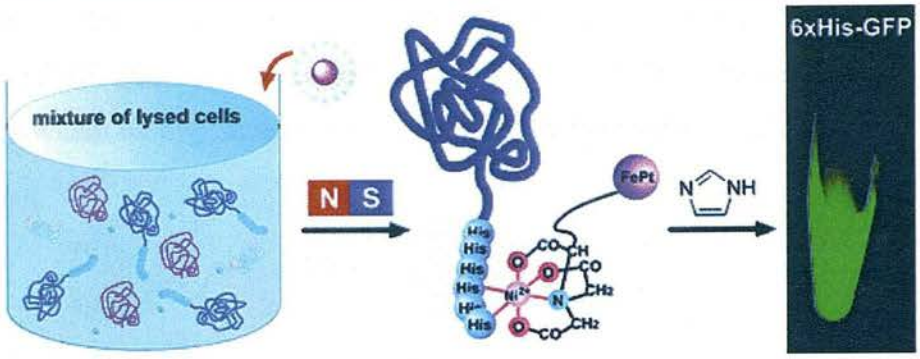

Figure 2.5 Ni-NTA-modified magnetic nanoparticles selectively bind to histidine-tagged proteins in a cell lysate *(taken from Xu et al.[7]).*

In a different approach Lim and co-worker[8] reported the encapsulation of highly monodisperse magnetic (Fe_2O_3) nanoparticles inside micelles formed by a mixture of PEG and NTA-Ni modified phospholipids (Figure 2.6). This self-assembly approach which exploits hydrophobic interactions has the advantage of requiring fewer synthetic steps.

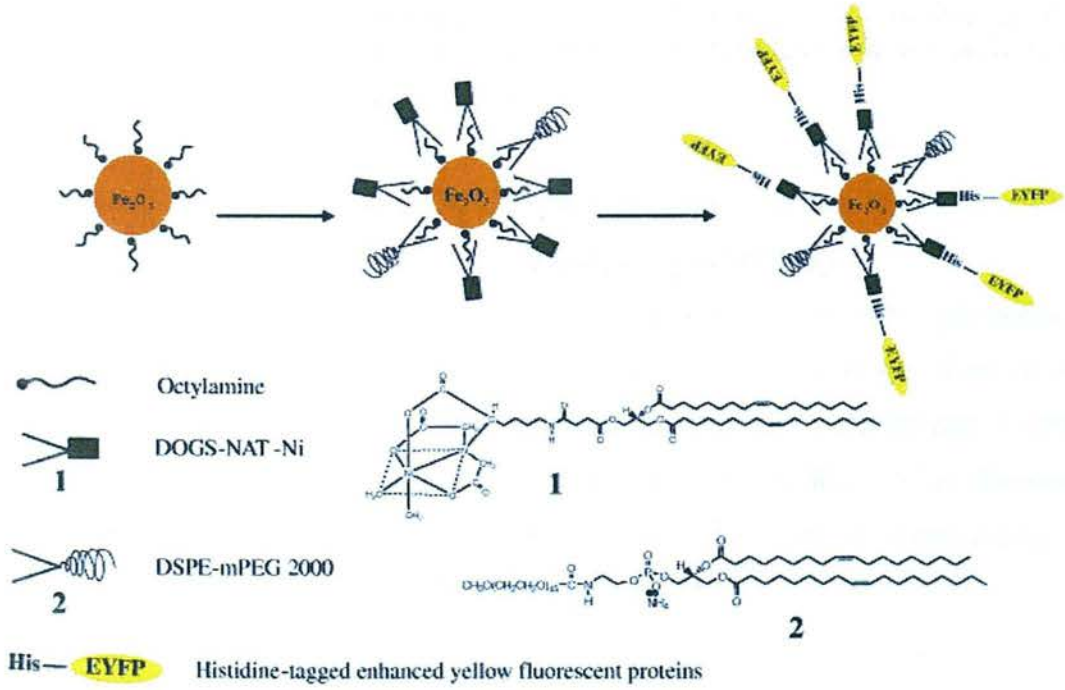

Figure 2.6 Schematic illustration of the surface modification strategy of iron oxide magnetic nanoparticles with NTA-phospholipids and subsequent immobilization of histidine-tagged EYFP *(taken from Lim et al.[8]).*

Gold nanoparticles have also been attached to Ni-NTA units for site-specific labelling of his-tagged proteins. For example Abad *et al.*[9] prepared NTA-Co(II) terminated gold nanoparticles for the site-specific immobilisation of his-tagged deglycosylated horseradish peroxidase (HRP_{rec}) and ferredoxin-$NADP^+$ reductase (FNR) (Figure 2.7).

They found that bound to the gold nanoparticles these enzymes had 93-97% of the activity of the free native enzymes; this is one of the few studies investigating the extent to which biological activity is preserved (critical aspect; *vide infra*).

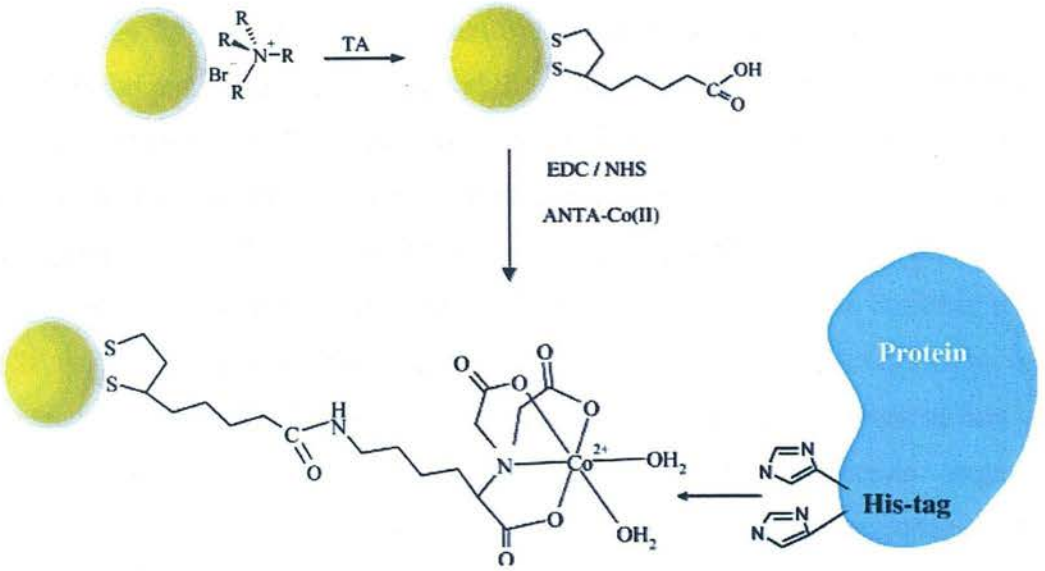

Figure 2.7 Reaction strategy showing the steps required for the construction of NTA-terminated nanoparticles for specific immobilization of His-tagged proteins *(taken from Abad et al.[9]).*

Lee *et al.*[10] used a very different approach for binding his-tagged proteins on nanoparticles. They found that in Ni/NiO core/shell nanoparticles the nickel surface itself provides a platform to bind the his-tagged protein effectively.

Finally, it is important to mention that it is possible to use non-metallic nanoparticles to achieve fluorescence site specific labelling of proteins. For example, Kim *et al.*[11] described the preparation and characterization of tetramethylrhodamine (TMR)-encapsulated silica nanoparticles and their functionalization with Ni-NTA. However, these constructs require many synthetic steps and the fluorescence characteristics of TMR is compromised by the Ni-NTA surface-modification.

2.1.2 Glutathione-S-transferases

2.1.2.1 General

Glutathione–S-Transferases (GSTs; E.C.2.5.1.18) are a large super family of enzymes found mainly in the cytosol, mitochondria and microsome.[12-15] They play a major role in the detoxification of xenobiotic compounds. The most significant catalytic activity of GST is the conjugation of the tripeptide glutathione (GSH) to electrophilic substrates, carcinogens and metabolites. This conjugation yields a more water soluble

product which is then excreted, and thus GST acts as a detoxifying enzyme of endogenous and xenobiotic electrophiles. GSTs exist as soluble enzymes in virtually every living species examined, including plants and bacteria.[12] The soluble form of GST exists as a dimeric protein with a monomer having a molecular weight of approximately 28 kDa. Each monomeric unit has an active site composed of two distinct functional regions: an hydrophilic G-site, which binds the physiological substrate glutathione (GSH), and an adjacent H-site which provides a non-polar environment for binding the electrophilic substrate (Figure 2.8).[12,16] The G-site is highly specific for GSH and it is conserved between all GSTs. Here, the enzyme uses multiple hydrogen bonding interactions to bind and activate GSH. In contrast, the H-site is quite divergent so that it can bind various substrates.[12,17] GSTs are over-expressed in myeloma cells causing resistance against chemotherapeutic agents used in cancer treatment. Consequently, they are promising therapeutic targets in anticancer therapy. GSTs isoenzymes are also over-expressed in neurodegenerative diseases, multiple sclerosis and asthma. There are two mechanisms by which GSTs cause resistance to anticancer drugs. In the first mechanism GST causes the direct detoxification of xenobiotics using glutathione as a reducing agent. In second mechanism, GST causes the inhibition of mitogen activated protein (MAP) kinase pathway, which is responsible for causing apoptosis of cells.[18]

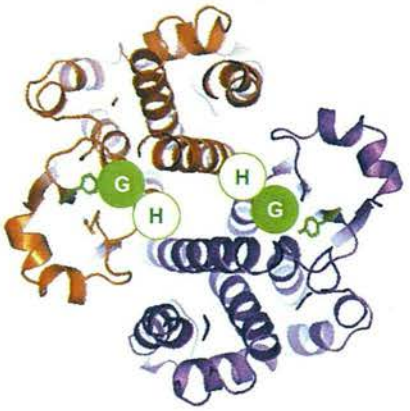

Figure 2.8 Crystal structure of hGSTP1-1 homodimer. The G (Glutathione) site of one monomer faces the H (Substrate) site of its partner. This figure was drawn using PyMol

2.1.2.3 Catalytic activity of GST

GSTs are enzymes that participate in the purification of xenobiotics and other carcinogenic compounds in living organisms by a GSH conjugation reaction. These reactions are of two types.[19]

1. Displacement reactions. In these reactions GSH displaces electron withdrawing groups such as halogens, nitriles and carboxylic acids.

2. Addition reactions. GSH is added to double bond structures or strained ring systems.

GST plays two basic functions to catalyse the modification of a substrate: 1) it brings the substrate into close proximity to GSH by binding to both substrate and 2) it activates the GSH sulphur atom for nucleophilic attack.[12]

A general reaction for GST catalysis is:

$$GSH + RX \xrightarrow{GST} HX + GSR$$

1-Chloro-2,4-dinitrobenzene (CDNB) is the universal electrophilic substrate for studying the catalytic activity of many kinds of GST but not all (Figure 2.9).[16]

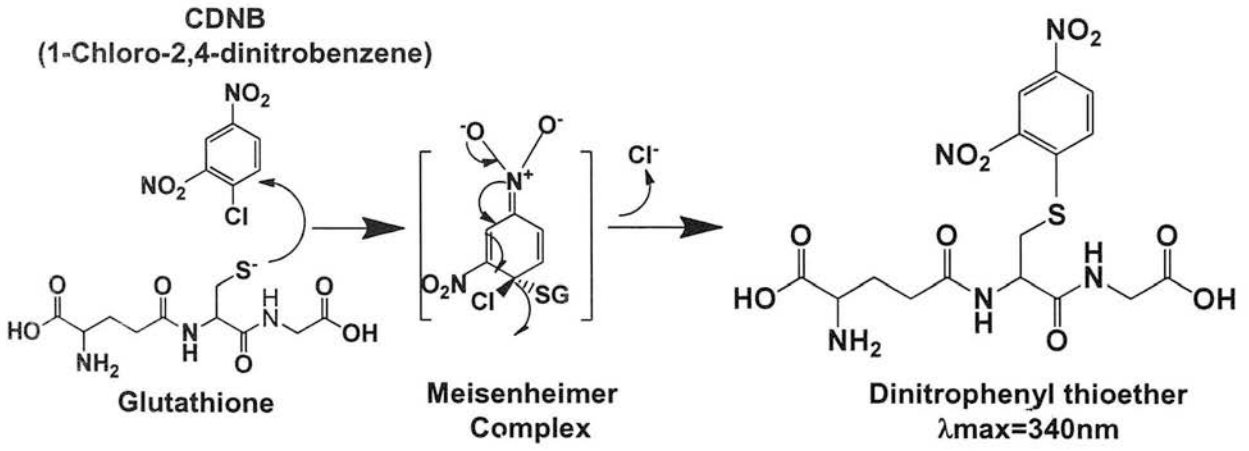

Figure 2.9 Glutathione conjugation to 1-chloro-2,4-dinitrobenzene (CDNB).

2.1.2.2 GSTs from *Schistosoma japonicum*

Schistosoma japonicum is a parasitic helminth worm that causes schistosomiasis. Schistosomiasis is parasitic disease infecting more than 275 million people worldwide which results in around 200 thousand deaths annually [20-21]. Two isoenzymes found in *S. japonicum* are of 26 kDa and 28 kDa. Like other GSTs the 218 residues of each subunit of the Sj26GST dimer form a small N-terminal α/β domain (residues 1-76), a shorter linker region (residues 77-84), and a larger α-helical C-terminal domain (residues 85-218). The Sj26GST dimer assembly creates a long (40 Å) and narrow (approximately 6-10 Å) inter-domain cleft. An essential catalytic residue is a tyrosine in position 7 (Figure 2.10).[22-23]

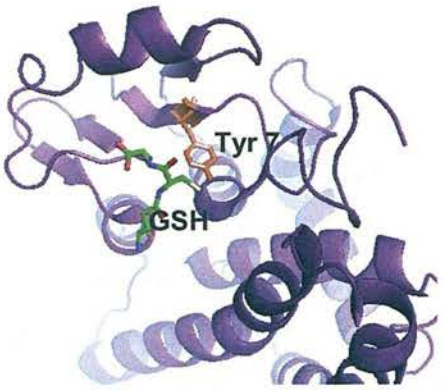

Figure 2.10 Crystal structure of the active site of sjGST. This figure was drawn using PyMol.

2.2 Motivation for the work

Currently, to conjugate QDs to biomolecules the QD surface is derivatized in such a way as to allow the attachment of the biomolecules through a covalent bond, electrostatic or hydrophobic interactions. A typical biomolecule contains many residues capable of forming covalent and non-covalent linkages with the QD. Thus, common problems associated with conjugating proteins to QDs in this way include non-specificity, irreversibility and limited control over the location and orientation of the QD in the biomolecule. Because QDs are large (e.g. similar in size to a protein) the functionality of the biomolecule cannot be taken for granted and must be proven experimentally. In most cases this has meant showing that molecular recognition with an appropriate partner does occur. However, biological activity may be more complex than this recognition, e.g. it may involve catalysing chemical reactions. In this Chapter we address these problems and issues by site-specific labeling of an his-tagged GST on Ni(NTA)-modified CdSe/ZnS nanoparticles. GST represents a challenging and interesting target because it is an enzyme which requires dimerisation and binding of two different substrates for catalysis.

2.3 Experimental

2.3.1 Materials

All chemicals were obtained from commercial sources and used as received. Cadmium oxide (CdO, 99.5%), tri-*n*-octylphosphine oxide (TOPO,99%), tri-*n*-butylphosphine (TBP, 97%), hexadecylamine (HDA, 98%), diethylzinc ($ZnEt_2$,1 M in hexane), hexametyldisilathiane [$(TMS)_2S$ 98%], thioctic acid , nickel(II)chloride, *N*-hydroxysuccinimide (NHS, 98%), *N*-*N*-bis(carboxymethyl)-L-lysine hydrate, 1-chloro-2, 4-dinitrobenzene and L- Glutathione were purchased from Sigma Aldrich. 1-Ethyl-3-[3'-(dimethylamino)propyl]carbodiimide was purchased from Ademtech. Stearic acid (98.5%) was purchased from Fluka. Selenium powder (Se, 99.999%) was obtained from Alfa Aesar. BCA protein Assay kit was purchased from Pierce Biotechnology. Recombinant forms of *S. japonicim* GSTs (histidine and untagged GSTs) were obtained from Anne Caniard and Dr. Dominic Campopiano from School of Chemistry, University of Edinburgh.

2.3.2 Synthesis of CdSe and CdSe/ZnS QDs

Hydrophobic CdSe and core-shell CdSe-ZnS QDs were synthesised and purified adapting a previously reported procedure with some modifications.[24]

In a typical synthesis, CdO (0.013 g, 0.1 mmol) and stearic acid (0.254 g, 0.89 mmol) were loaded into a three-neck flask and heated to 225°C under N_2 flow and stirring. Once the mixture was completely dissolved, it was allowed to cool to room temperature. Then, TOPO (3 g) and HDA (1 g) were added and the mixture was heated to 225 °C under N_2 flow and vigorous stirring. At this temperature, 1 mL of freshly prepared TPB-Se solution (1 M) was quickly injected into the flask [tri-*n*-butylphosphine selenide (TBP-Se, 1 M)] was prepared in a N_2-filled glove box by shaking 0.08 g of selenium powder in 1 mL of TBP). Following injection the temperature was adjusted to ~200 °C to promote nanocrystal growth for 5 h. Different aliquots were removed from this reaction mixture at different time intervals. On reaching the desired nanoparticle size, as determined by UV/vis and fluorescence spectroscopy the reaction mixture was cooled down to room temperature. The nanocrystals were then dispersed in chloroform and precipitated by addition of methanol. After centrifugation the supernatant liquid phase was removed. This

procedure was repeated at least three times. The precipitates were combined and dried under a stream of N_2 at room temperature.

For CdSe-ZnS QDs, on reaching the desired nanocrystal (CdSe) size, the temperature was lowered to ca. 100 °C to stop further growth. Then, the solution was heated to 210 °C. At this temperature, 0.5 mL of the ZnS stock solution was slowly injected into the reaction pot [a ZnS stock solution was prepared in a N_2-filled glove box by reacting $(TMS)_2S$ (0.5 mL, 2.5 mmole) with $ZnEt_2$ (3.5 mL, 3.5 mM in hexane) in TOP (6 mL)].The temperature of the mixture was set to 100 °C and stirred for 2 hr. After cooling to room temperature, the nanocrystals were dispersed in chloroform and precipitated by addition of methanol. After centrifugation the supernatant liquid phase was removed. This procedure was repeated at least three times. The precipitates were combined and dried under a stream of N_2 at room temperature.

2.3.3 Preparation of dihydrolipoic acid

Dihydrolipoic acid (DHLA) was prepared according to the method given by Uyeda *et al.*[25] Thiotic acid (1.22 g) was dissolved in an aqueous solution of $NaHCO_3$ (25 mL, 0.25 M) and the resultant solution was cooled to 0 °C. $NaBH_4$ (0.9 g) was added and the temperature was maintained at ca. 5 °C with continuous stirring for about 2 hr under nitrogen. The reaction mixture was acidified with HCl (3.3 M) to pH 1. The product was extracted with toluene (~30 mL) dried by adding $MgSO_4$. The final product (Figure 2.11) was isolated as colourless oil and a ^1H NMR of the product was obtained.

^1H NMR (250 MHz, $CDCl_3$) δ/ppm: 2.90 (1H, m, H^6), 2.69 (2H, m, H^9), 2.37 (2H, t, H^2), 1.89 (1H, m, 1/2H^8),1.80-1.40 (7H, m, H3, H4, H5, 1/2H^8), 1.35 (1H, d, H^7), 1.30 (1H, t, H^{10}).

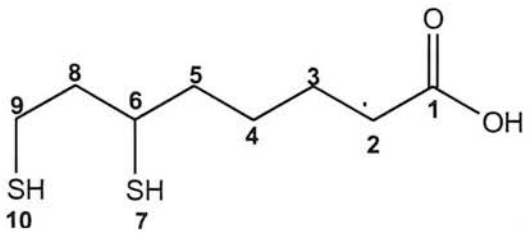

Figure 2.11 DHLA with NMR numbering assignments

2.3.4 Synthesis of water soluble quantum dots

The water-soluble DHLA-coated CdSe/ZnS QDs were prepared according to the method given by Mattoussi *et al.*[26] with some modifications. In a typical reaction, stearic acid-coated CdSe-ZnS QDs (50 mg) and DHLA (50 mg) were mixed in DMF (15 mL). The solution was heated to 60-70 °C and stirred overnight. Then, potassium-*tert*-butoxide (100 mg) was slowly added to deprotonate the terminal lipoic acid groups. The nanoparticles were separated by centrifugation at (700 *g*) and the supernatant liquid was discarded. The resulting QDs were dried under vacuum. The QDs were further purified by re-dissolving them in water and passing this solution through a 100 kDa microsep filter.

2.3.5 Modification of quantum dot surface by NTA and NTA-Ni^{2+} complex

N-N-Bis(carboxymethyl)-L-lysine hydrate (NTA) (5 mg, 0.0132 mmole) was dissolved in 3 mL of HEPES (20 mM, pH 7.5). Activation of carboxylate groups of the DHLA-coated QDs was performed by mixing the QDs (9 mg) in 1 mL of EDC (3 mM in HEPES) and 1 mL of NHS (3 mM in HEPES) with stirring for 30 min (this gives a QD concentration of 3.5 μM). Then, 1 mL of NTA (4.4 mM) was added and the solution was stirred for 24 h. The resulting NTA-modified nanocrystals were purified using a Nanosep 100 kDa omega membrane filter (low protein-binding, modified polyethersulfone on polyethylene substrate). The Ni-NTA coated nanocrystals were prepared in the same way using the preformed complex, which was prepared by mixing of *N,N*-bis(carboxymethyl)-l-lysine hydrate (NTA) (5 mg, 0.0132 mmole) and $NiCl_2$ (5 mg, 0.021 mmole) in 3 mL of HEPES (20 mM) with stirring for 1 h . NTA and NTA-Ni^{2+} modified QDs were re-dissolved in phosphate buffer (600 μL, 20 mM, pH 6.7) for specific immobilization of enzymes.

2.3.6 Optical characterization

Optical absorption spectra of the CdSe/ZnS QDs were measured using the Perkin Elmer Lambda 900 UV-vis spectrometer and the cuvettes had a path length of 1 cm. Fluorescence studies were carried out with an Edinburgh Instruments FS900 fluorometer using quartz cell. Excitation was at 350 nm with bandwidths of 2 nm for excitation (unpolarised) and emission (unpolarised). Temperature was maintained at

25 °C. The concentration of the CdSe QDs was estimated using the method reported by Yu *et al.*[27] in which equation I is used.

$$\varepsilon = 5857\ (D)^{2.65} \qquad (I)$$

In equation I, D is the diameter of the nanocrystal determined using the equation II

$$D = (1.6122 \times 10^{-9})\lambda^4 - (2.6575 \times 10^{-6})\lambda^3 + (1.6242 \times 10^{-3})\lambda^2 - (0.4277)\lambda + (41.57) \qquad (II)$$

where λ is the position of the first excitonic absorption peak of the QD. The concentration of the CdSe QDs samples was determined by using Lambert-Beer's law

$$A = \varepsilon cL$$

where, A is the first absorption peak intensity, ε is the extinction coefficient, L is the path length of the light beam, and C is the concentration of the nanocrystal.

2.3.7 X-Ray photoelectron spectroscopy

XPS studies of nanocrystals were performed by binding the QDs to self-assembled monolayers (SAMs) of 1,6 hexanedithiol on gold surfaces.[28] Gold slides were chemically cleaned by immersing in a piranha solution (a mixture of H_2O_2 and conc.H_2SO_4 in 1:3 ratio) for 5-10 minutes. *Caution: piranha solution reacts violently with organic materials and therefore must be handled with extreme care.* Then, the slides were rinsed with water and methanol, dried under N_2 and used immediately. Monolayers of 1,6 hexanedithiol (10 mM) were prepared by immersing the cleaned gold strips into the methanol solution for about 15 h. Then SAM modified gold surfaces were rinsed with methanol and water. After this the SAM modified gold slides were transferred to a solution of nanocrystals (CdSe and CdSe/ZnS, 3mg) in toluene (0.5 mL) for 6 h. X-ray photoelectron spectra were obtained with a VG Scientific Sigma Probe (UK) XPS system. The Al Kα anode X-ray source ($h\upsilon$ = 1486.6 eV) was operated at 200 W and the take-off angle for photoelectrons was 37°. Samples were mounted with a spring clip. In a typical experiment, a few survey scans in the 100 to 1200 eV kinetic energy range were collected at a resolution of 1 eV. hen, detailed scans of 20-60 eV over a single feature were collected at a resolution of 0.2 eV. During the measurements the pressure was 10^{-9}-10^{-10} Torr.

2.3.8 High-resolution transmission electron microscopy

High-resolution transmission electron microscopy (HRTEM) studies were conducted on a JEOL JEM-2011 electron microscope operating at 200 kV. The samples were prepared by depositing a drop of a solution of nanocrystals in pyridine onto a copper specimen grid coated with an holey carbon film and allowing it to dry.[28]

2.3.9 Inductively coupled plasma - optical emission spectrometry (ICP-OES)

For ICP-OES samples were prepared by digesting QDs (40 μL) with 960 μL of concentrated nitric acid for 5 days. The samples were then diluted to 10 mL with Millipore water. Samples were analyzed by using Perkin Elmer Optima 5300 DV ICP-OES. The concentrations of Cd, Se, Zn, S and Ni ions were estimated from calibration curves prepared by using standard solutions, from which the total amount of Cd, Se, Zn, S and Ni in the CdSe/ZnS QDs was estimated.

2.3.10 Protein binding studies by sodium dodecyl sulfate polyacrylamide gel electrophoresis (SDS-PAGE)

Protein binding studies were carried out by incubating 100 μL of the corresponding QD (3.75×10^{-6} M) with 75 μL of and H-GST and U-GST (1.09 mg/mL; 39×10^{-6} M) for 2.0 h at room temperature. Incubation was also performed in presence of salt (NaCl, 1M). The enzyme-QDs complexes were separated from the unbound enzyme molecules by passing this solution through a Nanosep 300 kDa Omega membrane filter (low protein-binding, modified polyethersulfone on polyethylene substrate). The retentate containing the QD-bound enzyme was treated with 175 μL of a PBS solution of imidazole (0.5 M, pH=7.4) to release the enzyme. Retentate and filtrate fractions were analysed by SDS-PAGE.[29] Similarly control retentate and filtrate fractions samples were prepared by using PBS.

Method for SDS-PAGE[29]

2x SDS-PAGE loading buffer was prepared by mixing Tris/HCL (1.5 M, pH 8.0, 1 mL), glycerol (2 mL), bromophenol blue (0.05%), sodium dodecyl sulphate SDS (10%, 1.6 mL) and β-mercaptoethanol (0.4 mL). Samples for SDS-PAGE were

prepared by mixing loading buffer and sample in a (1:1) volume ratio followed by heating (100 °C, 5 min) and centrifugation (11,000 g, 2 min). A stand method was used for production of acrylamide gel with running gel containing 15% acrylamide and stacking gel of 4% acrylamide. Briefly the running gel (acrylamide/ bis (29:1)15% w/v, SDS 0.1 w/v, TEMED 0.15 v/v and APS 0.1% w/v in Tris buffer (375 mM, pH 8.8) was poured between the glass plate levelled and set at room temperature. The stacking gel (acrylamide/bis (29:1) 4% w/v, SDS 0.1% w/v, TEMED 0.15% v/v and APS 0.1w/v in Tris buffer(125 mM, pH 6.8) was then added and set at room temperature using a comb(mould) to produce the wells in finished gel. Gels were run in buffer (25 mM Tris, 192 mM glycine and 0.1% SDS, pH 8.3) at 200 Vcm^{-1}(180 mA). After the electrophoresis was finished, the gel was stained overnight in a mixture of 0.1% Coomassie Blue R-250, 40% methanol and 10% acetic acid and then destained in the same solution without Coomassie blue R-250.

2.3.11. Estimation of protein by bicinchoninic acid (BCA) Assay

Enzyme concentrations of bound and unbound enzyme on QDs were calculated using a BCA™ protein Kit Assay (Pierce). BCA Protein Assay is a detergent-compatible formulation based on bicinchoninic acid (BCA). This assay is used for the colorimetric detection and quantification of total protein in samples. A standard curve was prepared with different concentrations of bovine serum albumin (BSA) and the samples were calibrated from the standard curve at 562 nm following the manufacturer's instructions. In brief 100 µL of retentate and filtrate fractions were prepared as stated in SDS-PAGE studies. Then 2 mL of working reagent was added to the fractions (retentate and filtrate) and incubated at 37°C for 30 min. After incubation absorbance of samples was measured at 562 nm in CARY 300 SCAN UV-vis spectrometer.

2.3.12 GST Activity Assay

The GST activity was determined spectrophotometrically by measuring the change in absorbance at 340 nm (ε = 9600 M^{-1} cm^{-1}).[30] The solution for the blank assay was composed of potassium phosphate buffer (850 µL, 0.1 M, pH 6.5), 1-chloro-2, 4-dinitrobenzene (50 µL, 40 mM) and GSH (100 µL, 80 mM). The solution for sample

assay was composed of potassium phosphate buffer (800 μL, 0.1 M, pH 6.5), 1-chloro-2,4-dinitrobenzene (50 μL, 40 mM), GSH (100 μL ,80 mM) and GST solutions (50 μl, free and immobilized on QD-NTA-Ni^{+2}). These GST solutions were prepared by adding 100 μL of the phosphate buffer solution or QD (4 μM) to 75 μL of His-GST (1.14 mg/mL; 41 μM) and Untagged-GST (0.62 mg/mL; 22 μM). The absorbance was measured at 340 nm for five minutes (T = 20 °C).

One unit of GST activity is defined as the amount of enzyme producing 1 μmol of CDNB-GSH conjugate per minute under the conditions of the assay, and was calculated using the formula:[30]

$$\text{Units/mL enzyme} = \frac{(\Delta A_{340}/\text{min}) \times \text{Total volume of Assay (in mL)}}{9.6 \times \text{Vol. of enzyme used (in mL)}}$$

where $(\Delta A_{340}/\text{min}) = A_{340}\,(\text{Time 2}) - A_{340}\,(\text{Time 1}) / \text{Time 2 (min)} - \text{Time 1 (min)}$.

2.4 Results and discussion

2.4.1 Synthesis and characterization of CdSe core and CdSe/ZnS Core/Shell QDs

QDs (CdSe and CdSe/ZnS) were prepared by using CdO as cadmium precursor instead of the extremely toxic, pyrophoric and expensive dimethyl cadmium $Cd(CH_3)_2$. At the temperature of around 225 °C, CdO powder dissolved in stearic acid, and then on addition of TOPO and hexadecylamine generated colorless clear solutions. The formation of CdSe nanocrystals took place immediately after injection of TBPSe as indicated by the formation of yellow to dark red solutions. The resulting stearic acid-coated CdSe nanocrystals were collected and purified by a precipitation process induced by the addition of MeOH. The precipitated nanocrystals were collected after centrifugation and redissolved in chloroform. This process was repeated several times to remove the free ligands and unreacted precursors. CdSe nanoparticles of different sizes were synthesised by changing the reaction time. The QD diameter and extinction coefficient were estimated by UV-Vis spectroscopy using equations I and II as given in experimental section, and the validity of these expressions to calculate QD concentration was checked against ICP-OES data.

For example a QD having λ_{max} = 620 nm has according to formulas I and II a diameter of 5.6 nm and an extinction coefficient (ε) of 564400.303 M^{-1} cm^{-1}. For such QD, the theoretical number of Cd and Se atoms per QD can be calculated using the bulk density (5.665 g/cm^3), formula weight of CdSe, and volume of a 5.6 nm spherical nanoparticle (equation III). This calculation estimates ca. 1600 Cd and Se atoms.

$$5.665\frac{g}{cm^3}\times\frac{4}{3}\pi 2.8^3 nm^3\times\frac{1cm^3}{1\times10^{21}nm^3}\times\frac{1molCdSe}{191.37g}\times N_A\times1\frac{molCdatoms}{molCdSe}=\sim1639\frac{Cdatoms}{nanopartide}\quad\text{.....III}$$

A 1.3 μM QD solution (according to the calculated extinction coefficient value of 5.64×10^5 M^{-1} cm^{-1}, Table 2.2) gave a concentration of Cd and Se of 0.942 mg/L (8.4 μM) and 0.619 mg/L (7.8 μM) respectively after 250-fold dilution. Thus, the agreement between concentrations calculated using ICP and UV-Vis data is excellent. Figure 2.12 and Figure 2.13 shows the photoluminescence absorption and emission spectra of QDs of five different sizes. HRTEM images of these QDs revealed that they are crystalline, spherical and monodisperse. Figure 2.14 shows the HRTEM image of CdSe QDs having the first absorption peak at 599 nm. It shows QDs with an average diameter of 4.4 nm, and therefore UV-Vis and equation II provided a good QD size estimate (4.22 nm based on the 590 nm absorption).

QDs Absorption (nm)	Diameter (nm)	Extinction coefficient (cm^{-1} M^{-1})
564	3.35	144226
575	3.66	182348
592	4.24	269274
599	4.53	320875
620	5.60	564400

Table 2.2. The calculated size of different nanocrystals and corresponding extinction coefficient (ε).

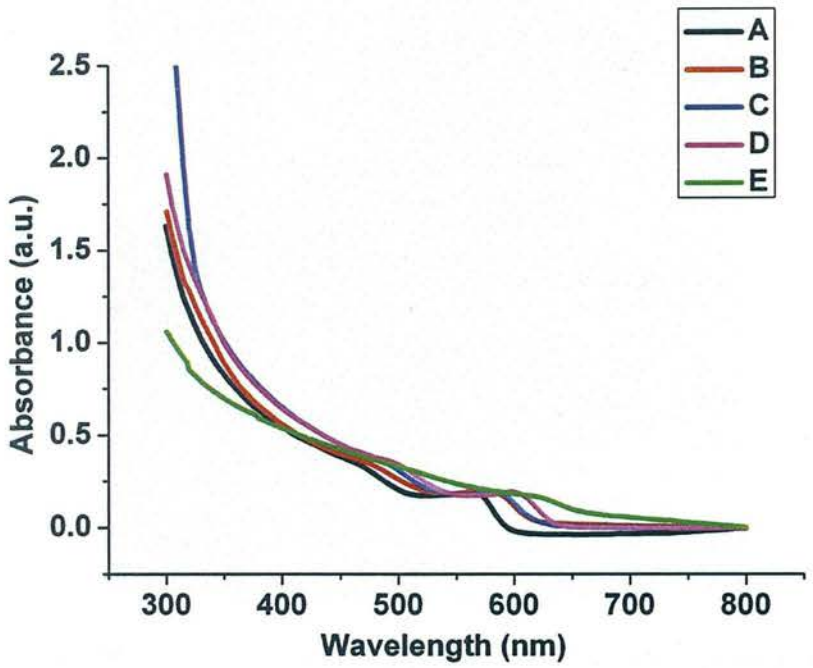

Figure 2.12 U.V-vis spectra of different CdSe nanoparticles (first absorption peak position: A= 564 nm, B = 575 nm, C= 592 nm, D= 599 nm, E= 620 nm).

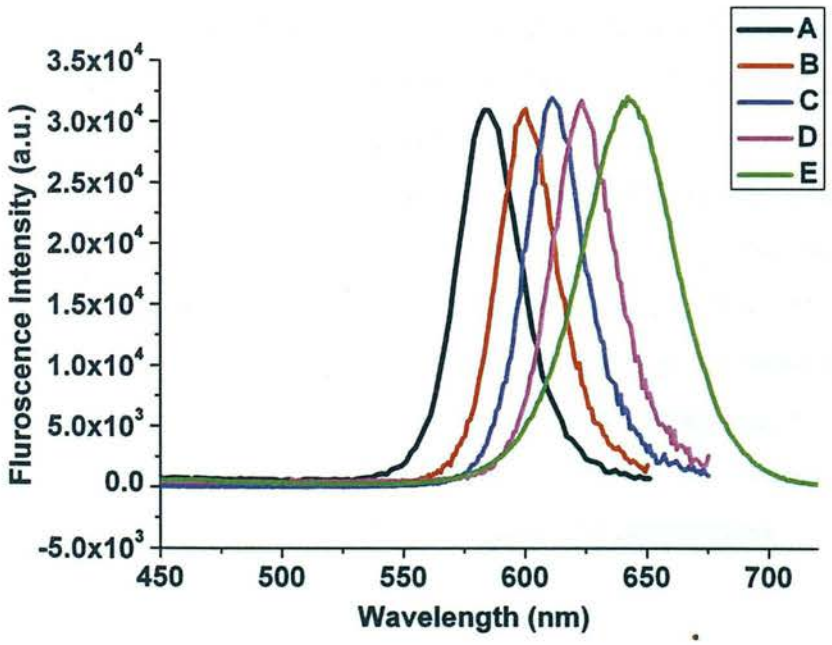

Figure 2.13 Fluorescence emission spectra of four different CdSe nanoparticles (emission peak position after excitation at 350 nm: A = 585 nm, B = 600 nm, C = 614 nm, D = 627 nm, E = 642 nm; Temperature = 25°C).

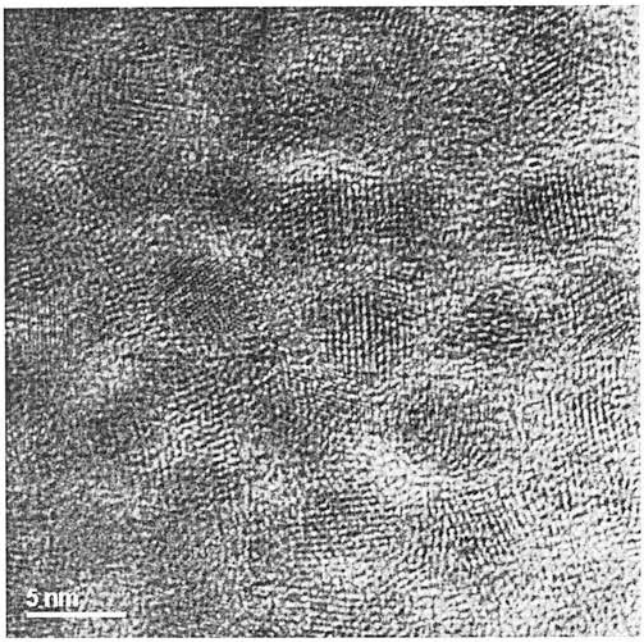

Figure 2.14 HRTEM images of CdSe QDs with a 1st absorption peak at 590 nm.

Core/shell QDs were prepared by overcoating the CdSe nanocystals with ZnS which is an higher band gap material. Diethylzinc ($ZnEt_2$) and bis(trimethylsilyl) sulfide ($(TMS)_2S$) in TBP (tri-*n*-butylphosphine) were used as Zn and S precursors in this work. The temperature at which the ZnS was added and growth temperature was 200 °C and 100 °C, respectively. These conditions avoided the self-nucleation of ZnS and ensured that most of the ZnS grew over the CdSe cores.[31] The resulting stearic acid-coated CdSe/ZnS (core/shell) nanocrystals were purified by several steps of precipitation-centrifugation (as in the synthesis of the CdSe core QDs). As expected[32], capping of CdSe core with ZnS shell increased the fluorescence of these QDs. There was also a small red-shift in the position of the first absorption peak (< 5 nm) and corresponding emission maximum (15-20 nm). This is due to the increase in size of the QD after capping, which decreases the band gap of the nanocrystals.

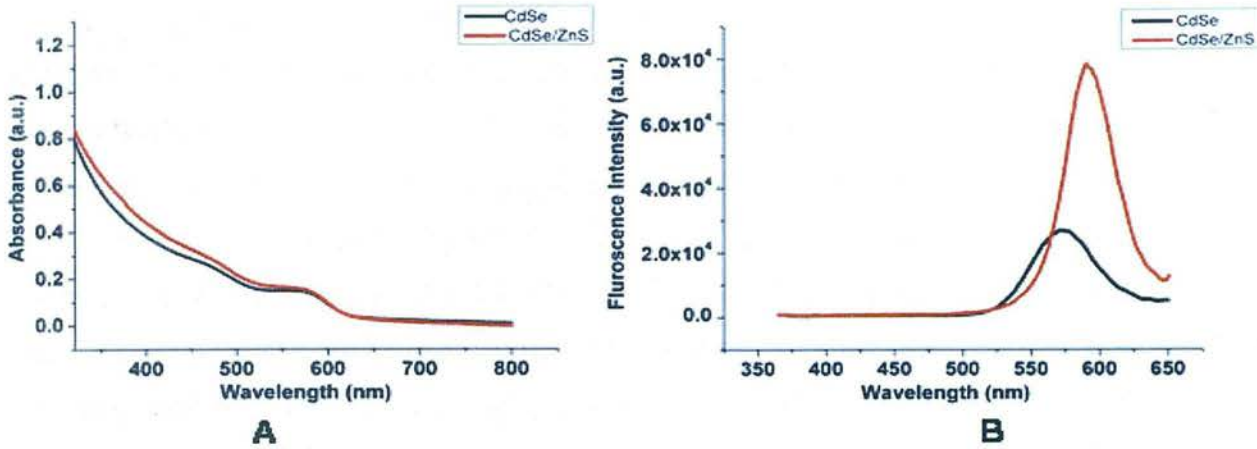

Figure 2.15 U.V-vis spectra and fluorescence emission spectra of CdSe and CdSe/ZnS QDs (Excitation at 350 nm, Temperature = 25°C).

Figure 2.15 shows the typical photoluminescence absorption and emission spectrum of CdSe and CdSe/ZnS QDs illustrating these changes. After formation of the ZnS shell, the size of QD increases. Figure 2.16 shows HRTEM images of the CdSe/ZnS QDs with a diameter of ~ 5.6 nm (compared to ~ 4.4 nm for the corresponding CdSe QDs; Figure 2.15). Since a shell of ZnS measures 0.31 nm[31] then an increase of 1.4 nm means that this particular QD had upto 4 monolayers of ZnS. It has been shown that overcoating CdSe QDs with 4-5 monolayers provides the best results in terms of fluorescence emission.[31, 33]

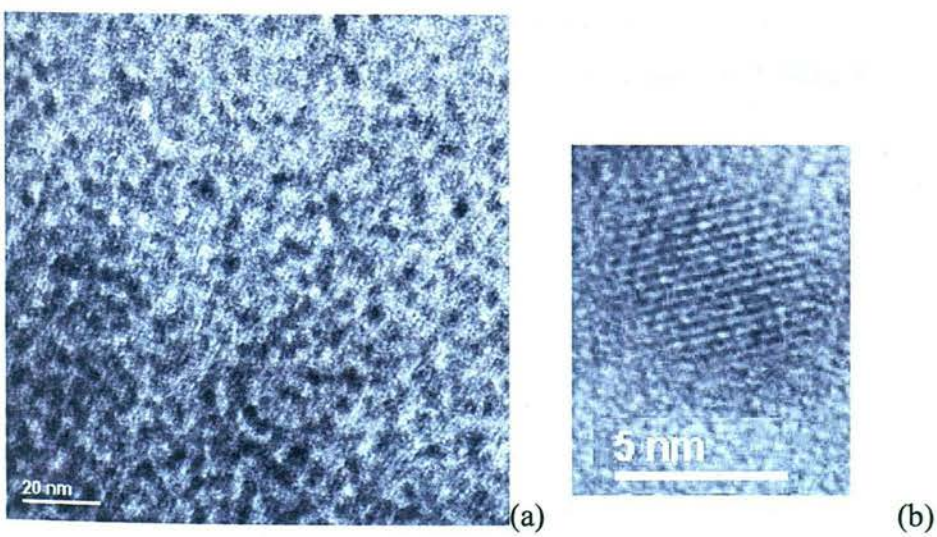

(a) (b)

Figure 2.16 TEM (a) images and HRTEM (b) images of CdSe/ZnS QD.

2.4.2 Synthesis of water soluble QDs

The first step in the QD water solubilisation process was to prepare dihydrolipoic acid (DHLA). The DHLA was successfully prepared by reduction of thioctic acid using sodium borohydride.[25] Then, CdSe/ZnS core/shell water soluble QDs were prepared by the ligand exchange method in which stearic acid on the QD surface was replaced with DHLA. Their optical properties were studied by UV-vis and fluorescence spectroscopy. For example a DHLA-coated CdSe/ZnS QD (QD-DHLA) with a first absorption peak at 561 nm (Figure 2.17) showed fluorescence emission maximum at 598 nm (excited with 350 nm light, Figure 2.18). HRTEM images of these nanocrystals revealed that they are spherical and monodisperse with a diameter of ~ 5.0 nm (Figure 2.19).

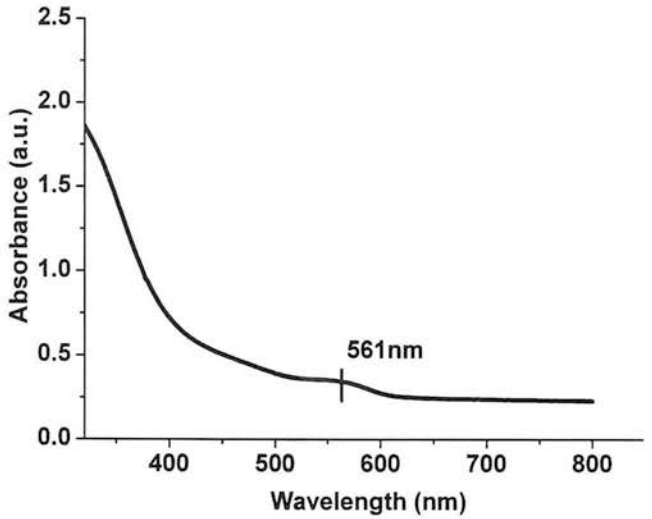

Figure 2.17 U.V-vis spectrum of water soluble QD-DHLA

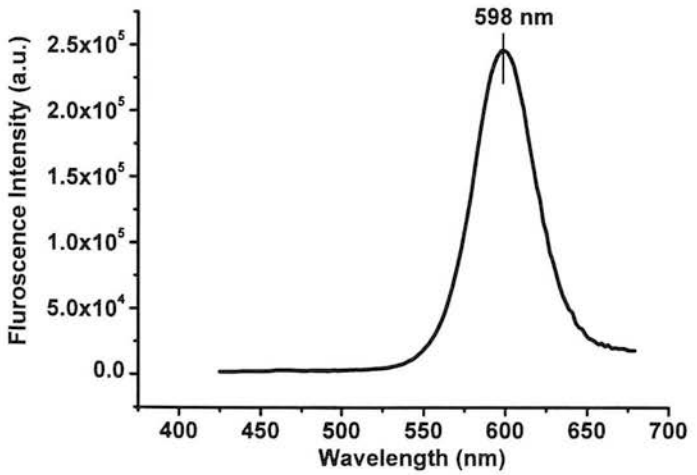

Figure 2.18 Fluorescence emission spectrum of water soluble QD-DHLA (Excitation at 350 nm, Temperature = 25°C)

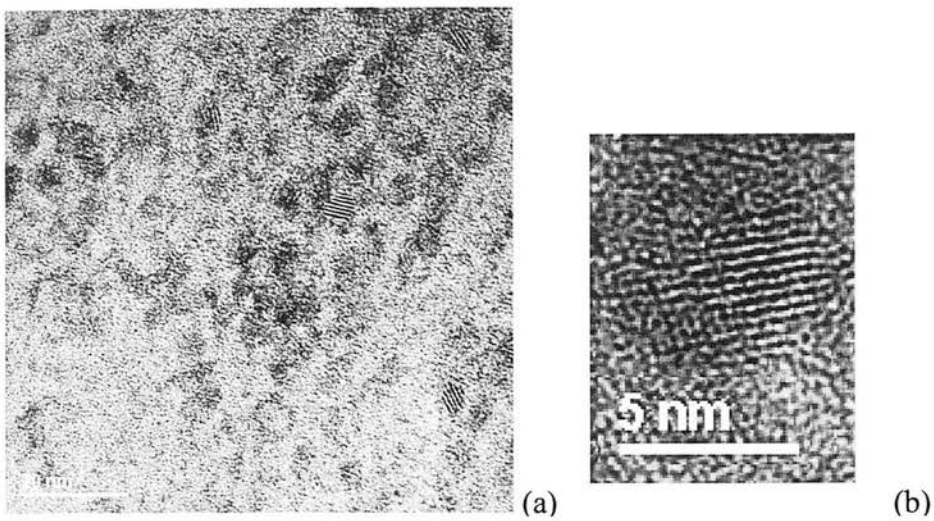

(a) (b)

Figure 2.19 TEM (a) images and HRTEM (b) images of water soluble QDs

2.4.3 Modification of QD surface by NTA and NTA-Ni^{2+} complex

The surface modification of DHLA-coated QDs with NTA-Ni^{+2} was accomplished as shown in Figure 2.20. It involved the reaction of DHLA-coated QDs with *N,N*-bis(carboxymethyl)-L-lysine hydrate (and its Ni^{2+} complex) using EDC and *N*-hydroxysuccimide as coupling agents in phosphate buffer solution. The position of the emission band did not change upon attachment of Ni-NTA units, and the photoluminescence intensity of the Ni-NTA-capped QD (QD-DHLA-Ni(NTA)) was found to be ca. 85% that of the metal free NTA-capped QD (QD-DHLA-NTA) (Figure 2.21). This is important because the paramagnetic Ni^{2+} was found to strongly quench the photoluminescence of some organic dyes, limiting their applications (see above).

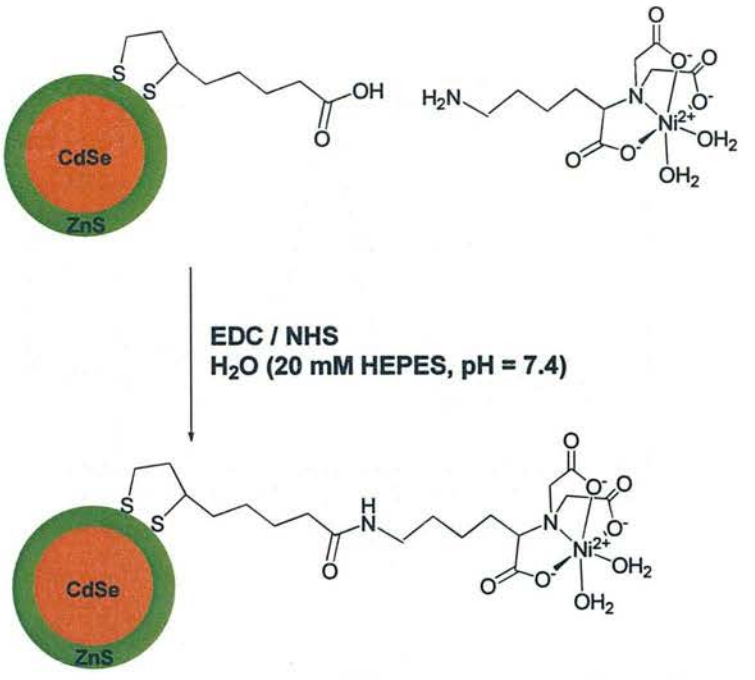

Figure 2.20 Scheme for the Ni(NTA)-functionalization of QDs.

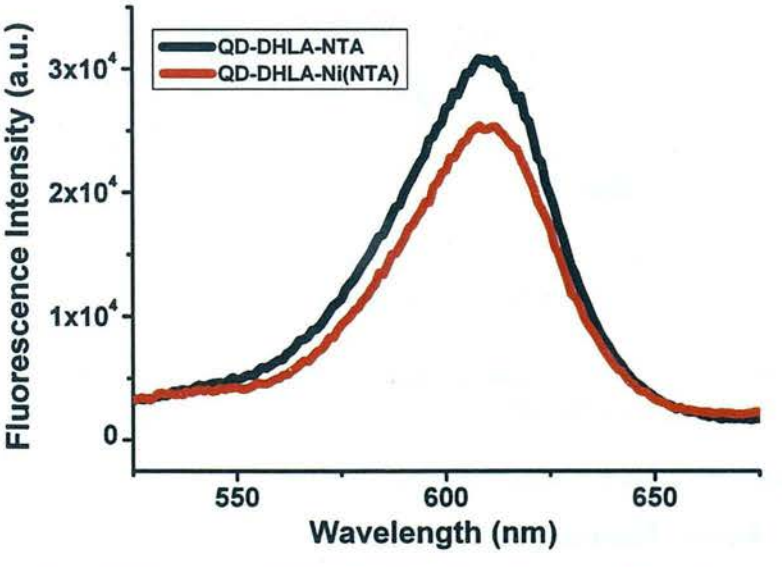

Figure 2.21 Pholuminescence spectra for CdSe-ZnS core-shell QDs coated with DHLA-NTA and DHLA-Ni(NTA) (Excitation at 350 nm, Temperature = 25°C)

The composition of the QDs was examined by X-ray photoelectron spectroscopy (XPS) and inductively coupled plasma-optical emission spectrometry (ICP-OES). The XPS spectra showed the main diagnostic peaks of the coupling of the NTA-Ni^{2+} units to the QD; a 2s peak at 400.1 eV due to N, and 2p3 and 2p1 peaks at 857.1 and 874.1 eV, respectively ,due to Ni^{2+} (Figure 2.22).

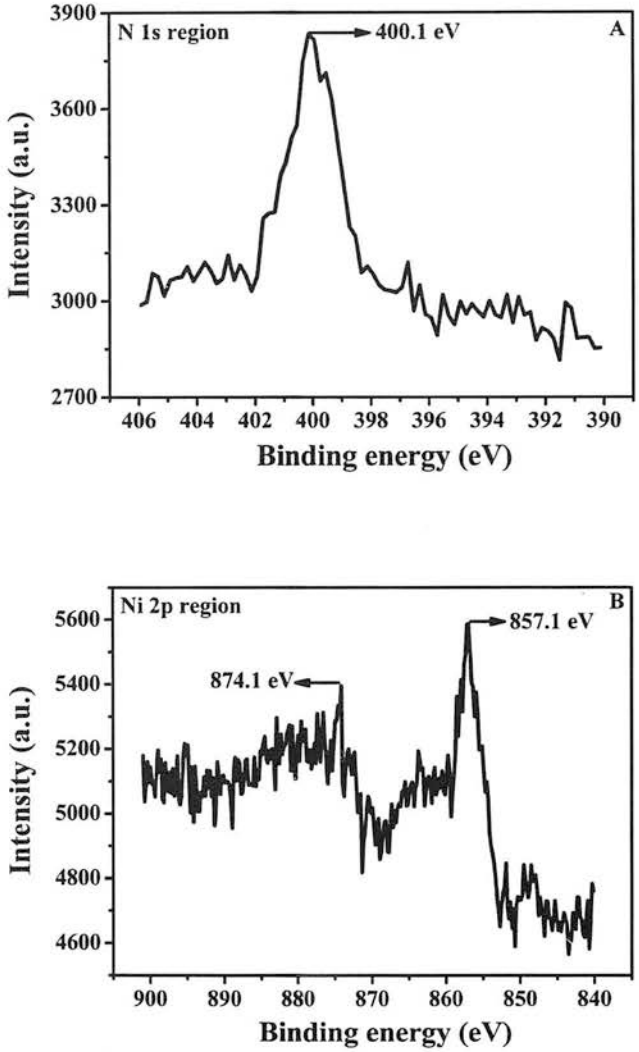

Figure 2.22 X-ray photoelectron spectra highlighting the (A) N 1s and (B) Ni 2p transitions of the DHLA-Ni(NTA) coated CdSe-ZnS core-shell QDs.

The amount of Ni-NTA units per QD was estimated by ICP-MS. For example QDs with a fluorescence emission maximum at 610 nm contained around 16 Ni-NTA complexes on the surface.

2.4.5 Protein binding studies

GST from the helminth worm *Schistosoma japonica* (SjGST, 26 kDa monomer) was selected as our target enzyme because it is amenable to overexpress GST in *E. coli* as an hexahistidine(His_6)-tagged construct and it is also well characterized.[34] It is important to note that the His_6-tag was genetically fused at the N-terminus. Site-specific attachment of GST to QDs was expected for the combination of QD-DHLA-Ni(NTA) and His_6-GST (Figure 2.23). To assess the extent to which this is the case a

series of protein binding study was carried out. Hexahistidine tagged GST (His_6-GST) and untagged GST (U-GST) were added to solutions of QD-DHLA-Ni(NTA), QD-DHLA-NTA, and QD-DHLA as stated in the experimental section. Nanosep 300 kDa Omega membrane (low protein-binding, modified polyethersulfone on polyethylene substrate) filters were used for isolation of the enzyme-QDs bioconjugates. Filtration was carried out for 1 h under ultracentrifugation, which gave enzyme-QDs conjugates in the concentrate and unbound enzyme molecules in the filtrate.

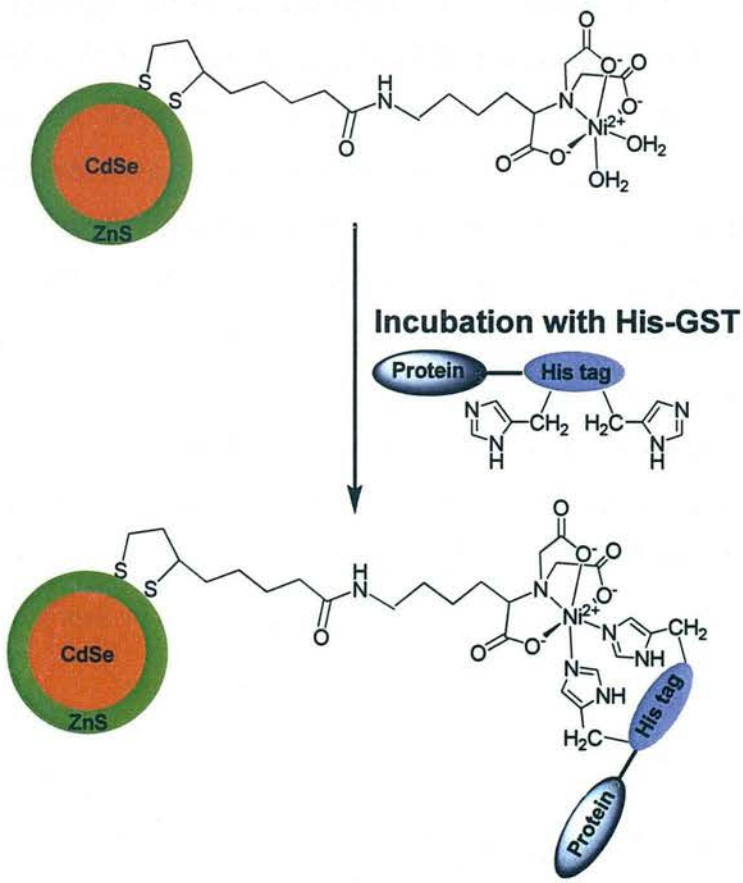

Figure 2.23 Scheme illustrating the strategy used for the attachment of His_6-GST on Ni(NTA)-functionalized QDs.

The non-covalent attachment of His_6-tagged and U-GST to the QD surface before and after derivatisation with Ni-NTA was analyzed by SDS-PAGE. A solution of the QD or PBS (as control) was incubated with the corresponding enzyme for 2 h and passed through a Nanosep 300kDa centrifugal device. The retentate was redissolved in PBS buffer, and both retentate and filtrate were analyzed by SDS-PAGE. In the absence of the QD, His_6-tagged and U-GST were found only in the filtrate. Several reports have shown that the DHLA-coated CdSe-ZnS core-shell QDs are capable of binding his-tagged proteins by coordination to Zn^{2+} ions at the nanocrystal surface.[35] Our SDS-

PAGE studies, however, did not find protein in the retentate (Figure 2.24). Lack of binding could be due to steric hindrance at the N-terminus location of the His_6-tag preventing access to the Zn^{2+} atoms of the nanoparticle. In contrast, using the same experimental conditions (QD: protein ratio 1:8) the Ni-NTA-capped QDs immobilized both enzymes. However, there was more His_6-GST than U-GST in the retentate (essentially no protein molecules were found in the filtrate), which is consistent with His-tag-Ni(NTA) recognition. Binding was also investigated in the presence of high salt concentrations. His_6-GST binding to Ni-NTA-capped QDs was not affected by 1 M NaCl. In contrast, U-GST did not bind to the QDs under these conditions, which suggests it is predominantly electrostatic. Thus, high salt concentrations can be used to avoid binding of untagged proteins while ensuring binding of the desired His-tagged target. The enzyme was easily released from the QD surface upon addition of 0.5 M (pH 7.4) imidazole, which competes for the Ni^{2+} binding sites. Thus, decorating the surface of the QD with Ni^{2+} complexes of NTA seems a good approach for non-covalent reversible site-specific fluorescent labeling of proteins, which can be used for instance if carboxylate-functionalized QDs lacking Ni^{2+} ions fail. Potential advantages of attaching Ni-NTA units to QDs could be stronger interactions with the histidine tag ($K_d \approx 10^{-13}$ M)[36] and less sensitivity to steric hindrance and surface properties by being further away from the nanocrystal surface.

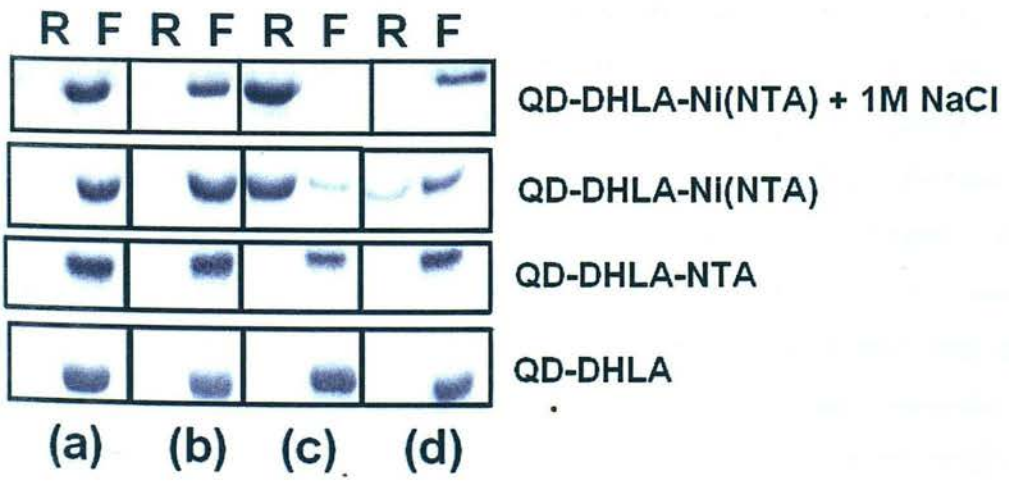

Figure 2.24 SDS-PAGE of the retentate (R) and filtrate (F) after ultrafiltration through a Nanosep 300 kDa filter of His_6-GST (a), U-GST (b), His_6-GST incubated with QD (c) and, U-GST incubated with QD (d). Coomassie blue staining was used in this study.

The loading capacity of Ni-NTA QDs for His_6-GST was estimated by BCA Assay. When Ni-NTA QDs (0.4 nanomole) were incubated with His_6-GST (2.7 nanomole) it was found that all the GST molecules had been attached to the QDs, consistent with the SDS-PAGE studies. After decreasing the amount of Ni-NTA QDs two-fold (0.2 nanomole) only 1.4 nanomole of His_6-GST protein molecules were attached to the QD; the remaining were found unbounded. When the amount of Ni-NTA QDs was decreased to 0.1 nanomole, only 0.27 nanomole of enzyme was attached and no protein binding was observed when the amount of Ni-NTA QDs was reduced to 0.05 and 0.025 nanomole. Based on this it seems that under these conditions ~7-8 molecules of His_6- tagged GST can be loaded on each QD. Since each QD had ~ 16 Ni(NTA) complexes, this suggests that only 50 % is available for protein binding.

The maximum number (purely based on geometric close-packing considerations) of His_6-GST molecules that can be loaded on each QD can be estimated using the equation IV.[26]

$$N_{His6} = 0.65\,(R_2^3 - R_1^3)/R_p^3 \quad \text{.....(IV)}$$

where R_1 is the core–shell nanocrystal radius with the lipoic acid and Ni-NTA cap and $R_2 \sim R_1 + 2R_p$ is the radius of the core–shell QD plus bound protein molecules. In this expression it is assumed that protein molecules are close-packed as spheres around a central QD and it takes account of the filling factor of hard spheres and adjusts the volume ratios by a factor of 0.65.[26] We have estimated the values for $R_1 = R_0$ + d(ZnS) + d(lipoic acid) + d(Ni-NTA) ~ 45 Å (where R_0 is QD core radius and d is the distance of ZnS shell, lipoic acid and Ni-NTA from the core radius) and R_2 ~100 Å ($R_p \cong 28$ Å where R_p radius of monomeric protein),[37] We have found theoretically ~ 27 His_6-GST molecules can be loaded per nanocrystal. For dimeric GST the theoretical maximum of GSTs per QD would therefore be ~13. Of course this theoretical estimate is subject to errors as the shape of the protein may not be spherical, nonetheless it gives a rough idea of the number of protein molecules which can be packed around the QD, and is consistent with the experimental result of 7-8 protein molecules per QD.

The protein purification efficiency of the Ni-NTA-capped QDs was also investigated by incubating *E. coli* cell lysates containing His_6-GST for 2 h. Remarkably, pure fluorescently labelled GST was obtained simply by ultracentrifugaton of this mixture

(Figure 2.25 B). Thus, by using the Ni-NTA-capped QDs it is possible to purify and fluorescently label histidine tagged proteins in a single step. Current methods for efficiently purifying and fluorescently labelling His-tagged proteins need various labour-intensive and expensive steps, such as conjugation of NTA derivatives on support materials or the preparation of suitable magnetic nanoparticles for purification purposes, followed by the attachment of fluorescent tags. Another construct suitable for one-step protein purification and site-specific labelling was recently developed and involves organic fluorophore-doped Ni-NTA-modified silica nanoparticles.[11]

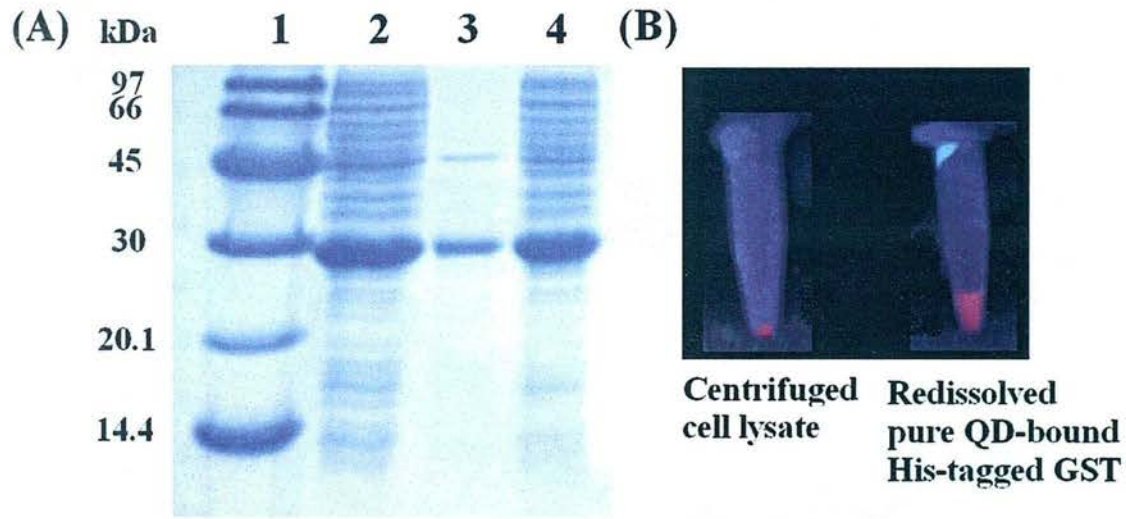

Figure 2.25 SDS-PAGE studies of the cell lysate containing His_6-GST (lane 2) and proteins released from the Ni-NTA-coated QDs treated with PBS containing 0.5 M imidazole (lane 3) and supernatant (lane 4) after ultracentrifugation. Lane 1 is the molecular weight marker. (B) Images of the cell lysate after ultracentrifugation and of the pure QD-bound His_6-tagged GST

2.4.6 Enzyme assay for biological activity

1-Chloro-2,4-dinitrobenzene (CDNB) was used as a substrate for measuring the catalytic activity of bound GST on QDs. The GST-catalysed reaction of GSH with CDNB produces a dinitrophenyl thioether which can be conveniently detected spectrophotometrically at 340 nm.[30] His_6-GST (14.93 U/mL) and U-GST (8.52 U/mL) were incubated with the same concentration of Ni-NTA-capped QD. It was found that His_6-GST retains full activity (14.7 U/mL) after binding to the QD, whereas non-specific binding of U-GST on QDs leads to ca. 70-75% of its activity (6.27 U/mL, Figure 2.26 A). Our hypothesis is that the ability of the His_6 -tag to control the position of the Ni-NTA-capped QD relative to the GST active site is responsible for

preserving the activity of the enzyme. The X-ray crystal structure of SjGST[23] shows that the N terminus, which is where the His_6-tag was placed, is ca. 25 Å away from the essential catalytic residue Tyr7 (Figure 2.26 B). On examining the distribution of positively and negatively charged residues it was found that there are positive and negative regions close to the active site. These are sites where in the absence of the His_6-tag non-specific electrostatic binding could occur, disrupting the enzyme activity. From the SDS-PAGE studies we estimated that ~25-30 % of the U-GST is captured non-specifically by the QD (see Figure 2.24), which suggests the activity found is only due to the unbound U-GST.

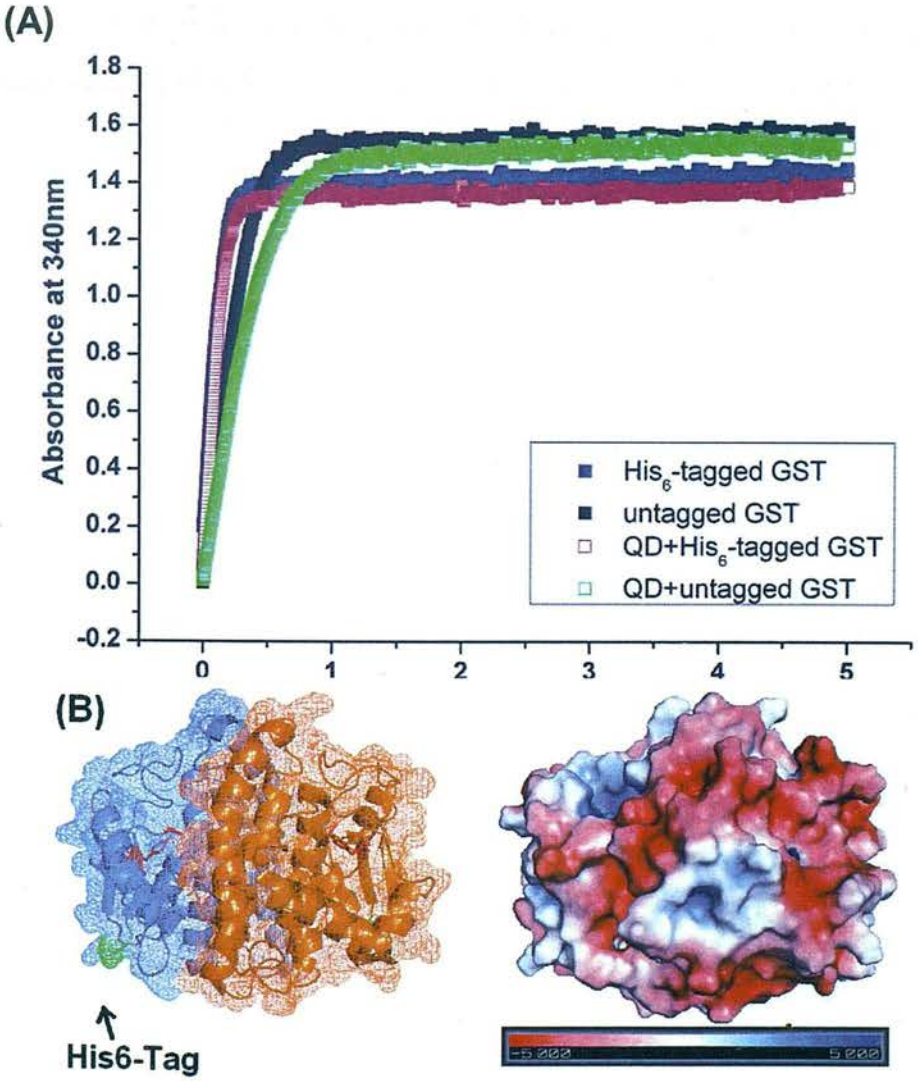

Figure 2.26 (A) Activity of His_6-tagged GST (N-terminal) and untagged GST in the presence of Ni-NTA coated QDs. Conditions: [GSH] = 8 mM, [CDNB] = 2 mM in PBS (pH 6.7), T = 25 °C. The QD alone did not have any activity. (B) X-ray crystal structure of the SjGST homodimer highlighting the catalytically crucial Tyr7 residue in red, and the N-terminus site for the hexahistidine- tagged in green (left); surface charge distributions (right).

2.5 Summary and Conclusion

In summary, in this study it was shown that Ni-NTA-coated QDs provide a straightforward method to, in one step, purify and fluorescently label proteins in a process that is reversible by addition of a competing ligand for His-tag. By using these Ni-NTA-coated QDs it is possible to purify and label the N-terminal His_6-GST which was impossible using QDs with carboxylates at the surface. Moreover, it was found that Ni^{2+} provides a docking site which helps to precisely orient the fluorescent nanoparticle on the protein surface, and that as a result, GST retained its activity. The use of His-tags has been broadly adopted in the molecular biology and biochemistry communities, and therefore this specific conjugation strategy should enable widespread use of these QDs for a broad range of biological applications.

2.6 References

(1) Arnau, J.; Lauritzen, C.; Petersen, G. E.; Pedersen, *J. Protein Expr. Purif.* **2006**, *48*, 1-13.

(2) Gaberc-Porekar, V.; Menart, V. *J. Biochem. Biophys. Methods* **2001**, *49*, 335-360.

(3) Hochuli, E.; Dobeli, H.; Schacher, A. *J. Chromatogr.* **1987**, *411*, 177-184

(4) Kapandis, A.N.; Ebright, Y.W.; Ebright, R.H. *J. Am. Chem. Soc.* **2001**, 123, 12123-12125.

(5) Lata, S.; Reichel, A.; Brock, R.; Tampe, R.; Piehler, J. *J. Am. Chem. Soc.* **2005**, *127*, 10205-10215.

(6) Goldsmith, C.R.; Jaworski, J.; Sheng, M.; Lippard, S.J. *J. Am. Chem. Soc.* **2006**,128, 418-419.

(7) Xu, C. J.; Xu, K. M.; Gu, H. W.; Zhong, X. F.; Guo, Z. H.; Zheng, R. K.; Zhang, X. X.; Xu, B. *J. Am. Chem. Soc.* **2004**, *126*, 3392-3393.

(8) Lim, Y. T.; Lee, K. Y.; Lee, K.; Chung, B. H. *Biochem. Biophys. Res. Commun.* **2006**, *344*, 926-930.

(9) Abad, J. M.; Mertens, S. F. L.; Pita, M.; Fernandez, V. M.; Schiffrin, D. J. *J. Am. Chem. Soc.* **2005**, *127*, 5689-5694.

(10) Lee, I. S.; Lee, N.; Park, J.; Kim, B. H.; Yi, Y. W.; Kim, T.; Kim, T. K.; Lee, I. H.; Paik, S. R.; Hyeon, T. *J. Am. Chem. Soc.* **2006**, *128*, 10658-10659.

(11) Kim, S. H.; Jeyakumar, M.; Katzenellenbogen, J. A. *J. Am. Chem. Soc.* **2007**, *129*, 13254-13264.

(12) Eaton, D.L.; Bammter, T.K. *Toxicol. Sci.* **1999**, 49, 156-164.

(13) Thom R.; Cummins I.; Dixon D.P.; Edwards R.; Cole D.J.; Lapthorn, A.J. *Biochemistry* **2002,** *41,* 7008-7020.

(14) Kaplowitz, N. *Am. J. Physiol.***1980**, *239,* G439-444.

(15) Hayes, J.D.; Flanagan, J.U.; Jowsey, I.R. *Annu. Rev. Pharmacol. Toxicol.* **2005**, *45,* 51-88.

(16) Armstrong, R.N. *Chem. Res. Toxicol.* **1997**, *10,* 2-18.

(17) Ladner, J.E.; Parsons, J.F.; Rife, C.L.; Gilliland, G.L.; Armstrong, R.N. *Biochemistry*. **2004,** *43,* 352-361.

(18) Townsend, D. M.; Tew, K.D. *Oncogene.* **2003**, *22*, 7369–7375

(19) Morel, F.; Rauch, C.; Petit, E.; Piton, A.; Theret, N.; Coles, B.; Guillouzo, A. *J. Biol. Chem.* **2004,** *279*, 16246-16253.

(20) Smith, D. B. *Applications of Chimeric Genes and Hybrid Proteins, Pt A* **2000**, *326*, 254-270.

(21) Zhan, Y.; Song, X.; Zhou, G. W. *Gene* **2001**, *281*, 1-9.

(22) Cardoso, R. M. F.; Daniels, D. S.; Bruns, C. M.; Tainer, J. A. *Proteins-Structure Function and Genetics* **2003**, *51*, 137-146.

(23) McTigue, M. A.; Williams, D. R.; Tainer, J. A. *J. Mol. Biol.* **1995**, *246*, 21-27.

(24) (a) Qu, L.; Peng X.; *J. Am. Chem. Soc.* **2002**, *124*, 2049-2055. (b) Jin, T.; Fujii, F.; Sakata, H.; Tamura, M.; Kinjo, M. *Chem. Comm.* **2005**, *34,* 4300-4302. (c) Jin, T.; Fujii, F.; Yamada, E.; Nodasaka, Y.; Kinjo, M. *J. Am. Chem. Soc.* **2006**, *128*, 9288-9289.

(25) Uyeda, H.T.; Medintz, I. L.; Jaiswal, J.K.; Simon, S.M.; Mattoussi, H. *J. Am. Chem. Soc.* **2005** , *127,* 3870-3878.

(26) (a) H. Mattoussi, J. M. Mauro, E. R. Goldman, G. P. Anderson, V. C. Sundar, F. V.Mikulec and M. G. Bawendi, *J. Am. Chem. Soc.* **2000**, *122,* 12142-12150.(b) Spurlino, J. C.; Lu, G. Y.; Quiocho, F. A. *J. Biol. Chem.***1991**, *266*, 5202−5219.

(27) Yu, W. W.; Qu, L. H.; Guo, W. Z.; Peng, X. G. *Chem. Mater.* **2003**, *15*, 2854-2860.

(28) Katari, J.E.B; Colvin, V.L.; Alivisatos, A.P.; *J. Phys. Chem.***1994**, 98, 4109-4117.

(29) Laemmli, U. K. *Nature* **1970**, *227*, 680-685.

(30) Habig, W. H.; Pabst, M. J.; Jakoby, W. B. *J. Biol. Chem.* **1974**, *249*, 7130-7139.

(31) Dabbousi, B.O; Veiejo, R.J.; Mikulec, F.V.; Heine, R.J.; Mattoussi, H.; Ober, R.; ensen F.K.; Bawendi, G.M. *J. Phys. Chem B.* **1997**, *101,* 9463-9475.

(32) Hines, M. A.; Guyot-Sionnest, P. *J. Phys. Chem.* **1996**, *100,* 468-471.

(33) Protasenko, V. V.; Kuno, M.; Gallagher, A.; Nesbitt, D. J. *Opt. Commun.* **2002**, *210*, 11-23.

(34) Esposito, D.; Chatterjee, D. K. *Curr. Opin. Biotechnol.* **2006**, *17*, 353-358.

(35) Medintz, I. L.; Clapp, A. R.; Mattoussi, H.; Goldman, E. R.; Fisher, B.; Mauro, J. M. *Nat. Mater.* **2003**, *2*, 630-638.

(36) Kim, J.; Park, H. Y.; Ryu, J.; Kwon, D. Y.; Grailhe, R.; Song, R. *Chem. Commun.* **2008**, *28*, 1910-1912.

(37) Spurlino, J. C.; Lu, G. Y.; Quiocho, F. A. *J. Biol. Chem.* **1991**, *266*, 5202-5219.

3.1 Introduction

In Chapter 1 various strategies for making water-soluble QDs were discussed. In Chapter 2, we applied the ligand exchange method to make water-soluble QDs with the ability to site-specifically label proteins as requirement for retention of biological activity. This chapter deals with using hydrophobic interactions and amphiphilic biomolecules for making bioactive hydrophilic QDs. Moreover, it investigates for the first time the extent to which the large size and multivalent nature of the resulting QDs can be useful for novel biological applications, specifically to mimic pathogens and elucidate how they interact and are processed by the immune system.

3.1.1 Hydrophobic-hydrophobic interactions for making biocompatible QDs

In 2002, Dubertret *et al.*[1] used hydrophobic-hydrophobic interactions to synthesise water-soluble QD-filled micelles. Phospholipids like 1,2-dipalmitoyl-sn-glycero-3-phosphoethanolamine-N-[Methoxy (polyethylene glycol](mPEG-200 PE) and 1,2 dipalmitoyl-sn-glycero-3-phosphocholine (DPPC) were used to encapsulate hydrophobic CdSe/ZnS QDs. In these amphiphilic polymers the hydrophobic part interacts with TOPO and other hydrophobic molecules on the QD surface and the hydrophilic part imparts water solubility.

In another interesting approach Osaki *et al.*[2] conjugated amphiphilic saccharides to CdSe QDs. These compounds have four alkyl chains and eight saccharide moieties (cellobiose, lactose, maltose or maltoheptaose) attached on opposite sides of calix[4]resorcarene. The four alkyl chains provided a site for hydrophobic association with TOPO on the QD surface while the hydrophilic saccharide units provided aqueous solubility to the assembly.

Recently Peng[3] encapsulated CdSe/ZnS QDs with the amphiphilic alginate natural polymer (Figure 3.1). It was based on the hydrophobic interactions between the QD's TOPO molecules and the octyl chain of alginate. These interactions result in phase transfer of hydrophobic QDs from organic solvents to aqueous solutions via the hydrophilic backbone (i.e. alginate).

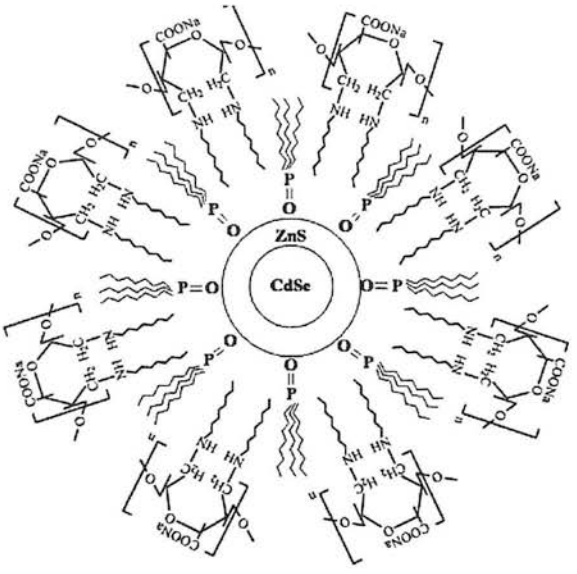

Fig. 3.1 Schematic drawing of CdSe/ZnS QDs encapsulated by amphiphilic alginate surfactant. (*Taken from Peng et al.*[3]).

3.1.2 Lipopolysaccharide (LPS)

3.1.2.1 Brief History of Endotoxins

Endotoxins are the compounds which cause "endotoxic" or "septic" shock.[4] Eugenio Centanni was an Italian pathologist who in 1894 extracted endotoxin from *Salmonella typhi* and other Gram-negative bacteria and which he called "Pirotoxina" because of its fever-inducing pyrogenic properties.[5] Centanni described at the time endotoxin as ubiquitous to many bacterial genera (pathogenic and non-pathogenic), and an agent which induces potent immune responses. In 1950 the chemical identity of endotoxin as lipoploysaccharide (LPS) was established, and in late 1970's the physical and biological properties of LPS were confirmed scientifically.[6] Chris Gallones and co-workers found lipid A (see below) as the active centre responsible for the endotoxic properties of LPS. They found lipid A to be the toxic and pyrogenic material which induces local Schwartzman reaction (skin lesions).[7]

3.1.2.2 Architecture of LPS

In LPS there are three different domains/regions which determine its properties. These are the O-polysaccharide or O chain containing repeating sugar units which are species-specific, the strain-specific core polysaccharide and the structurally-diverse lipid portion termed as lipid A (Figure 3.2).[8] Lipid A is the very hydrophobic and

endotoxically active part of LPS. The polysaccharide core region is covalently attached to lipid A and has an inner and outer core region. The inner core contains a high proportion of unusual sugars such as 3-deoxy-D-manno-octulosonic acid (Kdo) and L-glycero-D-manno-heptose (Hep) while the outer core contains more common sugars such as hexoses and hexosamines. The polymer of repeating saccharide subunits (O-polysaccharide) is attached to the outer core.[9]

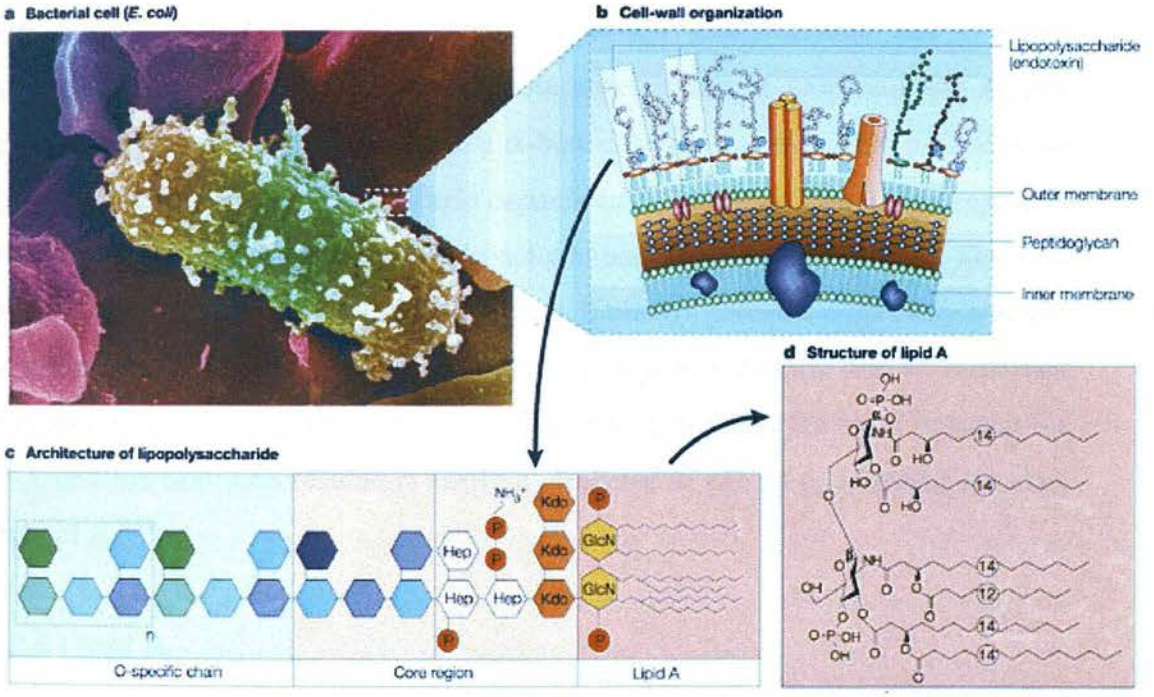

Fig 3.2 (a) Electron micrograph of *Escherichia coli.* (b) Schematic representation of the location of lipopolysaccharide (LPS; endotoxin) in the bacterial cell wall. (c) Architecture of LPS. (d) Primary structure of the toxic centre of LPS; the lipid A component . GlcN, D-glucosamine; Hep, L-glycero-D-manno-heptose; Kdo, 2-keto-3-deoxy-octulosonic acid; P, phosphate. *(Taken from Beutler et al.[11]).*

3.1.2.3 O-polysaccharide / O-region

This region contains between one and eight glycosyl residues which differ between strains in terms of sugars, sequence, chemical linkage, substitution, number of sugar units and ring forms utilized. As a result the O-region leads to limitless diversity; hundreds of serotypes have been observed for Gram negative bacteria. Moreover, the chain can contain between 0 and 50 subunits. In fact a single organism will produce a range of these lengths due to incomplete chain synthesis. In smooth type Gram-negative bacteria the O-region is the outermost part of their outer membrane, therefore it is a major antigen targeted by host antibody responses. This is a reason why sometimes the O-region is called the O antigen.[9] For some organisms, these O-

polysaccharide / O-region is essential to escape from lytic action by the compliment complex (i.e. survival in host serum) of the host. It also shields bacteria from numerous antibiotics.

3.1.2.4 Core polysaccharide

LPS structures have less variability in the core part than in the O-polysaccharide region. The outer core of LPS is generally more variable and is made up of common hexose sugars such as glucose, galactose, N-acetyl galactosamine and N-acetyl glucosamaine. The inner core is less variable and consists of more unusual sugars, particularly Kdo and heptose, which are α-bound to the carbohydrate backbone of lipid A. *Acinetobacter and Burkholderia cepacia* LPS are exceptions in this regard in that they have a 2 keto-D-glycero-D-talo-actonic acid (Ko) instead of Kdo. The Kdo domain is very important for bacterial viability. It always contains negatively charged substituents (such as phosphate groups). The core polysaccharide has an important role in modulating the endotoxin activity of lipid A. Typically, the bond between the lipid A and the first Kdo residue is easily hydrolyzed at pH <4.4, releasing the core form lipid A.[9,10]

3.1.2.5 Lipid A

The term lipid A is referred as the lipid domain of the LPS molecule. In 1985, it was found that lipid A is the part of LPS responsible for its endotoxic activity.

Lipid A consists of a β-1,6 linked diphosphoryl–D-glucosamine (D-GlcN) disaccharide with phosphate groups at positions C-1 and C-4' and up to seven hydroxylated fatty acid residues in ester or amide linkages (Figure 3.3). In some bacteria additional negatively and positively charged moieties such as phosphoethanolamine (PEtN), 4-amino-4-deoxy-L-arabino-pyranose and D-galacturonic acid are present. Lipid A is the part of LPS which anchors to the host cells.[8]

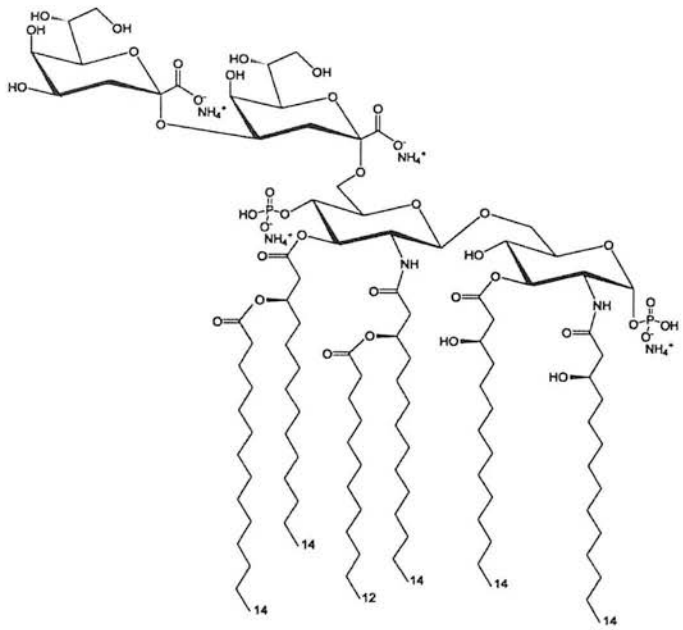

Fig 3.3 Structure of Kdo_2-lipid A. *(Taken from Sasaki et al.[12]).*

3.1.2.6 Mode of endotoxin action

The mammalian innate immune system senses pathogen associated molecular patters (PAMPs; evolutionary conserved, pathogen-derived motifs which the host uses to discriminate self from non-self) using a range of pattern recognition receptors (PRRs), among which the Toll-like receptors (TLRs) are particularly important.[13] In the case of LPS, it is widely accepted that the Lipid A unit activates TLR4 on the extracellular side of the membrane of cells of the innate immune system. There is also widespread agreement that TLR4 is required for signalling through a group of Toll/interleukin-1 receptor (TIR)-adaptors (TIRAP (also known as Mal), MyD88, TRIF and TRAM).[14] However, it is known that other receptors are involved in LPS-induced cell activation and that these form receptor clusters. LPS binding protein (LBP), CD14, MD2, the macrophage scavenger receptor (SR-A) and β2 leukocyte integrins CD11b/CD18 have been shown to participate in LPS-induced cell activation.[15] It has been shown that both CD14 and CD11/18 are capable of initiating signals to cell, resulting in phagocyte activation, bacterial internalization (phagocytosis, endocytosis), and the activation of bactericidal defences.[16] These complex binding/signalling events then lead to the production and release of cytokines and various other effects which result in the killing and clearance of the invading pathogen (Figure 3.4). However, the biologic importance of LPS internalization and its relationship to signalling are

disputed, and it is also not clear if the aggregation state affects the mode of internalization and signalling.[17]

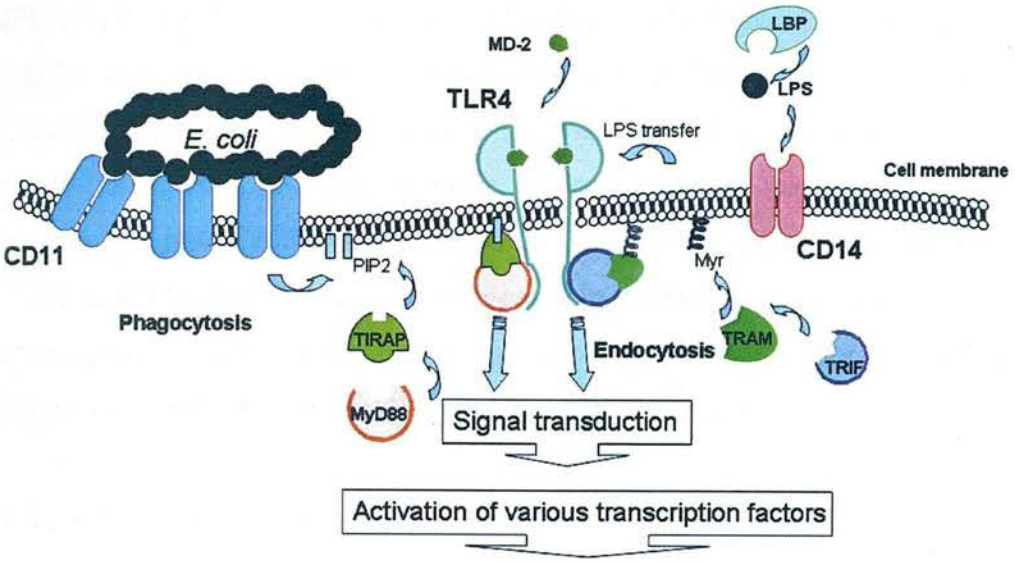

Fig 3.4 Mode of interaction of LPS with immune cells.

3.1.2.7 Role of LPS derivatives in vaccine technology

Vaccines are the best weapons for combating infectious diseases but for many of these diseases effective vaccines are yet to be developed. For example, vaccines are needed for parasitic diseases like HIV, malaria and tuberculosis which kill over 5 million people per year. Vaccines are also urgent for diseases like hepatitis C, shigellosis, respiratory synctitial virus, dengue fever, schistosomiasis and influenza.[18] Finding an effective vaccine requires not only an antigen but also an immune potentiator (adjuvant) and a delivery system.[19] The role of the adjuvant is to trigger early innate immune responses, which then lead to the generation of robust, long-lasting adaptive immune responses. The list of adjuvants which are already in use in vaccines or in clinical trials includes mineral salts (e.g. alum which is aluminium hydroxide),emulsions and surfactant-based formulations (e.g. MF59), organic particulate-based delivery vehicles (e.g. liposomes), microbial derivatives (e.g. LPS/MPLA), whole cells and cytokines (e.g. dendritic cells, IL-12), saponins (QS-21) and CpG oligos.[19] All these adjuvants have significant limitations, and thus finding new adjuvants and delivery systems has become a major target and bottleneck in the development of new and more effective vaccines. Moreover, it has been suggested that the combination of delivery systems, immune potentiators and isolated antigens will be required for optimal immune responses.[19] LPS derivatives like

monophosphoryl lipid A (MPLA, Fig. 3) are strong candidates to become the first approved adjuvant for widespread use since alum.[19] However, the stimulatory effects of MPLA (and LPSs) rely on a complicated sequence of events which involve a range of proteins as stated in the previous section (3.2.1.6). These events have not been structurally characterised in live cells or *in vivo*, and are likely to differ for each chemically different LPS. For example, it is interesting that MPLA generates clinically useful immune responses with only 0.1 % of the inflammatory toxicity of LPS. This could be due to structural changes (e.g. having only one phosphate ester) inducing subtle changes in the molecular interactions with these proteins.[20] Thus, attachment of LPS derivatives to QDs could lead to exciting results.

3.1.2.8 LPS and septic shock

Immune responses to LPS also play a key role in sepsis and septic shock, which is the most common cause of mortality in intensive care units worldwide.[21] Sepsis is a harmful and damaging response from bacterial infection and when sepsis causes life-threatening low blood pressure, this condition is called septic shock. Several peptides natural and synthetic bind and block LPS activity by exploiting electrostatic and H-bonding interactions e.g. polymyxin B, defensins, buforin, lactoferricin B and magainin.[21] The prototype is polymyxin B (PMB), for which the K_d of the PMB-LPS complex has been estimated to be 1 μM.[22] But due to PMB toxicity it is only used in topical applications and extracorporeal removal of endotoxins. Since many new nanomaterials can potentially bind to LPS investigating the immune responses to LPS when is attached or interacting with nanoparticles is becoming increasingly important.

3.1.3 Nano/microparticle containing LPS

Because of its high toxicity LPS cannot be used directly for immunization in humans. Thus, some researchers have started to investigate if the toxicity of LPS can be reduced by encapsulation inside polymer micro/nanoparticles.

Murillo *et al.*[23] encapsulated a hot saline antigenic extract (HS) from *Brucella ovis (B. ovis)* in poly-ε-caprolactone (PEC) microparticles. This vaccine was tested against *B. ovis* and *B. abortus* infection in mice. It was found to induce high amounts of IFN-γ (peptide responsible for activation of T-helper 1 [T_h1] immune cells) and IL-2 (growth factor for all immune cells) but low quantities of IL-4 (peptide responsible

for activation and growth of T-helper 2 [T_h2] immune cells) suggesting a combined T_h1/T_h2 cellular response. Subcutaneous and oral vaccination protected mice against *B. ovis* infection. Free HS or empty polymer microparticles did not produce any protective effect against brucellosis.

Recently in another study Gantrez ® (poly(methyl vinyl ether-co-maleic anhydride, MW 200,000) nanoparticles were used to deliver the *B. ovis's* LPS for effective vaccination against anaphylactic shock. LPS of *B. ovis* co-encapsulated with ovalbumin (OVA) were used as model allergen inside nanoparticles. They demonstrated that these modified nanoparticles can induce high level of IL-10 (peptide which suppress inflammatory reactions) thus showing highly interesting adjuvant properties for immunotherapy.[24]

In another study LPS functionalized iron oxide nanoparticles were used for antibody detection purposes. The iron oxide nanoparticles were functionalized with LPS from *B. abortus* by adsorption. Variation in magnetic relaxation in these particles was related to their hydrodynamic volumes and measured using an A.C. susceptometer. The changes in relaxation frequencies for the LPS functionalized nanoparticles was used as a proof of attachment of LPS on the nanoparticle surface. When these LPS functionalized nanoparticles were mixed to the biological sample (serum) for detection of *Brucella* antibodies, it led to particle size increases of 25-35%, which were consistent with antibody binding. The antibody detection limit was found to be 0.05 $\mu g\ mL^{-1}$.[25]

3.1.4 Liposomal preparations of lipid A

Liposomal preparations containing Lipid A have also been prepared with the intention of reducing the immunogenicity of this biomolecule for use in vaccine therapy.

The first liposome containing Lipid A was prepared by Schuster *et al.*[26] in 1979. The Lipid A used was isolated from *Shigella flexneri* LPS. They demonstrated that when one adjuvant (liposome) served as the carrier for the other adjuvant (lipid A) then the combination resulted in enhanced antibody formation against Lipid A in rabbits. They also confirmed that the liposome alone do not trigger any detectable immune response. In another study the biological activity of LPS and lipid A from *Salmonella minnesota* encapsulation within liposomes was studied. The liposomes formed were used to activate peritoneal macrophages which initiate both innate and cell mediated

immunity. It was found that *in vitro* the liposomal LPS was 100-1000 fold less potent inducing IL-1 (a peptide which induces and promotes inflammatory responses) and TNF (a mediator of inflammatory responses) that LPS alone.[27] Similarly, in another study *Neissera meningitis* LPS was incorporated into a liposome and 1000 fold decrease in the endotoxin activity was observed.[28] Dijkstra *et al.*[28] proposed that a direct interaction of Lipid A with appropriate plasma membrane components is necessary to trigger the biological response efficiently. Insertion of LPS into liposome can prohibit this interaction leading to less immunological activity.

In an interesting study the circumsporozite protein (CSP, a major malaria parasite surface protein during the sporogonic cycle) from *Plasmodium falciparum* was encapsulated inside a liposome made up of LPS. These immunogenic liposomes were used in phase I human preclinical studies, in which it was found that these immunogenic liposomes containing this malaria antigen cause very strong specific humoral immunity without any acute toxicity.[29]

3.1.5 Fluorescent sensing for phosphorylated peptides /proteins

Protein phosphorylation is widely involved in switching enzymatic activity and signalling transduction cascades of living cells. As a result the development of molecular probes which can selectively recognize phosphorylated proteins and enzymes has become an important target.[30]

Recently, artificial receptors containing dinuclear complexes have been found useful in recognizing and sensing phosphorylated proteins. This is because they exploit metal-ligand interactions which are stronger and more effective for phosphate binding/recognition in aqueous medium than other more commonly used interactions like hydrogen bonding and electrostatic interactions.[31] Zinc complexes which use dipicolylamine (DPA) as metal binding ligand have been proven to be particularly effective, providing association constants of around 10^7 M^{-1} in water.[32,33]

For example receptor **1** (Figure 3.5) combines the phosphate binding ability of the Zn-DPA units with the fluorescent properties of the anthracene unit to form 1:1 complexes with phosphorylated peptides with affinities ranging from 10^4 to 10^6 M^{-1}, depending on the peptide sequence. Binding of the phosphate species to the receptor is reported by an increase in fluorescence (~ four-fold increase). It was found that the

fluorescent enhancement was due to a three-stage assembly process (Figure 3.6): 1) binding to the first Zn(II), 2) phosphate binding and 3) binding of the second Zn(II) ion. Importantly, this sensor has excellent selectivity for the phosphorylated peptides over other common biologically relevant anions like chloride, inorganic phosphate and carboxylate.[33]

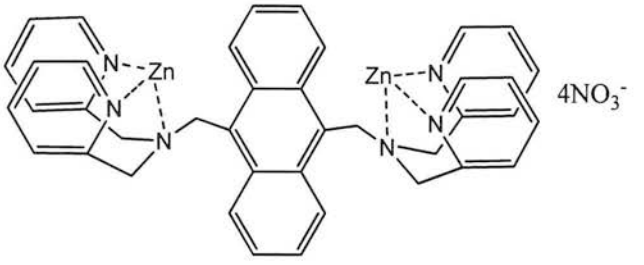

Figure 3.5 Molecular structure of an artificial phosphate receptor/sensor (1).

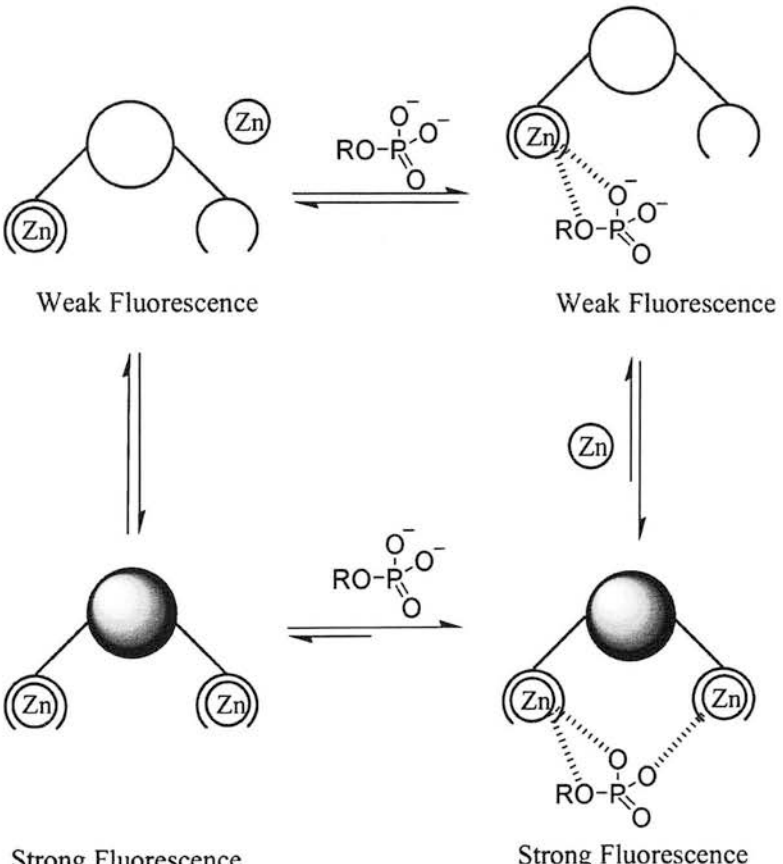

Figure 3.6 Mechanism of fluorescent enhancement and PET quenching.
(Taken from O'Neil et.al.[31])

Smith *et al.*[31] used the same principle for sensing bilayer membrane surfaces (liposomes) that were enriched with anionic phospholipids such as phosphatidylserine.

We have found that this anthracene-derived bis(Zn^{2+}–DPA) complex, and related Zn-DPA complexes can act as effective pattern recognition receptors for LPS sensing purposes via recognition of the anionic phosphate esters within lipid A.[34] Recently, Smith *at al.*[35] have reported that as a result of this latter property these complexes selectively target the surface of bacterial cells.[35]

3.1.6 Multivalency and its importance in biological systems

The 'valency' of a molecule or particle is the number of groups of the same type which this compound possesses. Thus, multivalent species are those which carry several groups of the same type. Many biological systems are activated through simultaneous binding of groups or ligands to the same receptor, and thus it has become an important tool for designing drugs and vaccines.[36] Because the interactions which arise from multivalent species are stronger than those of monovalent species they are very useful in initiating signal transduction responses. An interesting example of multivalency is the adhesion of the influenza virus to the surface of the bronchial epithelial cells, which results in binding of several copies of the virus hemagglutinin (HA) to sialic acid (SA) on bronchial epithelial cell (Figure 3.7).[36]

Gold nanoparticles have been used as a scaffold for exploiting multivalency of biomolecules (pathogenic polysaccharides) with the intention of developing more effective synthetic vaccines. For example, Manea *et al.*[37] prepared sacccharide-functionalized gold nanoparticles by self assembly as fully synthetic analogs of type A *Neisseria meningitides* antigens for protection against meningitis. They found that these nanoparticles were two times more antigenic than the corresponding oligomeric saccharides and that this was the result of the multivalent character of the nanoparticles.

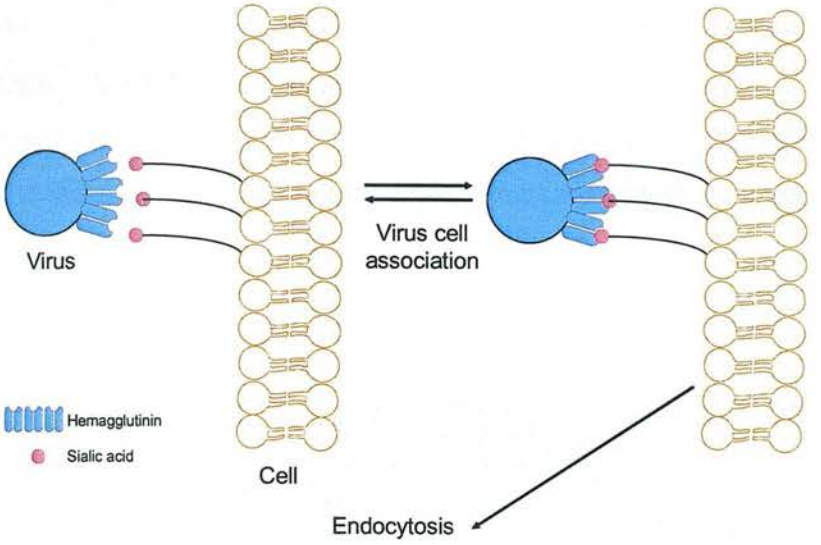

Figure 3.7 The influenza virus attaches to cells by interaction of trimeric hemagglutinin (HA_3, shown as protruding cylinders on the virus) with sialic acid (SA, shown as caps on the cells).

3.2 Motivation for the work

In Chapter 1 we have described why colloidal quantum dots (QDs) have become important materials in biology as alternatives to traditional organic dyes. But there are important differences between conjugation of biomolecules to QDs and organic dyes. An important one is that QDs are multivalent and have a size comparable or larger than most biomolecules, and therefore, a relatively large number of biomolecules can be conjugated to a single QD. Indeed, it is difficult to ensure that a single biomolecule is attached to them and is still biologically active. In most cases proving that the biomolecule is active has meant showing that molecular recognition with an appropriate partner does occur. However, this is not enough proof and biological activity may be more complex than this e.g. it may involve catalysing chemical reactions with specific efficiency or coupling molecular recognition with signalling events. Studies which have investigated this aspect reported both loss and preservation of biological activity.[38-41]

We considered that the nanometer-size and multivalency of QDs could be particularly useful to mimic and study how biomolecules and/or a combination of biomolecules in the proximity of each other behave and interact with cells, tissues, organs etc., possibly more so than to study the behaviour of biomolecules which may require being in isolation (focus so far in QD labelling of biomolecules). In Chapter 3 *E. coli*

LPS is attached to QDs by hydrophobic interactions so that it could mimic the surface of Gram negative bacteria and therefore be useful model materials to investigate how pathogens interact and are processed by the immune system (Figure 3.8). The interaction of LPS with the QD and of the QD-LPS conjugates with cells of the immune system is investigated, as are the immune responses generated *in vivo* and *in vitro*.

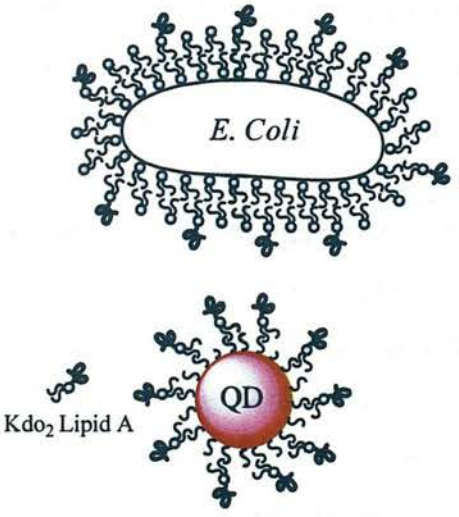

Figure 3.8 Illustration of strategy used in this study to create a biomimetic, artificial and fluorescent bacteria.

3.3 Experimental

3.3.1 Materials

All chemicals were obtained from commercial sources and used as received. Cadmium oxide (CdO, 99.5%), tri-*n*-octylphosphine oxide (TOPO,99%), tri-*n*-butylphosphine (TBP, 97%), hexadecylamine (HDA, 98%), diethylzinc ($ZnEt_2$,1M in hexane) and hexametyldisilathiane [$(TMS)_2S$ 98%], were purchased from Sigma Aldrich. Stearic acid (98.5%) was purchased from Fluka. Selenium powder (Se, 99.999%) was obtained from Alfa Aesar. *E. coli* LPS (Kdo2-lipid A) was obtained from Avanti Polar Lipids. The Purity of *E. coli* LPS (Kdo2-lipid A) was checked by gel electrophoresis (DOC-PAGE) in Dr. Dominic Campopiano lab from School of Chemistry, University of Edinburgh. This material is a mixture of 6 LPSs from E. coli strain WBB06 which is deep rough. The hydrophobic CdSe/ZnS QDs were prepared as described in Chapter 2, the results presented here were obtained with QDs which had the first absorption band at 628 nm, and a maximum emission peak at 642 nm with excitation at 350 nm. BCA protein Assay kit was purchased from Pierce Biotechnology. The *in vitro* and *in vivo* biological studies were performed by Dr. Tom A. Barr and Martin Krembuszewski in the laboratory of Prof David Gray, School of Biological Sciences at the University of Edinburgh.

3.3.2 Synthesis of QD-LPS Micelles

QD-LPS micelles were prepared using two different methods (Method A and B).

Method A. Hydrophobic QDs (1.5 mg, 0.36 nanomole) were combined with pure Kdo_2-lipid A (*E.coli* LPS) (200 µl, 43 µM) and sonicated for 1 min. LPS functionalized nanoparticles forms a suspension after sonication. The suspension was kept for 4 h at room temperature to ensure the formation of micelles by hydrophobic interactions. This suspension contained both empty micelles and those containing QDs, the empty micelles were removed with ultracentrifugation cycles (5×60 min) at 11,000 g. The micelle containing QDs formed a pellet while the empty micelles stayed suspended. The successive supernatants were discarded and the final QD-micelles were resuspended in 250 µl of water, which gives a QD concentration of 0.089×10^{-6} M (according to ICP-OES studies).

Method B. As above but using 2.5 mg of QD (0.6 nanomole) and 250 μL of 430 μM LPS (1 mg/mL). This method gives a final QD concentration of 0.31×10^{-6} M. (according to ICP-OES studies).

3.3.3 Synthesis of QD-PC/PEG-PE Micelle

QD-PC/PEG-PE micelles were prepared according to a recently published procedure.[42] In a 5 mL round-bottomed flask, 100 μl of a chloroform solution of hydrophobic QD (2 mg in 100 μl of chloroform; 5 μM) and 50 μl chloroform solutions of 1,2-dipalmitoyl-*sn*-glycero-3-phosphoethanolamine-N-methoxy(polyethylene glycol)-2000] (ammonium salt) (2 mg in 50 μl of chloroform; 15 mM) and 1-palmitoyl-2-oleoyl-*sn*-glycero-3-phosphocholine (PC) (1 mg in 50 μl of chloroform; 26 mM) were mixed together. The flask was left open at room temperature for 3 h in a fume hood to slowly evaporate the chloroform solvent. Any remaining chloroform was removed under vacuum using a rotary evaporator to form a thin film. The flask containing the QDs was then heated in water bath set to 80°C for 30 s, after which 250 μl of doubly deionized water was quickly added. Addition of water forms a suspension containing both empty micelles and those containing QDs. Large aggregates were removed by two centrifugation cycles at 11,000 g and empty micelles were removed by centrifugation cycles (2 × 45 min) at 300,000 g. The micelles containing QDs formed a pellet while the empty micelles remained in suspension. The successive supernatants were discarded and the final QD-PC/PEG-PE micelles were resuspended in water.

3.3.4 Transmission Electron Microscopy (TEM)

High-resolution transmission electron microscopy (HRTEM) studies were conducted on a JEOL JEM-2011 electron microscope operating at 200 kV. The samples were prepared by depositing a drop of a solution of nanocrystals in pyridine onto a copper specimen grid coated with an holey carbon film and allowing it to dry.

3.3.5 Inductively coupled plasma - optical emission spectrometry (ICP-OES)

For ICP-OES samples were prepared by breaking down the QDs (40 μL) with 960 μL of concentrated nitric acid for 5 days. The samples were then diluted to 10 mL with Millipore water. Samples were analyzed by using Perkin Elmer Optima 5300 DV ICP-OES. The concentrations of Cd, Se, Zn, S ions were estimated from calibration curves prepared by using standard solutions, from which the total amount of Cd, Se, Zn, S in the CdSe/ZnS QDs was estimated.

3.3.6 Dynamic Light scattering (DLS)

DLS data was obtained on a Malvern's Zetasizer Auto plate sampler (APS) equipped with 50mW 830nm Single-mode fibre laser. A 384-well microplate was used as sample container and 45 μL of sample was used for each study. Because the solute was CdSe/ZnS, the reflective index was set to 2.50. Typically, the experiment was carried out for 3 runs of 2 minutes each, and analyzed using the "number" (first-order) Multimodal Size Distribution.

3.3.7 Fluorescent sensing and quantification of LPS molecules on QD micelle by anthracene-derived bis(Zn^{2+}–DPA) complex

Fluorescence studies were carried out with an Edinburgh Instruments FS900 fluorometer. Excitation was at 380 nm and 500 nm with bandwidths of 2 nm for excitation (unpolarised) and emission (unpolarised). U.V-vis studies were measured using the Perkin Elmer Lambda 900 UV-vis Spectrometrer and the cuvettes had a path-length of 1 cm.

QD-LPS and QD-PC/PEG-PE micelles were titrated with increasing concentrations of anthracene-derived bis(Zn^{2+}–DPA) complex {**1**} in HEPES (20 mM, pH 7.5). For each concentration of **1** a fluorescence spectrum was obtained in the presence and absence of the QD micelles. The QD-LPS micelle attached to **1** were separated from the unbound molecules of **1** by passing these solutions through a Nanosep 100 kDa centrifugal device.These solutions were then treated with EDTA (15 mM) to release the anthracene-$(DPA)_2$ ligand (Filtrate 1 in Figure 3.16).Retentate containing the QD-LPS-bound molecules of **1** were also treated with EDTA to release the anthracene-$(DPA)_2$ ligand from the QD-LPS micelles, and then passed through a Nanosep 100 kDa Omega membrane filter (Filtrate 2 in Figure 3.16). Both filtrate fractions were

analysed by UV-vis and the concentration of anthracene-$(DPA)_2$ was calculated from the extinction coefficient of **1** in the presence of EDTA (15 mM) at 260 nm (ε = 32,500 L • mol^{-1} • cm^{-1}) in HEPES (20 mM, pH 7.5).

3.3.8 *In-vitro* Studies

3.3.8.1 Cell culture

The J774A.1 macrophage/monocyte cell line was obtained from the European Collection of Cell Cultures (ECACC). Cell cultures were grown at 37 °C in a humidified atmosphere of 5% CO_2 in 30 mL of complete medium (Isocove's Modified Dulbecco's Modified Medium (IMDM) , containing phenol red, L-Glutamine (2 mM), Penicllin/Streptomycin (50 U/mL) (Pen/strep) and 5 % Foetal Calf Serum (FCS)). Cells were grown to confluence after which they were removed from the culture flask via gentle scraping and then resuspended in complete medium. Cell viability was determined using Trypan blue (0.1% solution) exclusion. Cells were adjusted to a suspension of 2.5×10^5 cells mL^{-1} in medium and used for the subsequent experiments.

3.3.8.2 Preparation of bone marrow-derived dendritic cells (BMDCs)

C57BL/6 mice at 6 weeks of age were bred at The University of Edinburgh animal facility. Bone marrow cells were cultured in RPMI 1640 medium, containing phenol red, L-Glutamine (2 mM), Pen/Strep (50 U/mL) , 10 % FCS and 20 ng /mL of Granulocyte-monocytes colony-stimulating factor (GM-CSF). The DC culture medium was replaced every 2 days to replenish GM-CSF and remove non-adherent cells. Cells were harvested by gentle aspiration on day 7 and then were used as immature DC for *in vitro* assays.

3.3.8.3 Cytokine Assay

In a 96 well-plate, 100 µL of BMDCs or J744 Macrophages in IMDM medium (2.5×10^5 cells mL^{-1}, 25,000 cells per well), 50 µL of IMDM medium and 50 µL of the QD solutions (15 nM), LPS (250 nM) or PBS alone were incubated for 16 h (macrophages) or 24 h (BMDCs) at 37 °C in an humidified atmosphere of 5% CO_2. Cultures were performed in triplicate in a final volume of 200 µL (100 µL cells, 50 µL compound and 50 µL PBS). An additional group of cultures were set up with the LPS

inhibitor polymyxin B (final concentration 250 μM) instead of PBS. The same studies were simultaneously carried out with ten-fold serially diluted samples. After 24 h, supernatants were harvested by centrifuging plates at 400g for 3 min. and gently removing medium from cells. Supernatants were then frozen at -20°C until used. Cytokine (IL-6) was quantified by capture ELISA. Plates were coated overnight with 50 μl (10 μg/mL) IL-6 capture antibody (clone MP5-20FS, BD Pharmingen, UK). The following morning plates were washed with PBS/Tween 20 (0.05%) (Sigma Aldrich) and non-specific binding blocked with 2% bovine serum albumin (BSA). Samples (and recombinant cytokine for standardisation at 20 ng/mL to 9.8 pg/mL) were then applied to the plate. Following a 1h incubation at RT, plates were washed three times with PBS/Tween and a detection antibody (biotin labelled MP5-32C11, BD Pharmingen) added. Following a further 1 h incubation at RT and washing, streptavidin-alkaline phosphatase was added to the plates. Plates were again incubated and washed and then 50 μL (1.35×10^{-4} M) *p*-nitrophenyl phosphate (PNPP) substrate added to the plate. Optical density at 405 nm was measured and cytokine concentration determined by extrapolation from the recombinant cytokine standard curve.

3.3.9 *In-vivo* studies

3.3.9.1 Animal vaccination

C57BL/6 mice at 6-8 weeks of age were bred at The University of Edinburgh animal facility. For intraperitoneal (i.p) vaccination with the DNP-OVA antigen, four groups of animals (n = 5 per group) were injected into the peritoneal cavity with:

- a 200 μl solution containing a single dose of 100 μg of DNP-OVA (20 μL, 5 mg/mL) co-administrated with QD-LPS nanoparticles (40 μL, 235 nM, 95 pmol) in PBS (140 μL);
- a 200 μl solution containing a single dose of 100 μg of DNP-OVA (20 μL, 5 mg/mL) co-administrated with LPS (40 μL, 43 μM, 4 μg) in PBS (140 μL);
- a 200 μl solution containing a single dose of 100 μg of DNP-OVA (20 μL, 5 mg/mL) co-administrated with 180 μL PBS.

For subcutaneous (s.c.) vaccinations with the DNP-OVA antigen, animals (n = 5) received a single dose of 100 μg of DNP-OVA antigen (20 μL, 5 mg/mL), co-administrated with *E. coli* LPS (10 μL, 43 μM, 10 μg) and 70μl PBS, emulsified

with 100 μL of incomplete Freund's Adjuvant (IFA), with 100 μL injected in each flank. Statistical analysis was performed by using GraphPad, Prism, version 4.0b.

3.3.9.2 Analysis of serum DNP-OVA antigen-specific antibodies

Blood was collected via the dorsal tail vein at 7 day intervals. Samples were allowed to coagulate by overnight incubation at 4°C. Serum was separated from coagulated blood by centrifugation at 13,000 g for 3 min and stored at −20°C for later analysis. Antigen-specific IgG titers were analyzed by ELISA.

Plates were coated with 50 μL DNP-BSA antigen (10 μg/mL) per well at 4°C overnight. The following morning the plates were washed with PBS/Tween and blocked using PBS with 2% BSA (100 μL). Serum was diluted (1:10) in the blocking buffer and added to the plates. After 2 h incubation at room temperature, plates were again washed and incubated with 50 μL of detection antibodies (Polyclonal Goat-mouse IgG streptavidin-alkaline phosphatase conjugate, 1:2500 dilution, anti-mouse IgG1 alkaline phosphatase conjugate, 1:2000 dilution and IgG2c alkaline phosphatase conjugate, 1:1000 dilution) for 2 h. Following the incubation 50 μL (1.35×10^{-4} M) p-nitrophenyl phosphate (PNPP) substrate was added and the plates were read at 405 nm. End-point antibody titre was determined by extrapolating the dilution which gave an OD of 0.2 for the titration curve.

3.4 Results and discussion

3.4.1 Synthesis and characterization of CdSe/ZnS Core/Shell Nanocrystals

The hydrophobic CdSe/ZnS QDs were prepared as in Chapter 2. These QDs are coated with stearic acid –a non-toxic naturally produced fatty acid commonly used in pharmaceuticals and cosmetics. The high-resolution TEM image shows a spherical QD particle with a diameter of ~ 5.8 nm (Figure 3.11). A chloroform solution of these QDs (2.5 μM) was prepared and gave a concentration of Cd and Se of 0.878 mg/l (7.7 μM) and 0.507 mg/l (6.4 μM) respectively after 250-fold dilution by ICP-OES. The concentration of Zn was found to be 0.95 mg/l (14.6 μM). This gives ~ 770 Cd atoms, 640 Se atoms and ~ 1460 Zn per QD. The number of Cd, Se, Zn and S atoms per QD was calculated theoretically using the bulk densities and formula weights of CdSe and ZnS, as described in Chapter 2, section 2.4.1). Based on this calculation spherical particles of ZnS with diameters of 5.8 and 4.4 nm should contain 2594 and 1134 Zn atoms respectively. Similarly a spherical particle of CdSe with a diameter of 4.4 nm would contain ~ 770 Cd atoms. Taking all this results into account we can estimate that the CdSe/ZnS QDs used in this study have a CdSe core of 4.4 nm and a ZnS shell of 1.4 nm. The position of the first excitonic peak for these QDs appeared at 628 nm, and the fluorescence emission maximum was 642 nm (Figures 3.9 and 3.10).

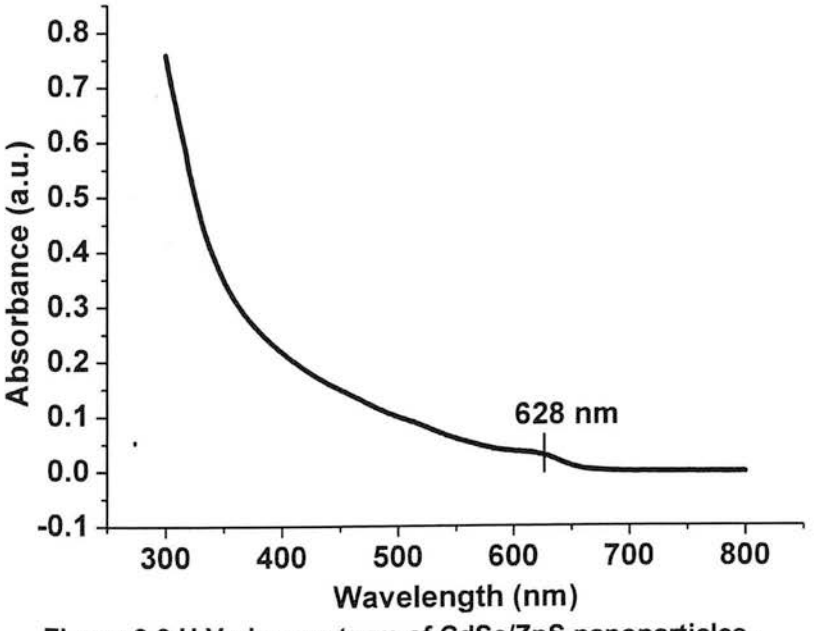

Figure 3.9 U.V-vis spectrum of CdSe/ZnS nanoparticles.

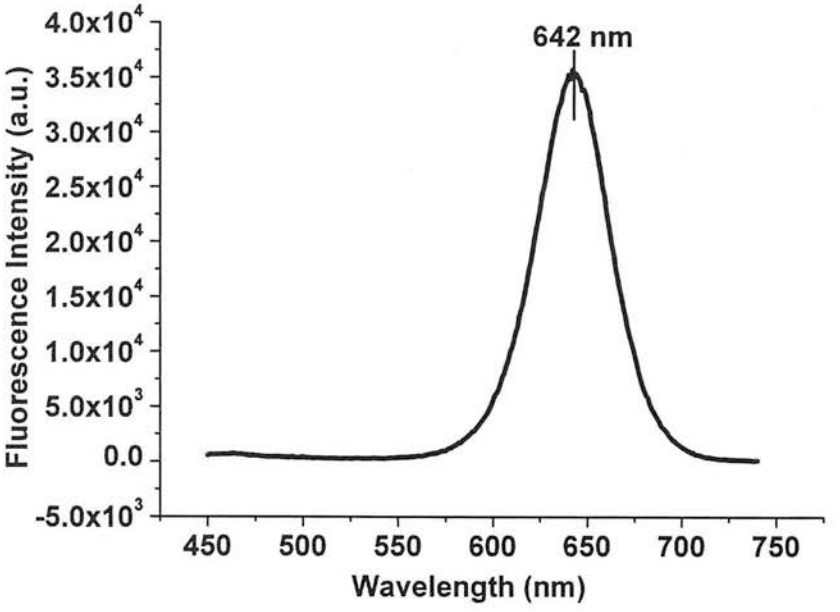

Figure 3.10 Fluorescence emission spectrum of CdSe/ZnS nanoparticles (Excitation at 350 nm, Temperature = 25°C).

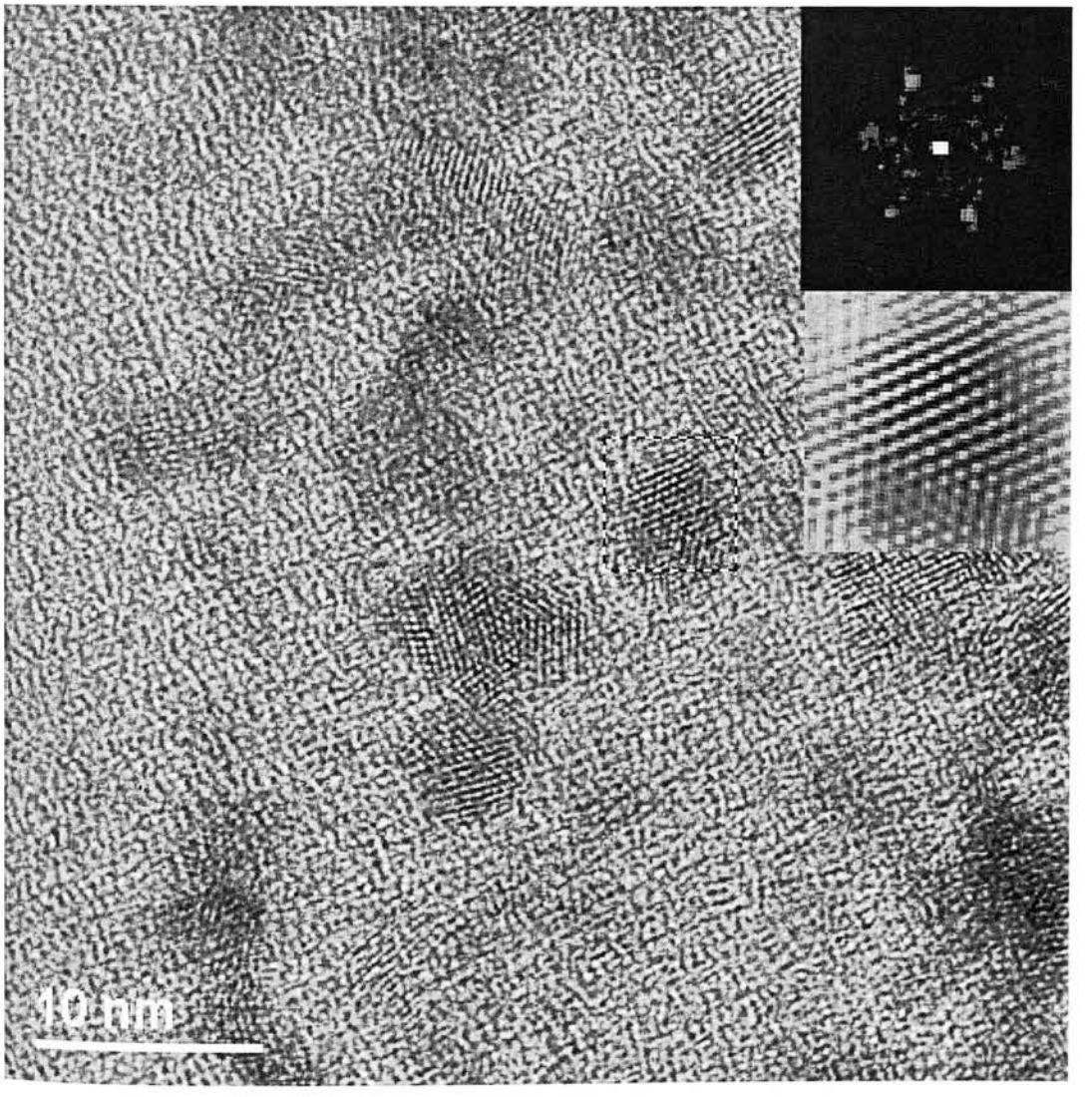

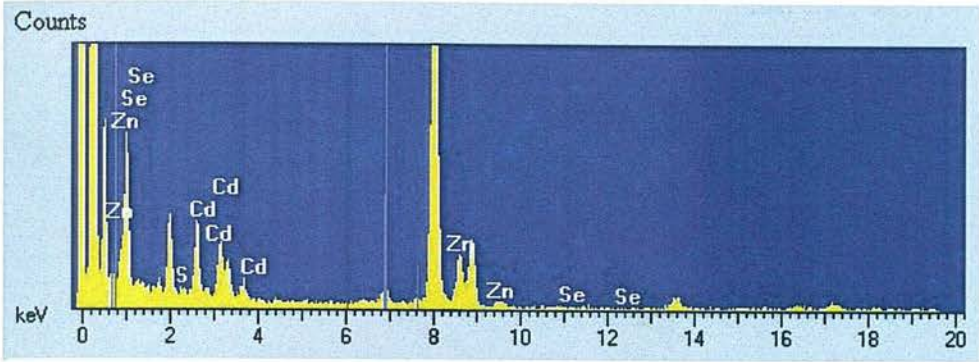

Figure 3.11 High-resolution transmission electron microscopy (HRTEM) image of several CdSe-ZnS QDs (a), fast Fourier transform (FFT) of the QD inside the box (5.72 × 5.72 nm) (b) and corresponding inverse FFT (IFFT) image, (c) EDX spectra of these QDs (d).

3.4.2 Synthesis of QD-LPS Micelles

Hydrophobic CdSe-ZnS QDs were attached to pure *E. coli* LPS (Kdo_2 lipid A, Figure 3.12). In these QDs hydrophobic chains of stearic acid (~ 2 nm long) provide sites for strong interaction with the six hydrophobic chains of this LPS (~1.5 nm long). QD-LPS micelles were prepared by mixing the hydrophobic QDs with excess of pure Kdo_2-lipidA by self assembly of the biopolymer chains around the hydrophobic core of the QD. We investigated the effect of biopolymer-to-QD ratio and we found that higher yields and smaller aggregates are obtained with higher ratios, presumably because the extra LPS prevents the formation of less water-soluble conjugates and the hydrophobic chains of QD from interacting with each other. Dynamic light scattering (DLS) studies revealed that using a LPS:QD molar ratio of 200:1 there are predominantly QD-LPS micelles which are between 11 and 15 nm in diameter in solution (Figure 3.14). This result correlates nicely with the size of the QD and Kdo_2 lipid A. The core-shell nanocrystal has a radius of 2.9 nm, stearic acid is 2 nm long and Kdo2-lipid A is ~ 3 nm long (Figure 3.13). If we consider that the QD at the point of interaction with the LPS chains has a radius of 4 nm as suggested by the DLS results, and that LPS has a surface area of 2 nm^2 based on the dimensions of Kdo2-lipid A[43], then the maximum number of LPS molecules that at single QD can hold in its 200 nm^2 surface is ~100. As one might expect there are also a small percentage of larger particles, presumably due to the formation of clusters containing more than one QD, but these larger aggregates can be removed in the first cycle of ultracentrifugation.

Figure 3.12 Gel electrophoresis of the LPS used in the study. [39] **K56-2 is the LPS from the *B. cenocepacia* parent strain K56-2 which has smooth LPS (O-antigen); SAL-1 is a mutant K56-2 strain which produces deep-rough LPS. Both of these are modified with Ara4N on the lipid A core 4' phosphate. Kdo_2-lipid A is LPS from an *E. coli* mutant strain WBB06 which is deep rough and commercially available from Avanti Polar Lipids. Silver Staining was used in this study.**

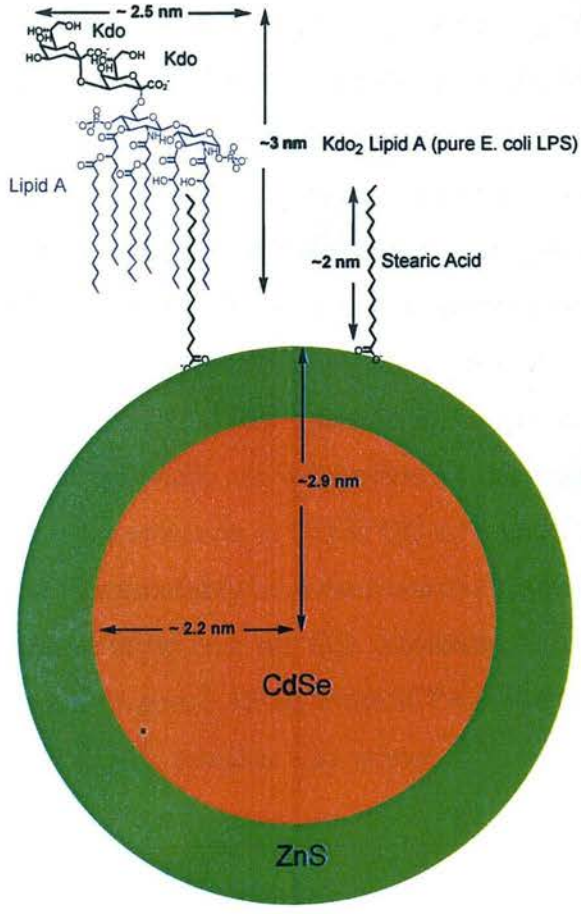

Figure 3.13 Schematic diagram of the self-assembled QD-LPS micelle, illustrating the relevant dimensions and molecular details.

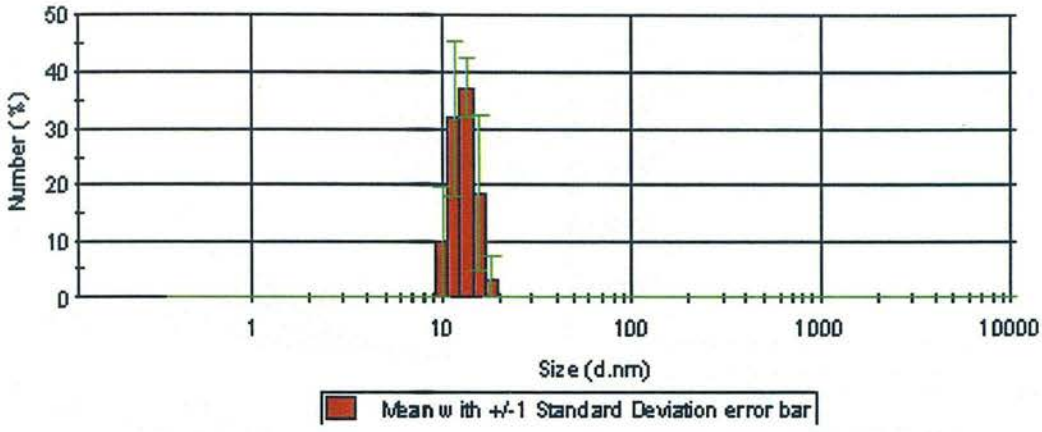

Figure 3.14 Size distribution (dynamic light scattering) of QD-LPS (LPS = Kdo_2-Lipid A).

3.4.3 Fluorescent sensing of LPS by anthracene-derived bis(Zn^{2+}–DPA) complex

QD-LPS and QD-PC/PEG-PE micelles were titrated with increasing concentrations of **1** (Figure 3.5) in HEPES (20 mM, pH 7.5) (Figure 3.15). In the presence of QD-LPS micelles the fluorescence of **1** is increased (Figure 3.15 A). In contrast, the fluorescence of **1** did not change in the presence of QD-PC/PEG-PE micelles (Figure 3.15 A). **1** selectively binds dianionic phosphate groups in QD-LPS. This result is consistent with the results obtained by Hamachi and coworkers[33] in which similar enhancement in the fluorescent intensity of **1** was observed after binding to phosphorylated peptides. It is also consistent with recent studies in our group in which **1** was found to be an effective pattern recognition receptor for Kdo_2-lipid A.[34] Also recently, Smith *et al.*[44] have found that **1** selectively targets and fluorecescently labels the surface of bacterial cell walls via recognition of the anionic phosphate esters of LPS. At the same time the emission of QD in QD-LPS and QD-PC/PEG-PE micelles was quenched by the **1**, presumably because **1** absorbs strongly at 380 nm (excitation energy used). However there was no QD quenching found when the excitation wavelength was 500 nm (Figure 3.15 B). From ICP-OES studies QD concentration in QD-LPS and QD-PC/PEG-PE micelles was estimated 50 nM.

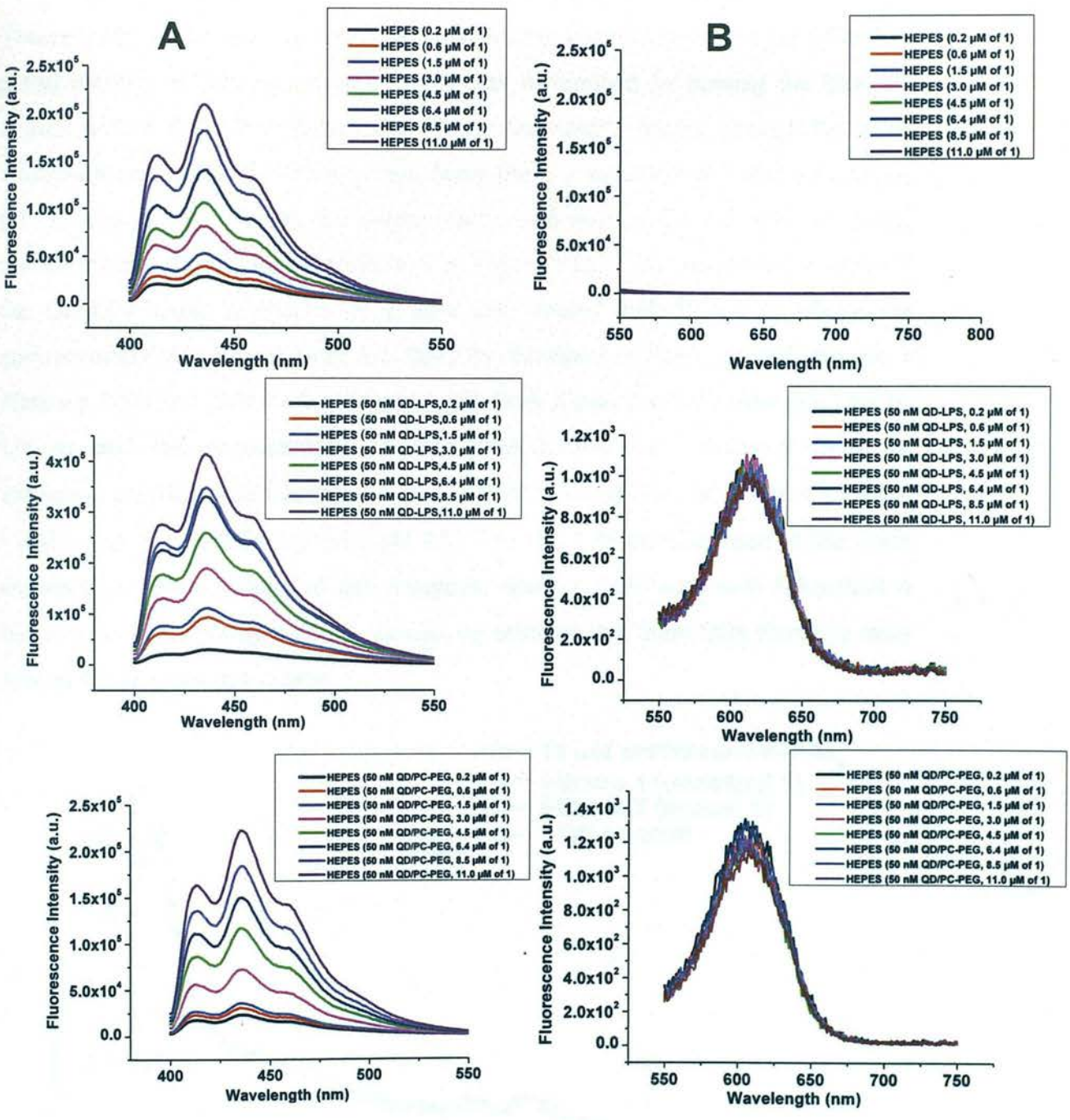

Figure 3.15 Fluorescence titration of Control [(HEPES buffer (20mM, pH =7.5)], QD-LPS and QD-PC/PEG-PE micelles using 1. A= Region for emission of zinc (II)-dipicolylamine complex in blank, QD-LPS and QD-PC/PEG-PE micelle (Excitation at 380 nm; Temperature = 25°C), B= Region for emission of CdSe/ZnS QDs in QD-LPS micelle and QD-PC/PEG-PE micelle (Excitation at 500 nm; Temperature = 25°C).

3.4.4 Quantification of LPS molecule on QD micelle

Theoretically a maximum of 100 LPS molecule can be accommodated per QDs. The actual number of LPS molecules per QD was determined by passing the QD-LPS treated with **1** through size-exclusion filters; unbound **1** passes through the filter, whereas bound to QD-LPS it does not. Since the UV spectrum of **1** and anthracene-$(DPA)_2$ ligand are different, the filtrate was treated with EDTA (15 mM) to release the anthracene-$(DPA)_2$ ligand (Filtrate 1 in Figure 3.16). The retentate s containing the QD-LPS-bound molecules of **1** were also treated with EDTA to release the anthracene-$(DPA)_2$ ligand from the QD-LPS micelles, and then passed through a Nanosep 100 kDa (Filtrate 2 in Figure 3.16). Both filtrate fractions were analysed by UV-vis and the concentration of anthracene-$(DPA)_2$ was calculated from the extinction coefficient of **1** in the presence of EDTA (15 mM) at 260 nm (ε = 32,500 L $\cdot$ mol^{-1} $\cdot$ cm^{-1}) in HEPES (20 mM, pH 7.5). The QD-LPS micelles used in this study captured ca. 130 molecules of this phosphate binding **1**. Because each Kdo_2-lipid A has two dianionic phosphate ester groups, we estimate that these QDs therefore carry around 65 LPS molecules each.

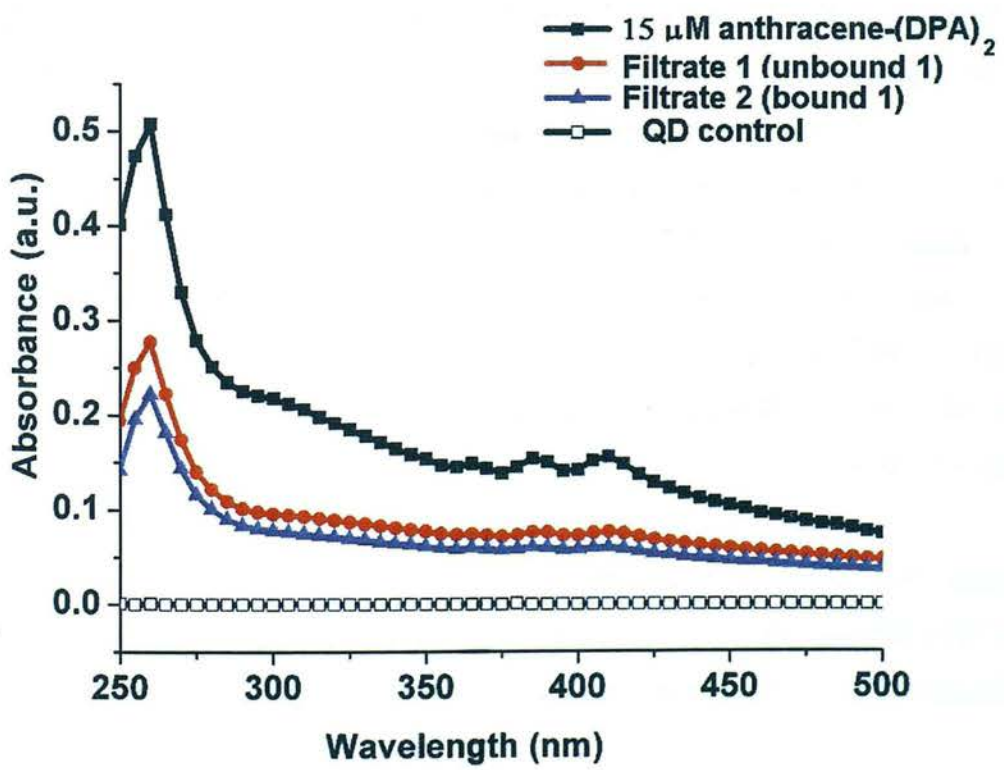

Figure 3.16 UV-vis spectra of 1 in HEPES (20 mM, pH 7.5) after addition of EDTA (15 mM) to release anthracene-$(DPA)_2$ from 1 (closed squares; 15 μM) and mixtures containing 1 (15 μM) + QD-LPS (50 nM). The molecules of 1 which did not bind to QD-LPS are in filtrate 1 (solid circles; 8.5 μM) and those which did bind to QD-LPS in filtrate

2 (solid triangles; 6.5 μM). The control QD micelles (coated with PEG-PE or PC/PEG-PE mixtures) did not bind 1 (open squares).

3.4.5 *In vitro* studies

3.4.5.1 Activation of immune cells

The immunostimulatory activity of the LPS-loaded QDs was evaluated with J774 macrophages and bone marrow-derived dendritic cells (BMDCs) from wild-type mice (data not shown).Controls we used were PBS, uncoupled Kdo_2-lipid A and phosphatidylcholine (PC) and n-poly(ethyleneglycol) phosphatidylethanolamine (PEG-PE) coated QDs.[1]

This involved quantifying IL-6 production by Enzyme linked immunosorbent assays (ELISA) (Figure 3.17). Increased IL-6 production was observed in both J774 macrophages and BMDC cultures subjected to QD-LPS conjugates stimulation than that achieved with LPS alone. J774 macrophages in the resting state released 1.85 ng/mL of IL-6 into the culture media during incubation for 12 h, whereas the cells markedly increased IL-6 production, up to 41.5 ng/mL and 2.4 ng/mL upon exposure to 250 nM LPS alone and LPS in the presence of the LPS inhibitor polymyxin B (PMB) respectively. IL-6 production by macrophages treated with 1.5 nM QD-LPS (prepared by method B; LPS content = 97.5 nM based on 65 LPS molecules per QD), was even greater; 64.1 ng/mL of IL-6 and suppressed to 0.02 ng/mL in the presence of PMB. So the activity of LPS attached to QD is greater than alone. The increase in immunostimulatory activity seems substantial: 35 ng/mL of IL-6 are released by cells stimulated with 0.45 nM QD-LPS (prepared by method A; QD: LPS content ~ 30 nM based on 65 LPS molecules per QD) was only slightly smaller than with 250 nM LPS alone. Moreover, more IL-6 is released with 0.15 nM QD-LPS (prepared by method B: LPS content = 10 nM based on 65 LPS molecules per QD) than with 250 nM LPS alone.

The fact that release of cytokines was strongly inhibited by the LPS antagonist polymyxin B (PMB), and that control QDs (QDs coated with PC and PEG-PE) lacked any activity proves that the immunostimulatory properties of the QD-LPS micelles are LPS-induced.

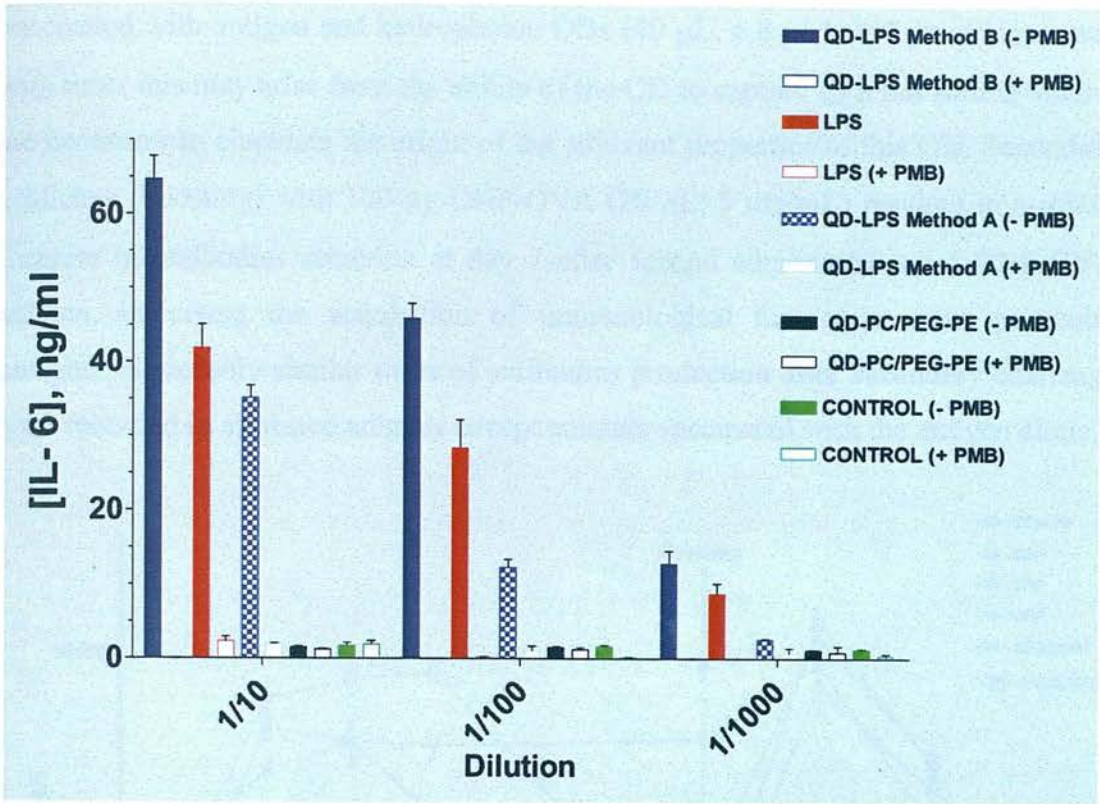

Figure 3.17 Cytokine IL-6 production by J774 macrophages. (IL-6 release from macrophages treated with QD-LPS. At 1/10 dilution; $[QD\text{-}LPS]_{Method\ A}$ = 0.45 nM; $[QD\text{-}LPS]_{Method\ B}$ = 1.5 nM; [LPS] = 250 nM; [control QD] = 2.5 nM. PMB is the LPS inhibitor polymyxin B; [PMB] = 250 μM . Control = phosphate-buffered saline (PBS), pH 7.4. The control QD is coated with PC and PEG-PE instead of Kdo_2-lipid A. Incubation time = 12 h.

3.4.6 *In vivo* studies

3.4.6.1 Analysis of serum DNP-OVA antigen-specific antibodies

Immunoglobulin G (IgG) is an antibody which protects against bacterial toxins. IgG is the most prevalent immunoglobulin (Ig) isotype in serum and is present also in extravascular spaces.[44] The formation of complexes of an antigen and IgG activates the complement system (a pathway which causes the lysis of bacteria) and facilitate phagocytosis by immune cells. IgG is also the primary circulating Ig produced after reexposure to an antigen (secondary immune response). Vaccination with 100 μg DNP-OVA (20 μL, 5 mg/mL) co-administrated with QD-LPS (40 μL, 235 nM, 95 pmol) had total IgG titers about 3-fold higher than that of the mice co-administrated with LPS (40 μL, 43 μM, 4 μg) and 52-fold higher than animals vaccinated with DNP-OVA antigen alone (Figure 3.18). Moreover, co-administration of QD-LPS micelles generated 2-fold greater response than the vaccination with incomplete Freund's adjuvant –a gold standard in adjuvant potency. IgG production in animals

vaccinated with antigen and hydrophobic QDs (40 μL, 6.8 μM, 340 pmol) increased with time; this may arise from the ability of the QD to capture LPS but further studies are necessary to elucidate the origin of the adjuvant properties of this QD. Secondary challenge (boosting) with 100 μg DNP-OVA (20 μL, 5 mg/mL) resulted in a robust increase in antibodies secretion at day 7 after second administration of DNP-OVA antigen, indicating the acquisition of immunological memory to this particular antigen. Noticeably similar titres of antibodies production after secondary challenge were recorded in all tested animals except animals vaccinated with the antigen alone.

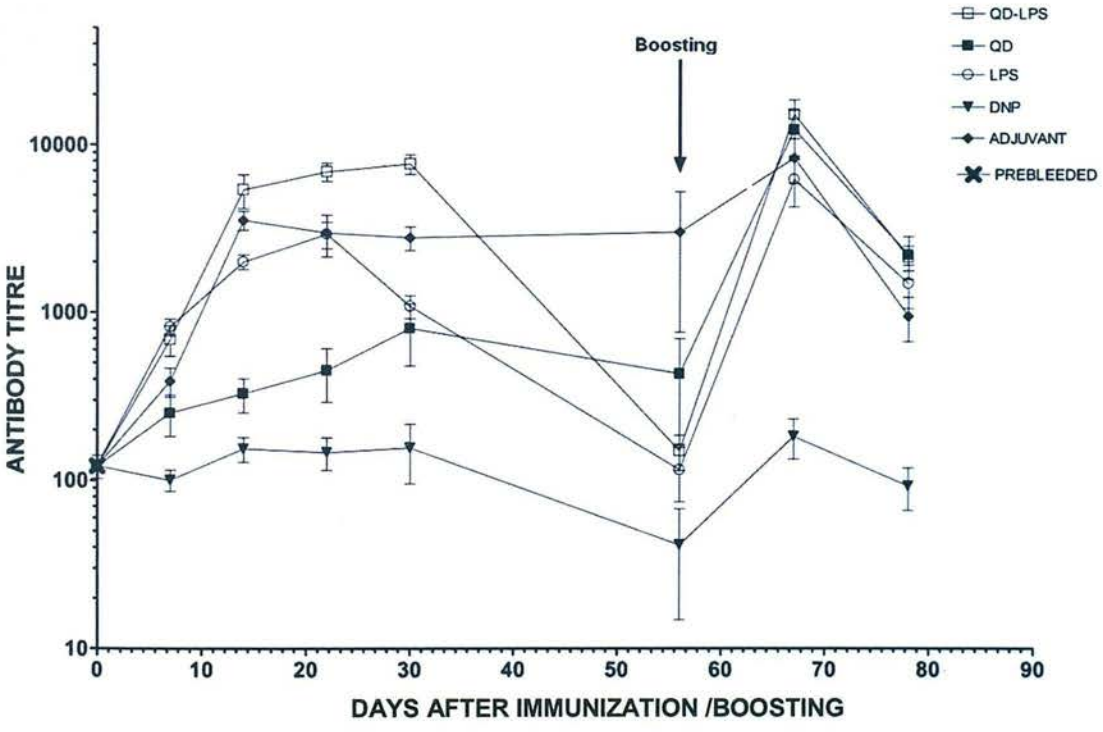

Figure 3.18 Total IgG class antibody production in mice.

3.5 Summary and Conclusion

We have demonstrated that the nanometer-size and multivalent nature of QDs which enables multiple biomolecules to be attached to a single QD can lead to higher activity *in vitro* and *in vivo* than that obtained when the biomolecule is isolated. The biomolecule attached was pure Kdo_2 Lipid A, a pathogen associated molecular pattern coating the surface of the outer membrane of *E. coli*. Like in *E. coli* the LPS molecules are held by hydrophobic interactions. We have tested the ability of these QD-LPS to bind and activate cells of the immune system with LPS receptors like

macrophages and dendritic cells. This requires binding to a number of receptors (e.g. TLR4 and CD14) and then signalling through a group of Toll/interleukin-1 receptor (TIR)-adaptors for cytokine production. The QD-LPS micelles are taken up by these cells and remarkably they induce greater production of cytokines than LPS alone. Importantly, these QD-LPS were found to be non-toxic, presumably because they were coated with a protecting layer of ZnS, stearic acid and LPS and extremely small amounts of QDs are sufficient to elicit these aforementioned immune responses.

3.6 References

(1) Dubertret, B.; Skourides, P.; Norris, D. J.; Noireaux, V.; Brivanlou, A. H.; Libchaber, A. *Science* **2002**, *298*, 1759-1762.

(2) Osaki, F.; Kanamori, T.; Sando, S.; Sera, T.; Aoyama, Y. *J. Am. Chem. Soc.* **2004**, *126*, 6520-6521.

(3) Wang, C.-H.; Hsu, S-Y.; Peng C-A. *Biosens. Bioelectron.* **2008**, *24*, 1012-1019.

(4) Rosenfeld, Y.; Shai, Y. *Biochim. Biophys. Acta.* **2006**, *1758*, 1513.

(5) H. Coley-Nauts, W. B. Swift and B. L. Coley, *Cancer Res.*, **1946**, *6*, 205–216.

(6) R. H. Raetz and C. Whitfield, *Annu. Rev. Biochem.* **2002**, 71, 635–700.

(7) Galanos, C.; Luderitz, O.; Rietschel, E. T.; Westphal, O.; Brade, H.; Brade, L.; Freudenberg, M.; Schade, U.; Imoto, M.; Yoshimura, H.; Kusumoto, S.; Shiba, T. *Eur. J. Biochem.* **1985**, *148*, 1-5.

(8) Bhor, V. M.; Thomas, C. J.; Surolia, N.; Surolia, A. *Mol. BioSyst.* **2005**, *1*, 213-222.

(9) Erridge, C.; Bennett-Guerrero, E.; Poxton, I. R. *Microbes Infect.* **2002**, *4*, 837-51.

(10) Caroff, M.; Karibian, D. *Carbohydr. Res.* **2003**, *338*, 2431-2447.

(11) Beutler, B.; Rietschel, E. T. *Nat. Rev. Immunol.* **2003**, *3*, 169-176.

(12) Sasaki, H.; White, S. H. *Biophys. J.* **2008**, *95*, 986-993.

(13) Andersen-Nissen, E.; Smith, K. D.; Strobe, K. L.; Barrett, S. L. R.; Cookson, B. T.; Logan, S. M.; Aderem, A. *Proc. Natl. Acad. Sci.* **2005**, *102*, 9247-9252.

(14) Latz, E.; Visintin, A.; Lien, E.; Fitzgerald, K. A.; Monks, B. G.; Kurt-Jones, E. A.; Golenbock, D. T.; Espevik, T. *J. Biol. Chem.* **2002**, *277*, 47834-47843.

(15) Jones, H. E.; Strid, J.; Osman, M.; Uronen-Hansson, H.; Dixon, G.; Klein, N.; Wong, S. Y. C.; Callard, R. E. *Cell. Microbiol.* **2008**, *10*, 1634-1645.

(16) Ingalls, R. R.; Monks, B. G.; Savedra, R.; Christ, W. J.; Delude, R. L.; Medvedev, A. E.; Espevik, T.; Golenbock, D. T. *J. Immunol.* **1998**, *161*, 5413-5420.

(17) Kitchens, R. L.; Munford, R. S. *J. Immunol.* **1998**, *160*, 1920-1928.

(18) Friede, M.; Aguado, M. T. *Adv. Drug Deliv. Rev.* **2005**, *57*, 325-331.

(19) Pashine, A.; Valiante, N. M.; Ulmer, J. B. *Nat. Med.* **2005**, *11*, S63.

(20) Singh, M.; O'Hagan, D. *Nat. Biotechnol.* **1999**, *17*, 1075-1081.

(21) Jerala, R.; Porro, M. *Curr. Top. Med. Chem.* **2004**, *4*, 1173-1184.

(22) David, S. A.; Balasubramanian, K. A.; Mathan, V. I.; Balaram, P. *Biochim. Biophys. Acta* **1992**, *1165*, 147-152.

(23) Murillo, M.; Grillo, M. J.; Rene, J.; Marin, C. M.; Barberan, M.; Goni, M. M.; Blasco, J. M.; Irache, J. M.; Gamazo, C. *Vaccine* **2001**, *19*, 4099-4106.

(24) Gómez, S.; Gamazo, C.; San, Roman B.; Ferrer, M.; Sanz, M.L.; Espuelas S, Irache, J.M. *Eur. J. Pharm. Biopharm.* **2008**, *717,* 711-717.

(25) Fornara, A.; Johansson, P.; Petersson, K.; Gustafsson, S.; Qin, J.; Olsson, E.; Ilver, D.; Krozer, A.; Muhammed, M.; Johansson, C. *Nano Lett.* **2008**, *8*, 3423-3428.

(26) Schuster, B. G.; Neidig, M.; Alving, B. M.; Alving, C. R. *J. Immunol.* **1979**, *122*, 900-905.

(27) Dijkstra, J.; Mellors, J. W.; Ryan, J. L.; Szoka, F. C. *J. Immunol.* **1987**, *138*, 2663-2670.

(28) Dijkstra, J.; Mellors, J. W.; Ryan, J. L. *Infect. Immun.* **1989**, *57*, 3357-3363.

(29) Alving, C. R.; Richards, R. L. *Immunol. Lett.* **1990**, *25*, 275-280.

(30) Ojida, A.; Miyahara, Y.; Kohira, T.; Hamachi, I. *Biopolymers* **2004**, *76*, 177-184.

(31) O'Neil, E. J.; Smith, B. D. *Coord. Chem. Rev.* **2006**, *250*, 3068-3080.

(32) B, Kabzinska. *Ann. Pharm. Fr.* **1964**, *22*, 685.

(33) Ojida, A.; Mito-oka, Y.; Inoue, M.; Hamachi, I. *J. Am. Chem. Soc.* **2002**, *124*, 6256-6258.

(34) Ganesh, V.; Bodewits, K.; Bartholdson, S. J.; Natale, D.; Campopiano, D. J.; Mareque-Rivas, J. C. *Angew. Chem., Int. Ed.*, **2009**, *48*, 356-360.

(35) (a) Leevy, W. M.; Johnson, J. R.; Lakshmi, C.; Morris, J.; Marquez, M.; Smith, B. D. *Chem. Commun.*, **2006**, *15, 1595*-1597. (b) Johnson, J. R.; Fu, N.; Arunkumar, E.; Leevy, W. M.; Gammon, S. T.; Piwnica-Worms, D.; Smith, B. D. *Angew. Chem., Int. Ed.*, **2007,** *46,* 5528-5531.

(36) Mammen, M.; Choi, S. K.; Whitesides, G. M. *Angew. Chem., Int. Ed.* **1998**, *37*, 2754-2794.

(37) Manea, F.; Bindoli, C.; Fallarini, S.; Lombardi, G.; Polito, L.; Lay, L.; Bonomi, R.; Mancin, F.; Scrimin, P. *Adv. Funct. Mater.* **2008**, *20*, 4348-4352.

(38) Zhang, C. Y.; Ma, H.; Nie, S. M.; Ding, Y.; Jin, L.; Chen, D. Y. *Analyst* **2000**, *125*, 1029-1031

(39) Kloepfer, J. A.; Mielke, R. E.; Wong, M. S.; Nealson, K. H.; Stucky, G.; Nadeau, J. L. *Appl. Environ. Microbiol.* **2003**, *69*, 4205-4213.

(40) Rosenthal, S. J.; TomLinson, A.; Adkins, E. M.; Schroeter, S.; Adams, S.; Swafford, L.; McBride, J.; Wang, Y. Q.; DeFelice, L. J.; Blakely, R. D. *J. Am. Chem. Soc.* **2002**, *124*, 4586-4594.

(41) Gupta, M. ; Caniard, A.; Touceda-Varela, A.; Campopiano, D. J.; Mareque-Rivas, J. C *Bioconjug. Chem.* **2008**, *19*, 1964-1967.

(42) Dubertret, B.; Skourides, P.; Norris, D. J.; Noireaux, V.; Brivanlou, A. H.; Libchaber, A. *Science* **2002**, *298*, 1759-1762; (b) Carion, O.; Mahler, B.; Pons, T. Dubertret, B. *Nat. Protocols* **2007**, *2*, 2383-2390.

(43) Kastowsky, M. ; Gutberlet, T. ; Bradaczek, H.. *Eur. J. Biochem.* **1993**, *217*, 771-779.

(44) Roitt, I, Rabson, A. *Really essential medical immunology;* Blackwell Science, 2000; pp 27-30.

4.1 Introduction

4.1.1 Pathophysiology of Malaria

Malaria is an infectious disease caused by the protozoan parasite *Plasmodium.* It has been estimated that Malaria kills at least two million people annually, and that at least one third of the world's population is at risk of acquiring it.[1] The four species causing all human infections are *P. falciparum, P. vivax , P. malariae* and *P. ovale.* Infection by *P.falciparum* is the most severe of the four and accounts for 90% of deaths due to malaria. The life cycle of *P.falciparum* consists of a sexual cycle which takes place in the anopheles mosquito, and an asexual cycle which occurs in man and is responsible for producing the clinical effects and pathology associated with malaria. After the bite of an infected female anopheles mosquito *sporozites* are transferred intravenously into the human body (Figure 4.1). Then these *sporozoites* enter the liver where they undergo multiplication from just a few to thousands. This stage is called pre-erythrocytic stage. After this stage rupturing of liver cells causes release of *merozoites* which invade red blood cells (erythrocytes). Binding of *merozoites* to erythrocytes begins the formation of intracellular parasites called *trophozoites*. In the erythrocytic stage, further development and multiplication of *plasmodium* within the erythrocyte takes place. Mitotic replication of the parasite nucleus inside the red blood cell takes place and then the parasite is called *schizont*. These *schizonts* are multiply rapidly for formation of further merozoites which will invade fresh erythrocytes.[2]

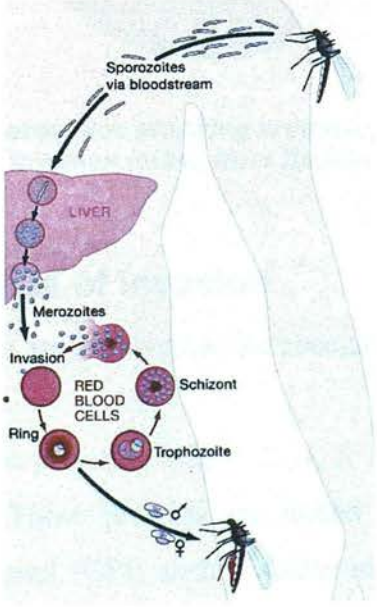

Figure 4.1 Illustration of the life cycle of *P. falciparum* in the human host and the anopheles mosquito vector *(taken from Cowman et al.* [2]*).*

4.1.2 Overview of merozoite Invasion to Erythrocytes

Malaria merozoites have the very important role of recognizing, attaching and entering erythrocytes (Figure 4.2 a). Initial attachment of merozoites to erythrocyte is relatively weak (low affinity) and reversible. After initial interactions the erythrocyte surface is deformed and wrapped around the merozoite; this ensures the closer interaction of the apical end of the merozoite with the erythrocyte membrane (Figure 4.2 b). Later a tight junction is formed between the merozoite and erythrocyte membrane aiding parasite entry. The actin myosin motor (proteins responsible for locomotion) of the merozoite helps this tight junction to move inside the cells. Once this assembly enters fully inside the cells sealing of the erythrocyte membrane takes place.[3]

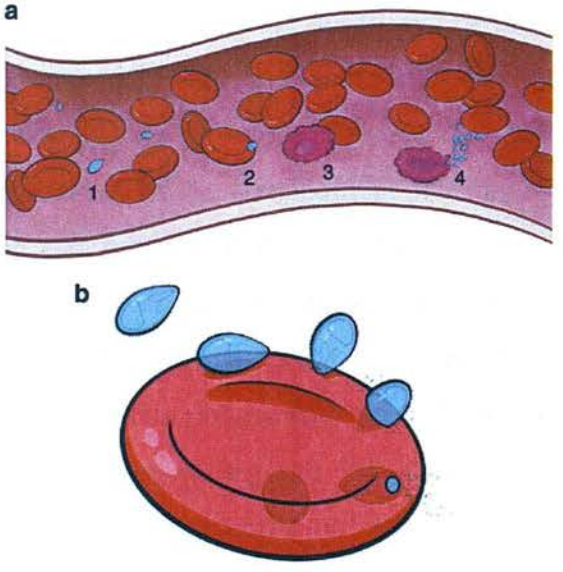

Figure 4.2 (a) Malaria merozoites attacking erythrocytes and (b) events in merozoite invasion *(taken from Richard et al.[4]).*

4.1.3 Molecular basis of invasion

A wide range of proteins are involved in the recognition and invasion of erythrocyte by the malaria parasite.

Several merozoite surface proteins (MSP-1, 2, 4, 5, 8 and 10) seem to be involved in the initial recognition. These proteins are linked to the merozoite surface by a glycosylphosphatidylinositol (GPI) anchor. Other merozoite surface proteins (MSP) like MSP-3, MSP-6 and MSP-7 and MSP-9 are also associated partly with the merozoite surface. MSP-1 was the first merozoite surface protein to be discovered. It

is a well characterized member of MSP family and the most abundant protein on the merozoite surface.[5] MSP-1 is essential for parasite survival and invasion. Although MSP-1 is considered a suitable candidate for facilitating initial contact of merozoite to the RBC definitive proof is still lacking. MSP-1 is formed during trophozoite and schizont stag and ranges in size between 180-225 kDa.[6] There are two proteolytic maturation steps for MSP-1. The first cycle takes place at the *schizont* stage producing four polypeptides products which remain attached to parasite surface by the GPI anchor. The fragments masses are 83 kDa (N-terminus), 30 and 38 kDa (central regions), and 42 kDa (C-terminus). The second step happens at the time of erythrocyte invasion forming $MSP1_{19}$ fragment (11 kDa). $MSP1_{19}$ is a leading candidate for malaria vaccine.[3,7,8]

After the initial contact/binding which is presumbably mediated by MSP-1, proteins harboured in secretory organelles in the apical end of the malaria parasite (rhoptries and micronemes; Figure 4.3) bind to specific receptors on the RBC; these proteins essential for invasion.[3,7,8] One of this proteins is the Apical Membrane Antigen 1 (AMA1); a leading antigen for the development of a malaria vaccine since antibodies directed against it can prevent invasion.[9] AMA-1 is a 83 kDa type 1 integral membrane protein which is stored in the microneme organelles of the malaria parasite (Figure 4.3). At the time of invasion AMA1 is transfered to the surface of the parasite through the rhoptry neck. The precise role of AMA1 and other proteins (e.g. actin myosin motors which seem to support the physical entry of parasite into the parasitophorous vacuole) in erythrocyte invasion is still unclear. Thus, the development of new ways to elucidate this important aspect is essential.

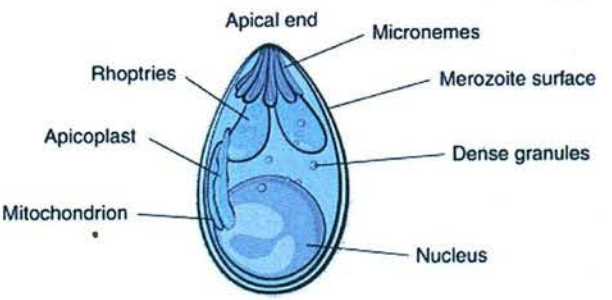

Figure 4.3 The structure of the *P. falciparum* merozoite *(taken from Richard et al.[4])*.

4.2 Controlling the number of functional groups attached to each QDs

For biological applications the ability to control the number of ligands or functional molecules bound to each QD is very important as these molecules act as binding sites to the cell or cell receptors. Controlling the number of binding sites per QDs can also reduce the chances of crosslinking and aggregation between QDs. However, in spite of recent synthetic advances, it is generally difficult to control the number of biomolecules which are attached to a single QD.[10-13] In a recent study Sperling *et al.*[14] separated QDs with discrete number of functional groups using gel electrophoresis. They prepared negatively charged polymer coated CdSe/ZnS QDs terminated with carboxylate groups and coupled each of them to individual NH_2-PEG molecules using the EDC coupling method. After conjugation the QDs were separated with zero, one and two NH_2-PEG molecules on the basis of their sizes using gel electrophoresis (conjugation of NH_2-PEG molecules to QDs increases their size after coupling). Also recently, Carstaris *et al.*[15] managed to monofunctionalise QDs with DNA.[15]
However, these methodologies are cumbersome and focused on minimising the number of biomolecules that are attached to the QD–this is required for some biological applications.

4.3 Motivation for the work

In Chapter 2 we developed an strategy [based upon Ni(NTA)] surface modification of QDs and his-tag protein labelling) for site specific attachment of proteins to QDs preserving biological activity. In Chapter 3 we used the large size and multivalent nature of QDs for developing strongly fluorescent materials which can be used to model the surface of Gram negative bacteria and study how they interact and activate immune cells. In this Chapter we are going to use QDs as new materials for studying malaria parasite invasion of RBCs.
The aim was to exploit Ni(NTA)-QDs to anchor MSP 1 expressed with an histidine tag. Because binding of MSP-1 to RBCs is weak multivalency may prove to be a critical aspect to achieve RBC binding (it has not been demonstrated using 'free' protein). Thus, another key objective of this work was to control the number of MSP-1 protein molecules attached to each QDs. For this, we employ different types of

water soluble QDs in which the distance between the Ni-NTA units and the nanocrystal surface is varied by different linker groups. The general strategy is illustrated in Scheme 4.3. The results presented in this Chapter pave the way for the first study in which fluorescent nanoparticles are used for studying and enhancing the weak interactions between merozoites and RBC (Future work section).

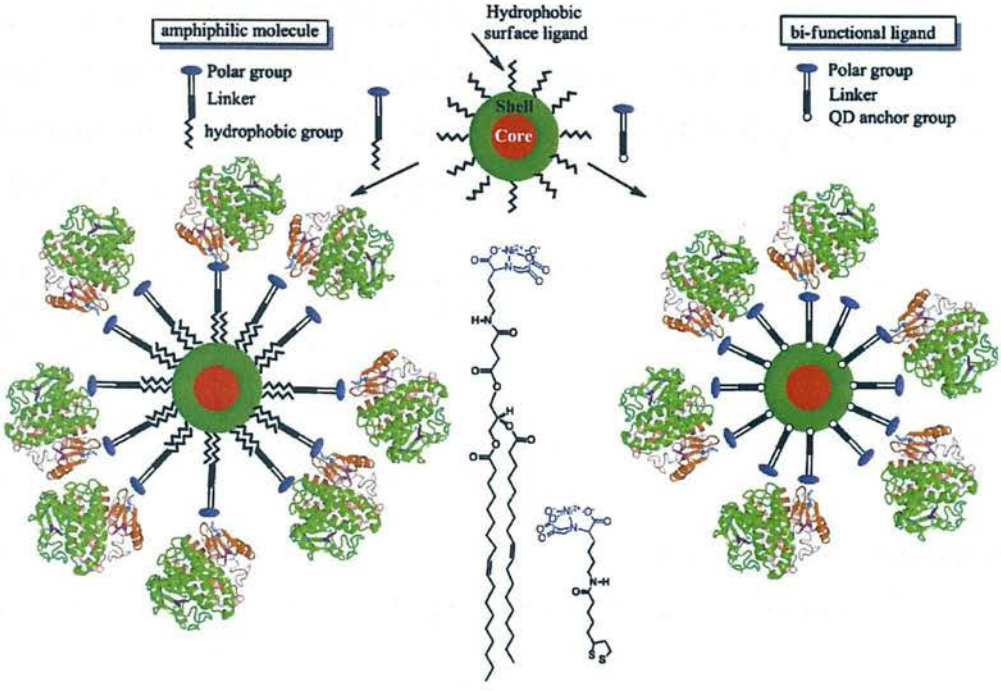

Scheme 4.3 Approach adopted to control the number of protein molecules that can be attached to a single QD (in green and orange represents an arbitrary protein).

4.4 Experimental

4.4.1 Materials

All chemicals were obtained from commercial sources and used as received. Nickel (II) chloride, *N*-hydroxysuccinimide (NHS, 98%) and *N*-*N*-bis(carboxymethyl)-L-lysine hydrate were purchased from Sigma Aldrich. 1-Ethyl-3-[3'-(dimethylamino)propyl]carbodiimide was purchased from Ademtech. The hydrophobic (CdSe/ZnS core/shell QDs) and water soluble QDs (CdSe/ZnS core/shell QDs coated with DHLA) were prepared as described in Chapter 2, and the results presented here were obtained with QDs which had the first absorption band at 615 nm, and a maximum emission peak at 620 nm with excitation at 380 nm. BCA protein Assay kit was purchased from Pierce Biotechnology. PBS 1X buffer (pH 7.4) was purchased from Invitrogen. 1,2-Dipalmitoyl-sn-glycero-3-phosphoethanolamine-N-

(methoxy(polyethylene glycol)-2000) (mPEG2000 PE), 1,2-dioleoyl-*sn*-glycero-3-[(N-(5-amino-1-carboxypentyl)iminodiacetic acid)succinyl] (nickel salt) and 1-palmitoyl-2-oleoyl-*sn*-glycero-3-phosphocholine (PC) were purchased from Avanti Polar Lipids. Water soluble commercial QDs (CdSe/ZnS core/shell QDs with carboxylic acid group) were purchased form Ocean NanoTech, LLC. In this chapter these commercial QDs will be referred to as CQDs. Deep Purple Total Protein Stain was purchased from GE healthcare. Recombinant His_6-MSP-1 (His_6 at the N terminus) was obtained from Lynne Harris and Dr David Cavanagh from The Institute of Immunology and Infection Research at the University of Edinburgh.[16] The MSP-1 hybrid sequence used in this Chapter was:

```
MVTHESYQELVKKLEALEDAVLTGYSLFHKEKMILNEEEITTKGASAQSGAS    50
AQSGASAQSGASAQSGTSAQSGTSGPSGPSGPSGTSGTSGTSGPSGTSGPSGTS 80
GPSGTSGTSGTSGTSAQSGTSGTSAQSGTSGTSAQSGTSGTSPSSRSNTLPRSN 120
TSSGASPPADASKDGANTQVVAKPADAVSTQSAKNPPGATVPSGTASTKGAI    160
SSPGAANPSDDSSNEGTSGTAVTTSTPGSKGSVASGGSGGSVASSGSVTSGGS   200
GGSVTSGGSVTSGGSGGSVASGGSVASGGSVASGGSVASGGSGGSVASVASV    247
ASVASGGSGGSVASGGSGNSRRTNPSDNSS                           250
```

This MSP-1 hybrid was chosen because recent studies have shown that antibodies to this sequence are associated with protection against clinical malaria.[17-19]

4.4.2 Modification of quantum dots surface by NTA and NTA-Ni complex

The nitrilotriacetic acid–Ni (II) complex (NTA-Ni) was prepared by mixing *N-N*-bis(carboxymethyl)-L-lysine hydrate (NTA) (15 mg, 0.0396 mmole) and Ni(II) chloride (15 mg, 0.063 mmole) in HEPES (3 mL; 20 mM, pH 7.5) with stirring for 1 hr. This complex was attached to DHLA-coated CdSe/ZnS QDs as described in Chapter 2. For CQDs, activation of carboxylate groups was performed by mixing 20 μL of QDs (8 μM). 100 μL of EDC (9 mM in HEPES) and 100 μL of NHS (9 mM in HEPES) with stirring for 30 min (this gives a QD concentration of 0.72 μM). Then, 100 μL of the NTA-Ni^{2+} complex solution was added and the mixture was stirred for 24 h. Excess nickel was removed by passing the solution through a 100 KDa nanosep filter. The NTA coated QDs were prepared in the same way using the NTA ligand instead of NTA-Ni^{2+} complex. NTA and NTA-Ni^{2+} modified QDs were re-dissolved 1X PBS buffer (50 μL, pH 7.4) for the protein binding studies with His_6-MSP-1.

4.4.3 Synthesis of QD-DOGS-Ni-NTA /PEG-PE and QD-DOGS-NTA /PEG-PE micelles

In a 5 mL round-bottomed flask, 100 μL of hydrophobic CdSe/ZnS QD (9.4 μM in chloroform), 50 μL of 1,2-dipalmitoyl-*sn*-glycero-3-phosphoethanolamine-N-methoxy(polyethylene glycol)-2000] (ammonium salt) (2 mg in 50 μL of chloroform; 15 mM) and 20 μL of 1,2-dioleoyl-*sn*-glycero-3-[(N-(5-amino-1-carboxypentyl)iminodiacetic acid)succinyl] (nickel salt) (0.2 mg in 20 μL of chloroform; 9.5 mM) were mixed together. The flask was left open at room temperature for 3 h in a fume hood to slowly evaporate the chloroform solvent. Any remaining chloroform was removed under vacuum using a rotary evaporator to form a thin film. The flask containing the QDs was then heated in water bath set to 80°C for 30 s, after which 600 μL of double distilled water was quickly added. Addition of water forms a suspension containing both empty micelles and those containing QDs. QD aggregates were removed from QD-DOGS-Ni-NTA/PEG-PE micelles by ultracentrifugation at 11,000 g for 2 min. Supernatant was collected which contains both empty micelles and those containing QDs. The empty micelles were removed with ultracentrifugation at 270,000g for 2×30 min. The micelles containing QDs formed a pellet while the empty micelles stayed suspended. The successive supernatants were discarded and the final QD-DOGS-Ni-NTA/PEG-PE micelles were resuspended in 600 μL of water (this gives a QD concentration of 30 nM). QD-DOGS-NTA/PEG-PE micelles were prepared by treating QD-DOGS-Ni-NTA micelles with EDTA (15 mM) and then passed through a Nanosep 100 kDa Omega membrane filter. Finally QD-DOGS-NTA micelles were resuspended in 400 μL of water (this gives a QD concentration of 25 nM).

4.4.4 Estimation of protein loading by BCA Assay (Enhanced Protocol)

The protein (His_6-MSP-1) loading capacity of the various QDs prepared was determined by BCA assays (Enhanced Protocol) as follows. Several QD: His_6-MSP-1 ratios were investigated. The following conditions were found appropriate to determine the maximum number of His_6-MSP-1 each type of QD can accommodate.

CQD-NTA and CQD-Ni(NTA) {10 μL; 1.6 μM} was incubated with His_6-MSP (10 μL; 14 μM) for 2.0 h at 4°C.

QD-DOGS-NTA/PEG-PE micelle and QD-DOGS-Ni-NTA/PEG-PE micelle (10 μL; 1.8 μM) was incubated with His_6-MSP (9 μL; 14 μM) for 2.0 hr at 4°C.

QD-DHLA-Ni-NTA (10 μL; 1 μM) was incubated with His_6-MSP (8 μL; 14 μM) for 2.0 h at 4°C.

In each case the QD-protein complexes were separated from the unbound protein molecules by passing the solution mixture through a Nanosep 300 kDa filter (low protein-binding, modified polyethersulfone on polyethylene substrate). The retentate containing the QD-bound protein was treated with 100 μL of a PBS solution of imidazole (0.5 M, pH = 7.4) to release the protein. The filtrate was also made up to 100 μL using PBS. Then 2 mL of working reagent [a mixture of solution A and B (50:1) as indicated in the manufacturer's instructions] was added to the fractions (retentate and filtrate) and incubated at 60°C for 30 min. After incubation the absorbance of the samples was measured at 562 nm using a CARY 300 SCAN UV-vis spectrometer.

4.4.5 Protein binding studies by sodium dodecyl sulfate polyacrylamide gel electrophoresis (SDS-PAGE)

Protein binding studies were carried out by incubating 100 μL of the corresponding QD (1.3 μM) with 75 μL of His_6-MSP-1 (4.8 mg/mL; 68 μM) and His_6-MSP-1 protein for 2.0 hr at 4°C. The protein-QDs complexes were separated from the unbound protein molecules by passing this solution through a Nanosep 300 kDa filter (low protein-binding, modified polyethersulfone on polyethylene substrate). The retentate containing the QD-bound protein was treated with 175 μL of a PBS solution of imidazole (0.5 M, pH = 7.4) to release the protein. Similarly control retentate and filtrate fractions samples were prepared by using PBS. Retentate and filtrate fractions were analysed by SDS-PAGE as stated in Chapter 2.[20] After the electrophoresis was finished, the gel was stained overnight using Deep Purple Total Protein Stain.

4.5 Results and discussion

4.5.1 Synthesis of NTA and NTA-Ni surface-modified QDs

The hydrophobic (CdSe/ZnS core/shell QDs) and water soluble QDs (CdSe/ZnS core/shell QDs coated with DHLA) were prepared as described in Chapter 2 (section 2.3.2 and 2.3.4). The surface modification of DHLA-coated QDs with NTA-Ni was accomplished as described in Chapter 2 (section 2.4.3). The absorption and emission spectrum of QD-DHLA-Ni (NTA) used in this study is shown in Figure 4.5 and Figure 4.6 respectively.

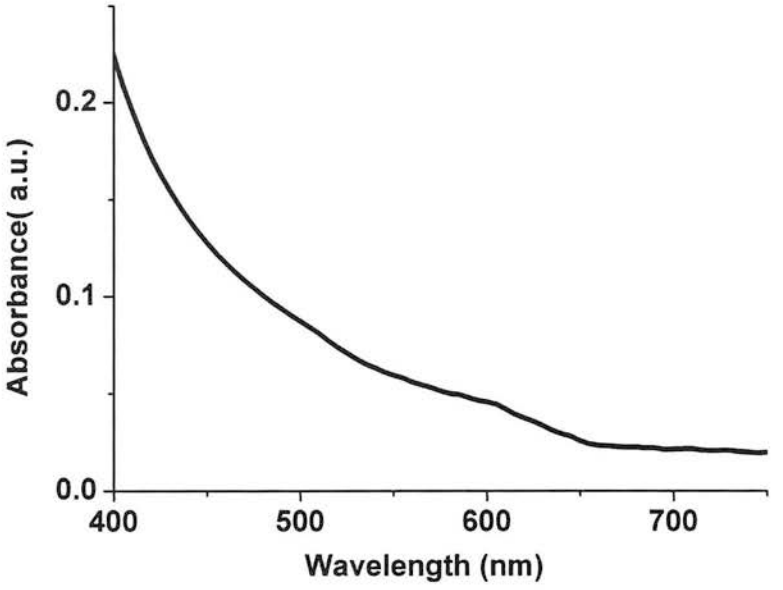

Figure 4.5 U.V-vis spectrum of QD-DHLA-Ni(NTA)(25 nM).

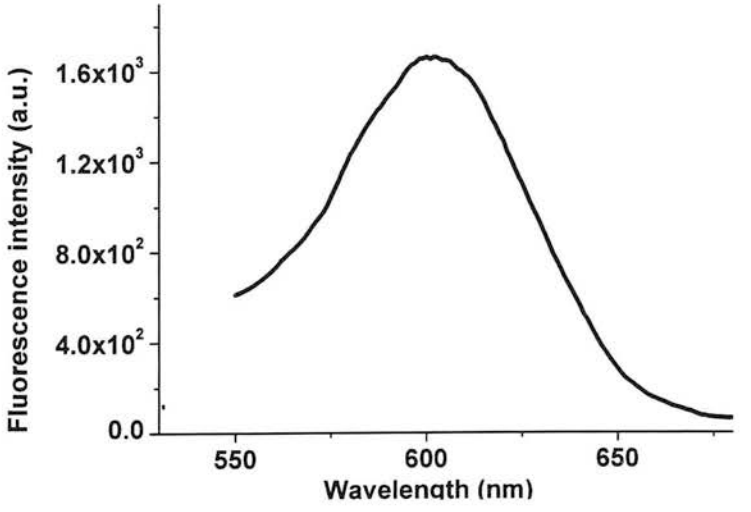

Figure 4.6 Fluorescence emission spectrum of QD-DHLA-Ni(NTA) (25 nM) [Excitation at 380 nm; Temperature = 25°C].

Commercial QDs with carboxylate groups on the surface (CQDs) modified with NTA and NTA-Ni (CQD-NTA and CQD-Ni(NTA) were prepared also by activation with EDC/NHS and reaction with *N*-*N*-bis(carboxymethyl)-L-lysine. The absorption and emission spectra of CQD, CQD-NTA and CQD-Ni(NTA) are shown in Figure 4.7 and Figure 4.8 respectively. The position of the first excitonic peak and of the emission band did not change upon attachment of NTA and Ni-NTA units to these QDs. The fluorescence emission intensity, however, was reduced by ca. 30 % and 47 % after attachment of NTA and NTA-Ni respectively.

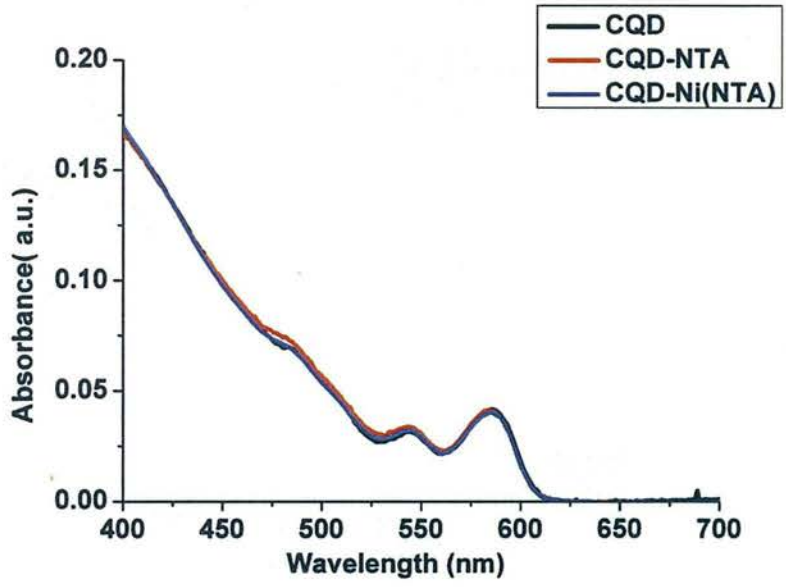

Figure 4.7 U.V-vis spectra of CQD-NTA and CQD-Ni(NTA) (160 nM).

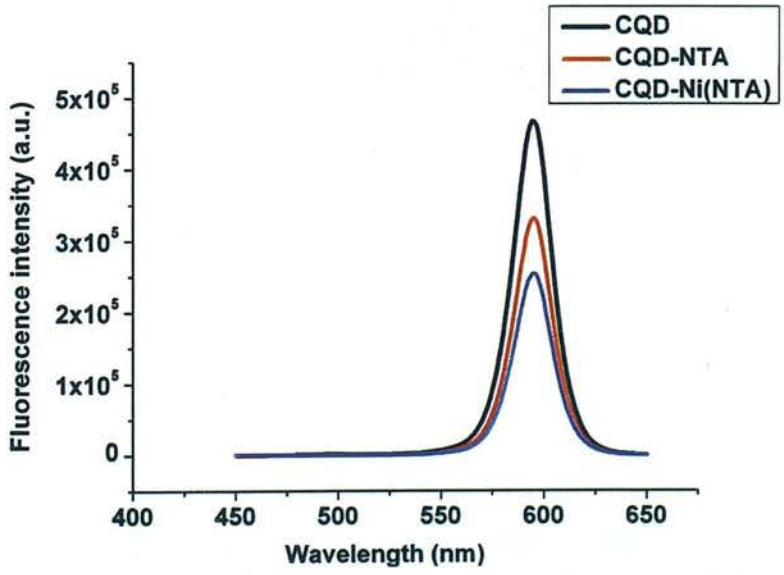

Figure 4.8 Fluorescence emission spectra of CQD, CQD-NTA and CQD-Ni(NTA) (160 nM) [Excitation at 380 nm; Temperature = 25°C].

QD-filled micelles decorated with NTA and Ni-NTA were prepared by adding DOGS-NTA-Ni and PEG-PE to hydrophobic QDs (QD-DOGS-NTA/PEG-PE and QD-DOGS-NTA-Ni/PEG-PE micelles). Several ratios of the three reagents were used. It was found that an excess of PEG-PE over DOGS-NTA-Ni is required (60:40 was found to be enough) for good water solubility. Moreover, better results were obtained when the excess of phospholipids relative to QD was high (500-1000:1). The absorption and emission spectra of these micelles are shown in Figure 4.9 and Figure 4.10 respectively. Also in this case the presence of Ni^{2+} ions does not affect the position of the emission band and the intensity is only reduced by ca. 10 %.

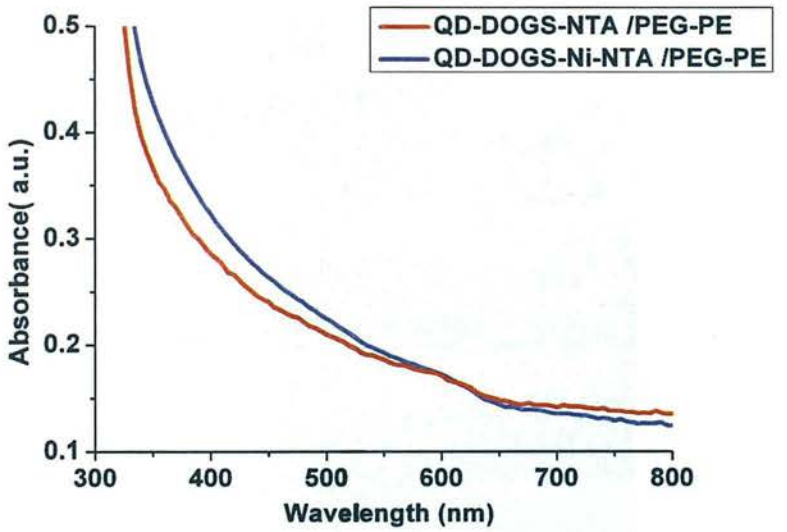

Figure 4.9 U.V-vis spectra of QD-DOGS-NTA /PEG-PE and QD-DOGS-Ni-NTA /PEG-PE (30 nM) micelle.

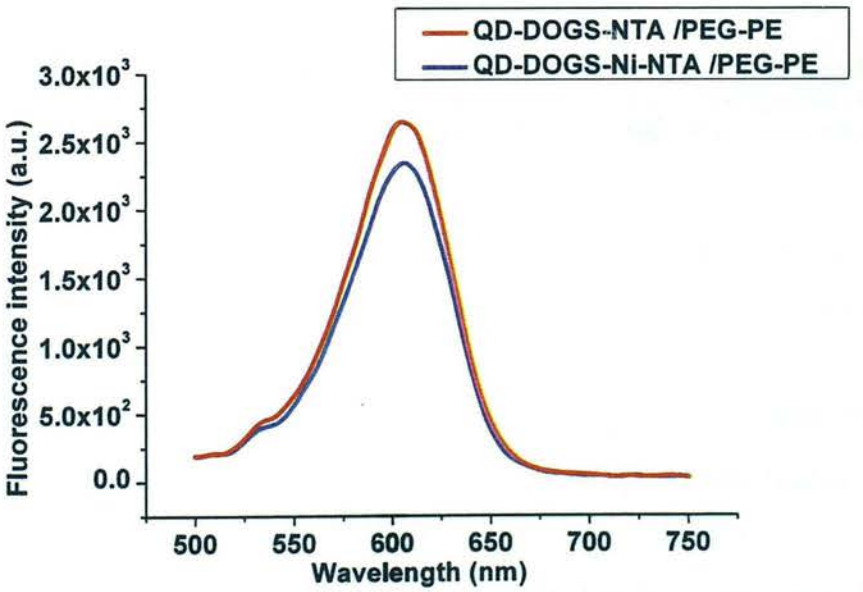

Figure 4.10 Fluorescence emission spectra of QD-DOGS-NTA /PEG-PE and QD-DOGS-Ni-NTA /PEG-PE micelles (30 nM) (Excitation at 380 nm; Temperature = 25°C).

4.5.2 Protein binding studies

The non-covalent attachment of His_6-MSP-1 to the QDs after derivatisation with Ni-NTA was analyzed by SDS-PAGE. A solution of the QD and control (PBS) was incubated with the His_6-MSP for 2 h and passed through a Nanosep 300 kDa centrifugal device. The retentate was redissolved in PBS buffer, and both retentate and filtrate were analyzed by SDS-PAGE. As expected from the results obtained in Chapter 2, His_6-MSP-1 was captured by the Ni-NTA modified QDs. Figure 4.11 shows the gel obtained when QD-DHLA-Ni (NTA) was incubated with 38 molar equivalent of His_6-MSP-1.

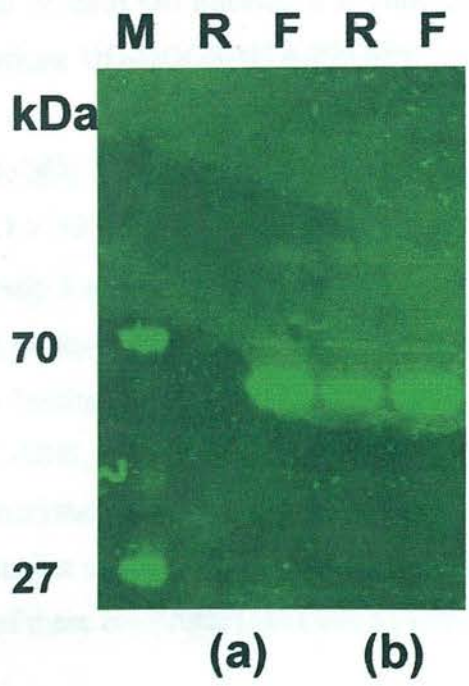

Figure 4.11 SDS-PAGE of the retentate (R) and filtrate (F) after ultrafiltration through a Nanosep 300 KDa filter of His_6-MSP (a) and His_6-MSP incubated with QD-DHLA-Ni(NTA) (b) Lane M contains size markers. Deep Purple Total Protein Stain was used in this study.

The loading capacity of CQD-NTA, CQD-Ni (NTA) QD-DOGS-NTA /PEG-PE micelle, QD-DOGS-Ni-NTA /PEG-PE micelle and QD-DHLA-Ni (NTA) for His_6-MSP-1 was estimated by enhanced BCA assays.

When CQD-Ni (NTA) (1.6×10^{-11} moles) were incubated with His_6-MSP (1.4×10^{-10} moles) it was found that all the His_6-MSP molecules had been attached to the QDs. Even after decreasing the amount of CQD-Ni(NTA) two fold (0.8×10^{-11} moles) it was found that all the His_6-MSP molecules had been attached to the QDs. When the amount of CQD-Ni(NTA) was decreased to 0.4×10^{-11} moles, only 2.23×10^{-11} moles

of protein was attached. Moreover, no protein binding was observed when the amount of CQD-Ni(NTA) was reduced to 0.2×10^{-11} moles. From these results it can be deduced that under these conditions ~18 molecules of His_6-MSP-1 can be loaded on each QD.

On incubation of QD-DOGS-Ni-NTA/PEG-PE micelle (1.82×10^{-11} moles) with His_6-MSP-1 (1.28×10^{-10} moles) it was found that all the His_6-MSP-1 molecules had been attached to the QD-DOGS-Ni-NTA /PEG-PE micelle. When the amount of QD-DOGS-Ni-NTA /PEG-PE micelle was decreased to 1.16×10^{-11} moles, only 7×10^{-11} moles of protein were attached. It seems that under these conditions ~7 molecules of His_6-MSP-1 can be loaded on each QD micelle. It is important to note that under the same experimental conditions QD-DOGS-NTA/PEG-PE micelle did not show any binding to His_6-MSP-1.

As expected, the smallest QDs had the lowest protein binding capacity. Thus, when QD-DHLA-Ni (NTA) (1.1×10^{-11} moles) were incubated with His_6-MSP-1 (1×10^{-10} moles) it was found that only 5×10^{-11} moles of His_6-MSP molecules were attached to the QD (i.e. ~5 molecules of His_6-MSP can be loaded on each of these QDs).

Thus, the highest protein loading capacity was found in CQD-Ni(NTA), whereas the lowest was found for QD-DHLA-Ni (NTA). In essence, by changing the size of the linker separating the nanocrystal surface from Ni-NTA (protein recognition unit) it is possible to control the number of MSP 1 molecules. It will be exciting to investigate the RBC binding ability of these constructs (see Future work).

4.6 Summary and Conclusion

We have demonstrated that NTA-Ni↔histidine tag recognition and the multivalent properties of QDs can be used for attaching multiple copies of His_6-MSP-1 proteins to a single QD. Several NTA-Ni modified QDs were successfully prepared. All exhibited His_6-MSP-1 binding capacity. The His_6-MSP-1 loading capacity ranged from 18 to 5, and is consistent with the length of the linker separating the nanocrystal and Ni-NTA complexes. This result paves the way for studies in which the binding ability of inorganic nanoparticles carrying a different number of MSP-1 molecules can be systematically investigated. Moreover, it provides further evidence that QDs

decorated with Ni-NTA are versatile and provide an effective way of purifying and fluorescently labelling His-tagged proteins for a range of biological applications.

4.7 References

(1) Snow, R. W.; Guerra, C. A.; Noor, A. M.; Myint, H. Y.; Hay, S. I. *Nature* **2005**, *434*, 214-217.

(2) Rang P H.; ***Rang & Dale's Pharmacology;*** Elsevier Health Sciences, 2009; pp 673.

(3) Cowman, A. F.; Crabb, B. S. *Cell* **2006**, *124*, 755-766.

(4) Richards, J. S.; Beeson, J. G. *Immunol Cell Biol.* **2009**, *87*, 377-390.

(5) O'Donnell, R. A.; Saul, A.; Cowman, A. F.; Crabb, B. S. *Nat. Med* .**2000**, *6*, 91-95.

(6) Qari, S. H.; Shi, Y. P.; Goldman, I. F.; Nahlen, B. L.; Tibayrenc, M.; Lal, A. A. *Mol. Biochem. Parasitol.* **1998**, 92, 241-252.

(7) Gaur, D.; Mayer, D. C. G.; Miller, L. H. *Int. J. Parasitol.* **2004**, *34*, 1413-1429.

(8) Bentley, G. A. *Curr. Opin. Microbiol.* **2006**, *9*, 395-400.

(9) Genton, B.; Reed, Z. H. *Curr. Opin. Infect. Dis.* **2007**, *20*, 467-475.

(10) Dahan, M.; Levi, S.; Luccardini, C.; Rostaing, P.; Riveau, B.; Triller, A. *Science* **2003**, *302*, 442-445.

(11) Courty, S.; Luccardini, C.; Bellaiche, Y.; Cappello, G.; Dahan, M. *Nano Lett.***2006**, *6*, 1491-1495.

(12) O. Lieleg, M. López-García, C. Semmrich, J. Auernheimer, H. Kessler, A. R. Bausch, *Small* 2007, **3**, 1560-1565.

(13) Bats, C.; Groc, L.; Choquet, D. *Neuron* **2007**, *53*, 719-734.

(14) Sperling, R. A.; Pellegrino, T.; Li, J. K.; Chang, W. H.; Parak, W. J. *Adv. Funct. Mater.* **2006**, *16*, 943-948.

(15) Carstairs, H. M. J.; Lymperopoulos, K.; Kapanidis, A. N.; Bath, J.; Turberfield, A. *Chembiochem* **2009**, *10*, 1781-1783.

(16) Cavanagh, D. R.; McBride, J. S. *Mol. Biochem. Parasitol.* **1997**, *85*, 197-211.

(17) Cavanagh, D. R.; Dodoo, D.; Hviid, L.; Kurtzhals, J. A. L.; Theander, T. G.; Akanmori, B. D.; Polley, S.; Conway, D. J.; Koram, K.; McBride, J. S. *Infect. Immun.* **2004**, *72*, 6492-6502.

(18) Conway, D. J.; Cavanagh, D. R.; Tanabe, K.; Roper, C.; Mikes, Z. S.; Sakihama, N.; Bojang, K. A.; Oduola, A. M. J.; Kremsner, P. G.; Arnot, D. E.; Greenwood, B. M.; McBride, J. S. *Nat. Med.* **2000**, *6*, 689-692.

(19) Polley, S. D.; Tetteh, K. K. A.; Cavanagh, D. R.; Pearce, R. J.; Lloyd, J. M.; Bojang, K. A.; Okenu, D. M. N.; Greenwood, B. M.; McBride, J. S.; Conway, D. J. *Infect. Immun.* **2003**, *71*, 1833-1842.

(20) Laemmli, U. K. *Nature* **1970**, *227*, 680-685.

5.1 Conclusions, Implications and Future Work

In this thesis various strategies for preserving and enhancing the activity of biomolecules on QDs were successfully devised (Figure 5.1).

In Chapter 2 hydrophobic CdSe-ZnS core-shell QDs made water-soluble by ligand substitution with the bifunctional ligand dihydrolipoic acid (DHLA) were further modified with nickel complexes of nitrilotriacetic acid (Ni-NTA). These QDs were able of in one step selectively purifying and labelling an His_6-tagged GST. An important aspect of this study was to investigate the extent to which the mode of attachment (site specific versus non specific) affects the catalytic activity of the GST on the QD surface. It was found that the Ni-NTA sites specifically recognize the His_6 tags. This recognition enabled docking the QD away from the active site of the GST homodimer resulting in retention of catalytic activity. In contrast, non-specific attachment of the Ni-NTA modified QDs to GST lacking the His_6 tag led to loss of activity. Because His-tags have been broadly adopted in the molecular biology and biochemistry communities, this specific conjugation strategy should enable widespread use of these QDs for a broad range of biological applications.

In Chapter 3 the possibility of exploiting the multivalency and large size of QDs to mimic pathogens like bacteria and viruses was investigated for the first time. An important discovery was that it seems that cooperativity between different biomolecules on the same QD can in some cases lead to enhanced biological activity. In this case hydrophobic interactions and micelle formation (instead of ligand substitution) were used to functionalize the hydrophobic CdSe-ZnS QDs with the lipopolysaccahride (LPS) Kdo_2-Lipid A LPSs are found in outer membrane of Gram-negative bacteria. Because LPS are potent stimulants of the mammalian immune response they can be both highly toxic and useful as adjuvants (immune potentiators) for the development of more effective vaccines.[1] QD-LPS micelles prepared in this thesis work induced stronger production of cytokines in macrophages and dendritic cells than control LPS *in vitro*. Importantly, when they were co-injected with a model antigen (DNP-OVA) in mice they generated higher production of antibodies *in vivo* than LPS alone and even than LPS emulsified in incomplete Freund's adjuvant –which is the gold standard in adjuvant potency. These results have important implications. It may be possible to exploit QDs both as tools to investigate how a wide range of pathogen associated

molecular patterns are processed *in vi*tro and *in vivo* and to modulate the immune responses they induce in a controllable way.

In Chapter 4 the discoveries made in the previous chapters were integrated towards creating the first example of a QD-based model for the *Plasmodium falciparum* malaria merozoite. In this parasite the surface is predominately coated with the protein MSP-1. An His_6-MSP-1 protein was successfully attached to three different Ni-NTA functionalized QDs. Importantly, it was possible to control the number of MSP-1 molecules loaded onto each QD by using different linkers. The implication of this work is that it will be possible to apply these or similar constructs to investigate the extent to which MSP-1 and it's density on the merozoite surface influences it's binding to red blood cells–a process which is critical in the malaria parasite life cycle.

In conclusion the results presented in this thesis work suggested that QDs can be used efficiently for preserving and enhancing the activity of biomolecules. These results open up new biological applications for QDs.

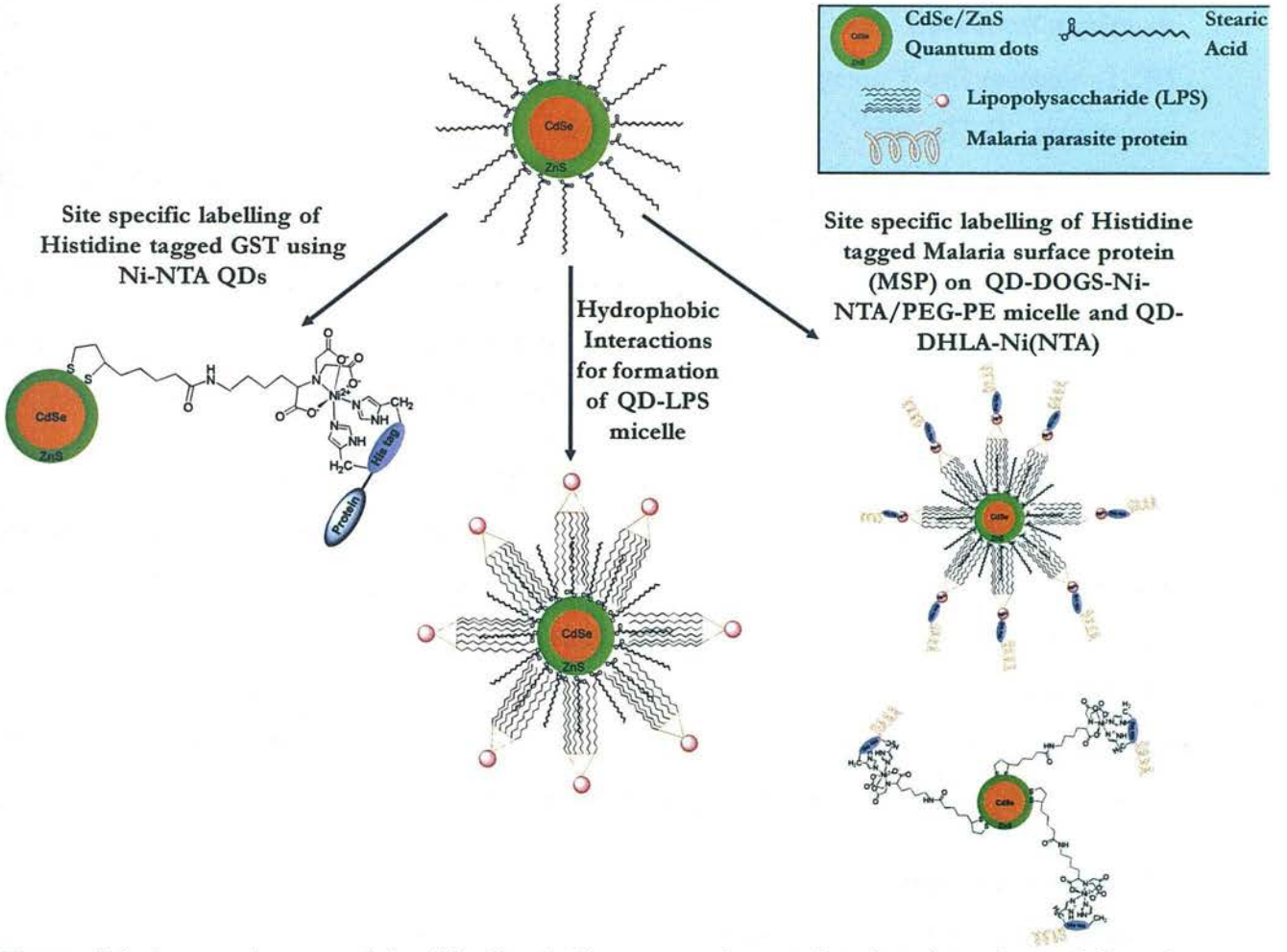

Figure 5.1 Approaches used in this thesis for preserving and enhancing the activity of biomolecules on QDs.

It should be possible to extend this work in many different ways.

First of all, antigen-containing micelles containing QDs should be prepared for studying if and how having an antigen and immune potentiator (e.g. LPS, CpG DNA etc.) attached to the same nanoparticle affects the immune responses generated. Recent studies have suggested that this is an extremely important aspect with exciting potential.[2] To accomplish this DOPGS-Ni-NTA/PEG-PE and LPS polymers could be co-incorporated in the QD-filled micelles for site specific immobilization of his-tag protein antigens. An important target antigen should ovalbumin (OVA). OVA is a well-characterised protein with a good availability of useful resources including T-cell receptor transgenic mice (e.g. OT-II), peptide antigens containing defined epitopes and monoclonal antibodies. It is also a highly manipulable antigen (e.g. it can be readily prepared in recombinant, immunogenic form with a His_6-tag[3] for site-specific binding to our Ni-NTA containing QDs). The native protein is a 45 kDa protein with a diameter of around 5 nm, so theoretical calculations based on the size

of QDs and this protein, the QD:OVA ratios can be varied from 1 to the theoretical maximum of ~12-17 (for 3-10 nm QDs). Peptide antigens encoding transgenic T-cell receptor (TCR) epitopes from the OVA protein will also be used (e.g. the OT-II epitope n-ISQAVHAAHAEINEAGR-COOH ; ~ 45-250 could be theoretically attached to 3-10 nm QDs). His_6-OVA could also be attached to the QD-DHLA-NTA-Ni, CQD-NTA-Ni, and QD-DOGS-Ni-NTA micelles already available from the work described in this thesis. It could be interesting to investigate the effect that the various linkers and different protein loading capacity provided by these systems have on antigenicity of ovalbumin attached to QDs

Later it would important to extend the results with OVA to an antigen with exciting medical potential like MSP-1, which is a protein expressed by *Plasmodium falciparum* and *Plasmodium chabaudi,* the protozoan parasites which cause malaria in humans, and it's corresponding model diseases in mice, *respectively.*[4] Also exciting would be the attachment of other pathogen associated molecular patterns (e.g. CpG DNA).[5] In doing so, it should be possible to better mimic the multivalency and 'cocktail' of biomolecules encountered by the immune system when interacting with microbial pathogens *in vivo.*

In Chapter 4 we have optimised the methods and conditions to control the stoichiometry of biomolecules for each QD. It would be interesting to examine the binding of this QD-His_6-MSP-1 hybrid to RBCs using techniques like fluorescence activated cell sorting (FACS) and confocal microscopy. As these techniques will allow to monitor in real time the binding events which may be responsible for the initial recognition and contact between the malaria merozoite and RBCs. These studies could be followed by *in vitro* and *in vivo* studies which investagate the antigenic activity of His_6-MSP-1 after binding to QDs.

5.2 References

(1) Mata-Haro, V.; Cekic, C.; Martin, M.; Chilton, P. M.; Casella, C. R.; Mitchell, T. C. *Science* **2007**, *316*, 1628-1632.

(2) Lande, R.; Gregorio, J.; Facchinetti, V.; Chatterjee, B.; Wang, Y. H.; Homey, B.; Cao, W.; Su, B.; Nestle, F. O.; Zal, T.; Mellman, I.; Schroder, J. M.; Liu, Y. J.; Gilliet, M. *Nature* **2007**, *449*, 564-569.

(3) Rupa, P.; Mine, Y. *Biotech. Letters* **2003**, *25*, 1917-2003.

(4) (a) Quin, S. J.; Langhorne, J. *Infect. and Immun.* **2001**, *69*, 2245;(b) Millington, O. R.; Di Lorenzo, C.; Phillips, R. S.; Garside, P.; Brewer, J. M. *J Biol* **2006**, *5*, 5.1-5.22.

(5) Latz, E.; Verma, A.; Visintin, A.; Gong, M.; Sirois, C. M.; Klein, D. C. G.; Monks, B. G.; McKnight, C. J.; Lamphier, M. S.; Duprex, W. P.; Espevik, T.; Golenbock, D. T. *Nat. Immunol.* **2007**, *8*, 772-779.